

TOPOGRAPHY AND FUNCTIONAL ORGANIZATION OF EXTRASTRIATE
AREAS V3 AND V4

By

Reuben H. Fan

Dissertation

Submitted to the Faculty of the
Graduate School of Vanderbilt University
in partial fulfillment of the requirements

for the degree of

DOCTOR OF PHILOSOPHY

in

Neuroscience

December, 2012

Nashville, Tennessee

Approved:

Professor Anna W. Roe

Professor Jon H. Kaas

Professor Vivien A. Casagrande

Professor Anita Mahadevan-Jansen

DEDICATION

To my wife Sunita, for always believing this day would come
And to my the rest of my family, for your constant love and support

ACKNOWLEDGEMENT

You will excuse me for breaking with normal protocol by starting with my wife. My time as a graduate student has not been smooth. Consequently many of the people I entered graduate school with have moved on well before this point. But my wife has been one of the few constants during my graduate phase and for that, I am eternally grateful.

I must thank my mentor, Anna W. Roe. My time in the Roe lab is a big part of how I reached this point. It was in this lab I found what I had been searching for in academics and Anna is responsible for building this incredible environment to work in. I also want to thank my Chair, Jon H. Kaas. I was a bit lost when I walked into Jon's office for the first time. He sat and listened to my tale gave me some words of encouragement. He later walked me down the hall and introduced me to Anna. That was the beginning of my life as a neuroscientist. I also need to thank my other two committee members Vivien A. Casagrande and Anita Mahadevan-Jansen. Vivien may be one of the most gracious people I have had the privilege to know. Her door was always open and she, as much as anyone, wanted me to succeed and to grow in this field. Anita and I have known each other since the beginning when I started as a BME graduate student here at Vanderbilt. She has been willing to help and guide me from the beginning which I have found is an extremely rare thing outside your family and dearest friends. I also must thank the Neuroscience program for taking me in, great people from top to bottom.

I truly feel all of the lab members that have come and gone have had a wonderful impact and I am grateful to have known all of them. I will mention a few because of their unique contribution to my growth. Dr. Robert M. Friedman, Rob was my first office mate

but was also a wonderful person to talk to about science and provided advice at every turn. He takes his role in the lab very seriously, especially when it comes to the growth of the students, and does it all with a smile. Dr. Haidong Lu, who is now a professor in China, I always say, everything I know about optical imaging is because of two people, Anna and Haidong. Dr. Hisashi Tanigawa, who is now a professor in Japan, without him, two thirds of this dissertation does not exist.

And finally, my friends, of which, I have managed to make a fair few who have all believed in me. I have managed to make lasting friends from many departments Pharmacology (Drs. Rich G. and Brett E.), BME (Johnathan C., Dr. Richard D., Dr. Chris W.), and Psychology (Christina C., thanks for the roof). I wish I could name them all but even short hand would take serious space. I do have to mention Dr. Megan Rothney, who started with me in BME many years ago. You could not wish for a better friend. I also need to mention Dr. Mary Baldwin. My first project as a neuroscientist partnered me with Mary and that work became the first chapter. We have gotten along great ever since.

I end with my family. While they did not quite understand why I insisted on doing this, they supported me the best they knew how and that was a great blessing. My mother always said, "If this is what makes you happy, then I am happy." Well I am pretty happy now I she certainly let me know she was happy to see me finish. My in-laws, they were just as excited for me as when my wife finished, thank you for that. I want to also mention my grandfather (on my mother's side). He was my inspiration for pursuing an academic path and my one regret is that I did not finish in time for him to know that I accomplished this goal. And I finish with a big thank you, thank you, thank you, to my wife Sunita, none of this happens without you.

TABLE OF CONTENTS

	Page
DEDICATION	ii
ACKNOWLEDGEMENT	iii
LIST OF FIGURES	ix
LIST OF TABLES	x
CHAPTER I	
INTRODUCTION	1
Primate V3	2
Primate V4	8
Intrinsic signal optical imaging.....	13
Research Goals.....	18
Specific aim 1: <i>The establishment and characterization of presumptive V3d in the prosimian galago (Otolemur garnetti) using intrinsic signal optical imaging (IOI).</i>	18
<i>Locate upper and lower visual field representations directly rostral to V2d.</i>	18
<i>Examine the retinotopy along the rostral border of V2.</i>	18
<i>Orientation selectivity.</i>	18
Specific aim 2: <i>Characterization of foveal V4 in the Macaque using IOI.</i>	19
<i>IOI characterization of V4 retinotopy in the awake Macaque.</i>	19
<i>Characterization of cortical magnification factors.</i>	20
<i>Characterization of size preference.</i>	20
<i>Characterization of spatial frequency preferences.</i>	21
References.....	22
CHAPTER II	
INTRINSIC SIGNAL OPTICAL IMAGING EVIDENCE FOR DORSAL V3 IN THE PROSIMIAN GALAGO (<i>OTOLEMUR GARNETTI</i>)	33
Abstract.....	33
Introduction.....	34
Materials and Methods.....	37

Animal Preparation/Surgery	37
Optical Imaging	38
Electrode Recordings	40
Data Analysis of Optical Images	41
Histological Procedures	43
Results.....	44
Overview.....	44
Alignment of cytochrome oxidase stained sections and optical images.....	44
Lower vs. Upper Visual Field Representation.....	46
Mapping with rectangular windows.....	49
Mapping with square windows	53
Electrophysiology	58
Orientation patch sizes in V1, V2, and V3	60
Discussion.....	66
Summary.....	66
Experimental considerations.....	67
Consistent with dorsal V3.....	68
Functional Organization.....	70
Conclusion	71
References.....	73

CHAPTER III

THE INFLUENCE OF MODULARITY ON V4 VISUAL TOPOGRAPHY	78
Abstract.....	78
Introduction.....	79
Material and methods.....	80
Animal preparation	80
Optical imaging in awake, fixating animal.....	80
Visual stimuli	81
Data analysis	82
Results.....	84
General retinotopic organization of foveal V4	84
Stability of maps in awake monkey V4	85
Modality-specific retinotopic organization of foveal V4.....	92
Modality-specific cortical magnification.....	96

Discussion.....	98
Summary.....	98
Modular level visual field representations in foveal V4.....	102
Center of Mass.....	103
Cortical Magnification of foveal V4.....	104
Conclusion.....	107
References.....	109
 CHAPTER IV	
SIZE AND SPATIAL FREQUENCY PREFERNCES OF V4 MODULES.....	113
Abstract.....	113
Introduction.....	114
Materials and methods.....	115
Animal preparation.....	116
Optical imaging in awake, fixating animal.....	116
Visual stimuli.....	117
Data analysis.....	118
Fitting procedures.....	122
Results.....	124
Optical imaging response of color and orientation preference domains to stimulus size.....	124
Optical imaging response of color and orientation preference domains to spatial frequency.....	131
Discussion.....	141
IOI signal vs. total domain area.....	141
Study of parameters of a modular V4 from IOI signal.....	142
Conclusions.....	145
References.....	146
 CHAPTER V	
SUMMARY.....	150
<i>Chapter 2: Galagos have a V3.....</i>	151
<i>Chapter3: Modular influence of V4 visual topography.....</i>	154
<i>Chapter 4: Size and Spatial frequency preferences in V4 modules.....</i>	156
Future directions.....	159

V3	159
V4	161
References	162

LIST OF FIGURES

	Page
Figure 2- 1. <i>V3 vs. DM.</i>	36
Figure 2- 2. <i>Alignment of histological tissue and optical images (Case 08-61).</i>	45
Figure 2- 3. <i>Alignment of histological tissue and optical images (Case 08-11).</i>	47
Figure 2- 4. <i>Lack of upper visual field representation anterior to V2 (Case 08-61).</i>	48
Figure 2- 5. <i>Retinotopic mapping with 20 degree bar stimuli (Case 08-11).</i>	50
Figure 2- 6. <i>Retinotopic mapping with 8 degree bars (Case 08-61).</i>	52
Figure 2- 7. <i>Retinotopic mapping with 4 degree bars (Case 08-11).</i>	54
Figure 2- 8. <i>HM mapping with 10 degree square windows (Case 10-10).</i>	56
Figure 2- 9. <i>VM mapping with 10 degree square windows (Case 10-10).</i>	57
Figure 2- 10. <i>Electrode array recording data.</i>	59
Figure 2- 11. <i>Orientation preference maps are not continuous along the anterior border of V2 (Cases 08-11/08-61).</i>	61
Figure 2- 12. <i>Procedure for orientation preference patch size determination (Case 08-49).</i>	63
Figure 2- 13. <i>Distribution of orientation preference patch sizes in V1, V2, and V3.</i>	64
Figure 3- 1. <i>General retinotopic organization of central V4.</i>	86
Figure 3- 2. <i>Stability of center of mass against different area thresholds.</i>	88
Figure 3- 3. <i>Stability of center of mass over different p-value thresholds.</i>	89
Figure 3- 4. <i>Stability of maps over time.</i>	90
Figure 3- 5. <i>Center of mass of the representation of two spots in V4. T-maps of color selective regions from two different eccentricities (Fig. 4B-8.0°; Fig. 4C-6.0°).</i>	91
Figure 3- 6. <i>Center of mass representations of eccentricity and angularity.</i>	93
Figure 3- 7. <i>Discontinuous representation of angular positions in Subject J.</i>	95
Figure 3- 8. <i>Modular comparison of cortical magnification for Subject L.</i>	97
Figure 3- 9. <i>Modular comparison of cortical magnification for Subject J.</i>	99

Figure 3- 10. <i>Comparison of cortical magnification factor vs eccentricity between Subject L and J.</i>	100
Figure 3- 11. <i>Comparison of cortical magnification factor vs. polar angle between Subject L and J.</i>	101
Figure 4- 1. <i>Extracting time courses.</i>	121
Figure 4- 2. <i>Example of color domain coverage due to different spot stimulus diameters</i>	125
Figure 4- 3. <i>Example of orientation domain coverage due to different spot stimulus diameters</i>	126
Figure 4- 4. <i>Effect of spot size on area from exemplar cases.</i>	128
Figure 4- 5. <i>Effect of spot size on signal strength</i>	130
Figure 4- 6. <i>Example of color domain coverage due to different spatial frequency.</i>	132
Figure 4- 7. <i>Example of orientation domain coverage due to different spatial frequencies.</i>	133
Figure 4- 8. <i>Effect of Spatial frequency on area from exemplar cases.</i>	135
Figure 4- 9. <i>Effect of Spatial frequency on signal at various eccentricities.</i>	137
Figure 4- 10. <i>Comparing the effect of Spatial frequency from foveal vs. parafoveal eccentricities.</i>	139
Figure 4- 11. <i>V2 spatial frequency preference at 0.75° eccentricity.</i>	140

LIST OF TABLES

	Page
Table 2- 1. <i>Orientation patch calculations for three visual areas.</i>	65

CHAPTER I

INTRODUCTION

Elucidating the inner workings of human visual processing requires a detailed understanding of the cortical areas involved and their properties. Although newer methodologies continually enhance direct study of the human cortex, shifting to a dogmatic focus of the human system would undoubtedly hamper progress. Comparative studies provide immeasurable value toward understanding human visual processing. Therefore considerable effort is spent to understand the visual system of other primates, particularly the macaque. There are potentially over 30 visual areas in the macaque (Felleman and Van Essen, 1991). However how many of those areas are homologous to all primates is an open question. Homologous visual areas are cortical subdivisions conserved over evolution. These select cortical regions likely provide vital roles in processing visual information. Currently we consider V1, V2, and the middle temporal area (MT) as homologous primate visual areas (Kaas and Lyon, 2001). Two candidates for addition to that exclusive list are the extrastriate areas V3 and V4.

Defining homology involves more than the simple demarcation of their borders and their visual field representation. Short of tracking common embryological developmental states of a particular visual area (Rosa and Manger, 2005), identifying homologous primate areas is an exercise in finding common traits among many different primate species. The idea that the more primates we can consistently describe a cortical area, the more likely it developed in a common ancestor and has been preserved. The usual tactic

in proposing a potential cortical subdivision is to first describe the sensory surface representation, visuotopy for visual areas, in as many species as possible. While it is an important beginning, it is also crucial to explore other aspects such as cortical connectivity, possible histological markers, and the functional properties of any proposed division (Kaas, 1982). Interestingly despite several decades of research into the visual topography of V3 and V4, we are still unsure about the homology of both areas. The inability to resolve issues centered on topography has likely limited our understanding of their function and contributed to our somewhat naïve belief that V3 and V4 only involve themselves in either the dorsal or ventral visual processing streams. An important step toward dissolving old associations is to better understand how visual areas topographically organize. By improving our understanding influences on visual area topography we can potentially find themes that all visual areas use to further our understanding of the visual system.

Primate V3

Cragg (1969) and Zeki (1969) described a third visual area (V3) similar in size to V2 with a reflected retinotopic organization across the rostral V2 border in macaques. Unfortunately, study of V3's role in the visual system has been relatively sparse when compared to areas like V1, V2, and MT. Studying macaque V3 is difficult due to its location. In V3 of larger primates like humans and macaques, the dorsal half is hidden from view because it is located within the lunate and its ventral half is not easily accessible. These particular features have created significant challenges to the study of V3. But despite limited study due to challenging anatomy, evidence of V3's cortical

connections and functional attributes fuels suggestion that V3 is a part of the dorsal pathway.

There is evidence that V3 and MT, a quintessential dorsal pathway area, are connected (Maunsell and van Essen, 1983). Functional parallels support the evidence for reciprocal connections. Like MT, V3 is selective for orientation and direction (Baizer, 1982; Felleman and Van Essen, 1987; Gegenfurtner et al., 1997; Zeki, 1978). It has also been reported that V3 is important to processing perception (Cowey et al., 2006). V3 appears to prefer 2nd order over 1st order motion processing and may be the first location where 2nd order motion processing occurs in visual cortex (Smith et al., 1998). Previously, MT was thought to be the first location for 2nd order motion processing. V3 also possesses disparity tuning (Poggio et al., 1988). While functional similarities between MT and V3 are interesting, they could simply be coincidences. However it has been demonstrated that selective inactivation of V2 and V3 in the macaque strongly inhibits many MT functions, which suggests that the functional parallels between V3 and MT are more than simple coincidence (Ponce et al., 2008). However there is evidence that V3 may be interconnected with V4 (Stepniewska et al., 2005; Zeki, 1971) as well and there is evidence that V3 can process color (Felleman and Van Essen, 1987) and the surface properties such as gloss and texture (Okazawa et al., 2012) potentially involving V3 in the ventral pathway as well.

While originally thought to be a single continuous area by Cragg (1969) and Zeki (1969), V3 for a time became strongly associated with a discontinuous model where the dorsal and ventral parts were proposed as completely separate visual areas. In this curious turn in V3 history, the moniker V3 was redefined as only representing the lower visual

field being completely contained in the dorsal half of the original V3 defined by Cragg (1969) and Zeki (1969) and the ventral half of V3 was renamed the ventral posterior area (VP) (Burkhalter et al., 1986; Burkhalter and Van Essen, 1986; Newsome et al., 1986). Although suggesting visual areas could be composed of only lower or upper visual field representations is bizarre, the V3/VP proposal was not without some justification. Tracer injections revealed connections between V3 and V1 but not VP and V1 (Burkhalter et al., 1986; Felleman et al., 1997a). Additionally, VP reportedly showed color selectivity and a lack of directional preferences where V3 showed the opposite, little interest in color and clear directional selectivity (Burkhalter et al., 1986; Burkhalter and Van Essen, 1986; Felleman et al., 1997a). With a functional and anatomical asymmetry, the proposal was made that these areas should be considered different and independent areas. This was a bold suggestion. Despite the recognition that both anatomical and functional information is needed to confidently propose a visual area, up until the V3/VP proposal, visual areas processed both the upper and lower visual field.

The most interesting aspect of the V3/VP proposal was not its suggestion but the lack of initial resistance. The proposal gained acceptance despite only representing half the visual field. Kaas (2001), later echoed by Zeki (2003), argued that there is little evidence to support the probable existence of an area only composed of the upper or lower visual field. Appropriately, new evidence began to accumulate that threw the VP/V3 model into question and it was eventually rejected. Emerging fMRI studies that mapped topography suggested the signal dynamics supported a unified V3 rather than a V3/VP model (Brewer et al., 2002; DeYoe et al., 1996; Engel et al., 1997; Press et al., 2001). The anatomical evidence showing asymmetry in macaques from V1 to VP and V3 was shown

to be an unlikely result (Lyon and Kaas, 2002b). And there are clear examples of functional symmetry between V3 and VP that originally were believed to only be associated with one of the two halves (Nishida et al., 2003; Smith et al., 1998).

Another issue that contributed to questioning the original V3 story was questions surrounding its existence in New World monkeys and prosimian primates. In the 1970's, Allman and Kaas performed studies in owl monkeys suggesting an alternative organization that excluded V3 (Allman and Kaas, 1975; 1976) proposing several visual areas along the rostral border of V2, dorsomedial area, dorsointermediate area, and the dorsal lateral crescent. Initial evidence from galagos was not promising for a V3 either, as mapping also suggested receptive fields for both upper and lower visual quadrants in a region similar to the original dorsomedial area (Allman et al., 1979; Rosa et al., 1997). The lack of V3 in other primates did not preclude the possibility of V3 in macaques. However it did pave the way for other proposals, most consequential to V3 was the continued work on the dorsomedial area (DM).

Proposed to lie along the rostral border of dorsal V2, DM slowly emerged as a main reason to question V3 homology. The modern concept of DM is not equivalent to the original definition by Allman and Kaas (1975; 1976). Based on studies in marmosets (Rosa et al., 2005; Rosa et al., 2000; Rosa and Schmid, 1995; Rosa and Tweedale, 2000; 2001), the modern concept of DM principally differs in the topographic representation from the one defined by Allman and Kaas (1975; 1976). However like the originally proposed, DM is a densely myelinated area with both upper and lower visual field representations (see Rosa and Schmid, 1995). Proposed as a complete visual area within the dorsal aspects of visual cortex, the modern DM seemed to have a great deal of

supporting evidence for its existence. First, DM had neighboring representations of the visual field. In the marmoset, the location of DM appears to coincide with a heavily myelinated region near the rostral border of dorsal V2 with connections to V1 and V2 that appear to be from both upper and lower visual fields (e.g. Jeffs et al., 2012; Rosa and Schmid, 1995). While the DM proposal is undoubtedly attractive, there are concerning issues. Studies in owl monkeys (which like marmosets are New World monkeys) show clear orientation selectivity in intrinsic signal optical imaging (IOI) studies along the rostral border of dorsal V2 (Xu et al., 2004a). IOI mapping of this region of owl monkeys reveals a topographic reversal consistent with a dorsal V3 and not a DM (Lyon et al., 2002). Additionally, injections into V1 in squirrel monkeys, owl monkeys, and titi monkeys support a V3 interpretation and not DM (Lyon and Kaas, 2002c). Acceptance of V3 in these other New World monkeys would isolate marmosets, which although possible, is certainly not probable. But, there are supportive tracer studies in marmosets for V3 over DM which allows for the possibility that marmosets are not outliers among New World monkeys and that alternative methods of examination may be required (Lyon and Kaas, 2001). It is also possible that in marmosets, V3 is slightly modified from other primates and consequently there is a DM like area bordering V2 in marmosets (Jeffs et al., 2012).

Another troubling issue is a distinct lack of evidence for functional symmetry in DM. Orientation preference is clearly demonstrated directly anterior to dorsal V2 using IOI in owl monkeys (Xu et al., 2004a) which is consistent with known functionality of V3 in macaques (e.g. Burkhalter et al., 1986; Felleman and Van Essen, 1987; Zeki, 1978). However study of DM functional selectivity only reported orientation selectivity on the

lower visual field and conspicuously omitted any report on symmetric upper visual field functional preferences despite having mapped receptive fields in the upper visual field (Lui et al., 2006). Moreover, the receptive field mapping performed for many of these supportive DM studies can be re-interpreted to allow for a dorsal V3 (see Lyon and Connolly, 2012) which would be consistent with the proposal by Kaas and Lyon (2001) calling for DM to border a thinner V3.

The V3 story is converging onto established homology among primates. Establishing a homologous visual area requires reliable identification of a proposed visual area across species. Currently we identify visual areas based on principles previously outlined by Jon Kaas (1982). When applied to the visual system, these principles suggest that a visual area should possess the following: (1) a representation of the upper and lower visual field, (2) an architectonically definable region, and (3) a unique connective pattern. Implicitly the three principle attributes suggest that the upper and lower visual field representation have “relatively symmetric” functional attributes. Therefore we should not expect one quadrant of a visual area to have an attribute that is completely omitted in another quadrant of that same visual area. Unfortunately, certain features may not be identifiable for a homologous visual area across different species making the task more difficult. For instance staining for cytochrome oxidase (CO) can reveal areas of high and low mitochondrial density (Wong-Riley, 1979). It has been shown that CO staining reveals stripes in V2 that has been identified in both Old World (Hubel and Livingstone, 1987) and New World monkeys (Kaskan et al., 2009). But, in galagos the CO bands are absent in V2 (Condo and Casagrande, 1990). Additionally, there is little to prevent the arbitrary combinations of various upper and lower visual field representations. Despite

this potential hurdle the different lines of evidence across primates species has succeeded in the cases of V1, V2, and MT (Kaas and Lyon, 2001). A convergence of evidence across primates in V3 is also forming. First there was a series of anatomical tracer studies showing consistency in V1 to V3 connections for dorsal and ventral parts of V3 in macaques (Lyon and Kaas, 2002b), various New World monkeys (Lyon and Kaas, 2001; 2002c), and galagos (Lyon and Kaas, 2002a). These studies reveal topographic connectivity consistent with a V3 interpretation. Supporting the visuotopy implied by the connections with V1 was IOI mapping rostral to dorsal V2 that demonstrated a retinotopic reversal consistent with V3 in owl monkeys (Lyon et al., 2002). Additional support for V3 came from fMRI studies in humans (DeYoe et al., 1996; Engel et al., 1997; Gegenfurtner et al., 1997; Reppas et al., 1997; Sereno et al., 1995; Smith et al., 1998; Tootell et al., 1997) and macaques (Adams and Zeki, 2001; Brewer et al., 2002; Press et al., 2001) all supportive of a reversal across the rostral border of V2 in both dorsal and ventral aspects. With the evidence across the various species producing a coherent story the strong possibility exists that V3 is a homologous area among primates. Therefore continuing to study V3 in various primates is important. Adding V3 to the basic plan of the primate visual system suggests this area has been conserved by all primates and would allow for more comprehensive comparative study to learn more about this understudied visual area.

Primate V4

V4 was first described based on lesions in V2 and V3 revealing degeneration patterns along the anterior bank of the lunate sulcus and rising out onto the prelunate gyrus and

into the posterior bank of the superior temporal sulcus (Zeki, 1971). Connections have been described between V4 and V2, V3, middle temporal area, and temporal cortex, and some parts of central V1 (Stepniewska et al., 2005; Ungerleider et al., 2008).

Interestingly, connections with inferior temporal cortical areas involved in object recognition (TE, TEO) seem to be concentrated in central vision representation of V4 while peripheral vision representations have connections with areas believed to be more involved with dorsal stream areas involved with spatial vision and attention (e.g. medial superior temporal sulcus area, ventral intraparietal area, lateral intraparietal area, posterior intraparietal area) (Ungerleider et al., 2008).

The diversity of cortical connections suggests roles in both object identification and object location. Early characterization of V4 revealed a large number of color selective cells (Zeki, 1983; Zeki, 1973). This led to V4 being considered a major color processing area in the visual system. However there is poor support for V4 being primarily a color processing area based on lesions in macaques (e.g. Heywood and Cowey, 1987; Heywood et al., 1992; Tootell et al., 2004; Walsh et al., 1992; Walsh et al., 1993). Instead lesion studies produced a loss in color constancy (Walsh et al., 1993) and various object/shape recognition deficits (De Weerd et al., 1996; De Weerd et al., 1999; Merigan and Pham, 1998; Schiller, 1993). Additionally, V4 responds to a variety of different functional preferences, such as orientation (Essen and Zeki, 1978; Schiller, 1993; Zeki, 1973), 3D orientation tuning (Hinkle and Connor, 2002), binocular disparity (Hegde and Van Essen, 2005; Hinkle and Connor, 2001; 2005), and contour curvature/shape (Pasupathy and Connor, 1999; 2001; 2002). Although still considered an important

component of its function, V4's association as a major color processing center has been tempered.

There has been substantial debate over many of the possible functions of V4. Considered a mid-tier visual processing area lying in the cortex between V2 and MT, V4 is believed to be critical in the progression of information through ventral stream visual areas (Tootell and Hadjikhani, 2001). The current body of evidence has led to a new proposal that V4 performs figure-ground segregation (differentiation of objects and features at various depths) based on "selective extraction" of appropriate feature domain networks which would explain V4's diverse set of functional properties (Roe et al., 2012). However there are inadequacies in our V4 knowledge base that prevents better progress.

Although our understanding of V4 has vastly improved since its initial identification, we are still debating fundamental aspects of V4 that continue to limit our understanding. One of these fundamental issues is the topographic organization of V4. Several decades ago, Gattass and colleagues (1988) mapped an area in macaques they deemed to be V4, where the anterior border was the horizontal meridian and posterior border was the vertical meridian lying in the anterior bank of the lunate progressing over the prelunate gyrus and into the posterior bank of the superior temporal sulcus. While this view of V4 has been influential, it has not been the only interpretation of V4 organization. Initially, this region in macaques was defined as two visual areas, V4 and V4A (Zeki, 1971). The initial Zeki model eventually gave way to the influential Gattass model (1988). The continuous retinotopic map in macaques was unchallenged until tracer injections into the V4 area suggested that the patterns of connections supported a version of V4 similar to

the original Zeki model where V4 is split into two areas, a rostral dorsolateral area (DLr) and a caudal dorsolateral area (DLc) similar to V4 and V4A (Stepniewska et al., 2005). The rostral/caudal division of V4/DL is complicated to confirm. Detailed receptive field mapping did not strongly advocate for a division of this nature (Gattass et al., 1988) and fMRI evidence favors a continuous visual area interpretation similar to the Gattass model (Brewer et al., 2002; Fize et al., 2003). The confusion over V4 organization has made efforts to establish V4 as a homologous area problematic.

The various speculations regarding V4 likely stem from incomplete understanding of how V4 maps the visual world. The visual area currently considered V4 in macaques is quite large with receptive fields with complex properties such as selectivity for various curvatures (Connor, 2003; Pasupathy and Connor, 1999; 2001; 2002) and apparent radial asymmetry inherited due to V1 cortical magnification (Motter, 2009). Efforts to map V4 topography suffers from this complexity and is likely the reason why dense electrophysiological sampling failed to reveal any clear functional organization (Youakim et al., 2001). However there is evidence that V4 is segregated into functional modules that are reminiscent of the stripes of functional modalities in V2. CO staining reveals patterns of thin and thick stripes (that stain darkly for CO) and pale stripes that can be revealed *in vivo* based on their functional preferences using IOI (Lu et al., 2010; Lu and Roe, 2007; 2008). In V2 each point of visual space has a representation in each stripe (Roe and Ts'o, 1995). This is similar to the repetition of visual space in layer IV in V1 that coincides with ocular dominance columns (Blasdel and Fitzpatrick, 1984; Hubel and Wiesel, 1974). In V4, there is no known histological technique that has revealed features like V2 stripes. Despite this limitation there is strong evidence for functional

modularity. Using IOI, Ghose and Ts'o demonstrated orientation preference in non-adjacent locations within V4 suggestive of modularity (1997). Also supporting V4 modularity, an electrophysiological study demonstrated a columnar like organization for color in V4 (Kotake et al., 2009). Modular like functional groupings is also supported by a fMRI study revealing “globs” (more color selective regions) and “interglobs” (more shape selective regions) in V4 (Conway et al., 2007). Cortical connections between V2 and V4 show a relationship with V2 stripes that also supports a modular V4 interpretation (Felleman et al., 1997b; Xiao et al., 1999; Zeki and Shipp, 1989). The best example of V4 modularity is from Tanigawa and colleagues whose use of IOI in awake macaques revealed segregation of orientation and color/luminance domains in V4 (Tanigawa et al., 2010). Consistent with anatomical results (Felleman et al., 1997b; Xiao et al., 1999), there appear to be regions where the two types of preference domains overlapped (Tanigawa et al., 2010). These V4 modules also appear to repeat visuotopic positions (Tanigawa et al., 2010). The visuotopic patterns among the different V4 preference modules is highly reminiscent to those reported among V2 stripes (Roe and Ts'o, 1995).

Continuing to elucidate the topographic organization of macaque V4 could present a crucial juncture in the history of this visual area. Currently there is a strong debate regarding V4 homology between humans and macaques. Initially, there appeared to be a human visual area with a similar retinotopic organization to that of macaque V4 (Serenio et al., 1995). However after numerous human mapping studies (Brewer et al., 2005; DeYoe et al., 1996; Smith et al., 1998; Tootell et al., 1997; Wade et al., 2002; Wandell et al., 2005) were unable to reveal a human V4 similar to macaque V4 (Brewer et al., 2002; Fize et al., 2003; Gattass et al., 1988), serious questions were raised about V4 homology.

This led many to suggest that there was a human specific V4 that only exists in the ventral cortex bordering ventral V3. However Hansen et al. (2007) attempted to end the debate by demonstrating that it was possible to reveal a human equivalent to macaque V4 bordering the length of V3. But, an fMRI study revealed color selectivity in the ventral V4 and not in the hypothesized dorsal V4 continuing to put the homology between human and macaque V4 in doubt (Goddard et al., 2011). However if V4 is modular as suggested by IOI evidence (Ghose and Ts'o, 1997; Tanigawa et al., 2010), fMRI evidence (Conway et al., 2007), and cortical connections with V2 (Felleman et al., 1997b; Xiao et al., 1999; Zeki and Shipp, 1989), then previous studies showing asymmetries will need to account for possible influences of a modular organization to the topographic organization of V4.

Intrinsic signal optical imaging

Intrinsic Signal Optical Imaging (IOI) is based on the detection of activity-dependent reflectance changes in cortical tissue using detectors that can differentiate these state dependent changes. This technique has been successfully applied to a wide variety of cortical regions such as somatosensory cortex (e.g. Chen et al., 2005; 2009), auditory cortex (e.g. Kalatsky et al., 2005), barrel cortex (e.g. Grinvald et al., 1986; Tsytsarev et al., 2010), and visual cortex (e.g. Grinvald et al., 1986; Lu and Roe, 2008; Lyon et al., 2002; Xu et al., 2004a; Xu et al., 2004b). This section will cover the basic principles behind IOI. A comprehensive treatment can be found in an excellent chapter by Tobias Bonhoeffer and Amiram Grinvald (1996).

From the perspective of applying IOI, when light hits the cortical surface, there are two outcomes for the light (photon fates) of particular interests. The first is *specular reflectance* where some of the photons reflect directly off the tissue surface. The second is *transmission*, photons that pass through the tissue surface. Once there are photons within the tissue, then there are two other possible photon fates of interest. First is photon *absorption*. These are lost photons. The second is *diffuse reflectance*. These photons enter the tissue and then travel back out the tissue surface. IOI is based on the detection of reflected light of which there are two sources mentioned, specular and diffuse reflectance. In the case of diffusely reflected light, the photons have entered and interacted with the tissue providing, in a sense, an “optical signature” of the current state of the sampled tissue in cortex. By collecting “optical signatures” of tissue over time, it is possible to detect time dependent changes.

The most common application of IOI is to target the hemodynamic change that accompanies neuronal firing. The phrase “hemodynamic change” refers to the alteration in the balance between oxy and de-oxy hemoglobin states of red blood cells. Hemoglobin is an iron carrying metalloprotein that is responsible for carrying oxygen to tissues via the vasculature. In cortex, increased neuronal activity results in correlated with oxygen demands (Devor et al., 2003; Li and Freeman, 2007; Offenhauser et al., 2005; Thompson et al., 2003). The increased demand results in an initial drop in the blood oxygenation followed by vasodilation (a standard physiological response due to an increase in carbon dioxide). The alteration of hemoglobin from oxy and de-oxy states and the subsequent influx of newly oxygenated blood provides a detectable difference in the optical signature. Due to the optical properties of oxygenated and deoxygenated blood, it is

common practice to use visible wavelengths in the visible orange to red spectrum; for example ~630 nm is a wavelength that has been used effectively (Tanigawa et al., 2010). Although IOI is most commonly performed in the visible orange to red range, IOI works over a wider spectrum (Frostig et al., 1990). Once the cortical tissue is exposed and a light source is chosen, a detector sensitive enough to detect the changes in reflectance is required.

It is important to understand that typical changes in diffuse reflectance are very small (on the order of 0.1%). Adding to the challenge of detecting such small changes is the persistent presence of normal physiological processes like breathing and the beating heart. However there are several strategies for combating these issues of signal to noise (see Bonhoeffer and Grinvald, 1996). Also of relevant note are the relative resolution scales. A neuron fires on the time scale of milliseconds. However a hemodynamic change happens on the order of seconds. Additionally the resolution of IOI is often on the order of 100 microns. Although the link between the events is strong (Devor et al., 2003; Li and Freeman, 2007; Offenhauser et al., 2005; Thompson et al., 2003), IOI looks at a change related to neuronal events, not neural events themselves.

In visual areas, IOI reveals cortical responses by comparing images generated from different visual stimuli conditions (or comparing conditions of visual stimuli and no visual stimuli condition) (for examples see Lu et al., 2010; Lu and Roe, 2007; 2008). Through these comparisons it is possible to reveal parts of visual areas where preferences between visual conditions occur. This concept is best understood when applied to areas where organization is well known. In V1, orientation preference is organized into “pinwheels.” By comparing various orientations to determine preferences in V1 based on

IOI signals, we can reveal pinwheels in V1 (e.g. Grinvald et al., 1986). Ocular dominance is also a clear example whereby comparing differences between left and right eye activation this characteristic feature of V1 can be exposed (e.g. Lu and Roe, 2008).

The link between cortical activity and functional structure with its optical properties due to neuronal activity is crucial to the utility of IOI since the signal detected is indirect in nature. Therefore support for the correlation of neural and microvascular responses and the indirect hemodynamic based signal are important. There have been a variety of studies linking optical changes in neurons and cortical tissue in response to neuronal activity (for review see Bonhoeffer and Grinvald, 1996; Cohen, 1973; Hillman, 2007). There have been numerous demonstrations of the correspondence of functional organization and the local changes detected via IOI. Grinvald et al. (1986) elegantly demonstrated that IOI could reveal whisker barrels in rat as well as orientation columns of the cat. In macaque V1, ocular dominance columns have been repeatedly demonstrated throughout the years (e.g. Frostig et al., 1990; Lu and Roe, 2008). In V2, Lu and Roe demonstrated that the stripes in macaque V2, which were first revealed by CO staining (Hubel and Livingstone, 1987), could be revealed *in vivo* by IOI (Lu and Roe, 2008). The hemodynamic correspondence also extends to fMRI. In squirrel monkeys the digit representations in somatosensory cortex based on measures from electrophysiology, IOI, and fMRI co-localize with astonishing accuracy (Chen et al., 2007; Roe and Chen, 2008). A similar association has also been demonstrated between two-photon imaging and IOI of orientation preferences in ferret V1 (Schummers et al., 2008). The correspondence of the IOI signal also extends beyond mapping. Spatial frequency tuning preferences of local areas in cat visual cortex derived from changes in the reflectance changes in IOI

correlate well with tuning functions found based on electrophysiological recordings (Issa et al., 2000).

The strength of IOI is its ability to reveal organization on a spatial scale ideal for revealing modular organization. This is done without the use of dyes or contrast agents. Combined with the ability to reveal stimulus tuning, IOI is a formidable technique for exploring and studying visual area organization and function.

Research Goals

The overall goal of this work is to extend our knowledge of the extrastriate areas V3 and V4. Here we present a set of experiments using intrinsic signal optical imaging (IOI) to study two visual areas, V3 and V4. For V3, our goal is to establish its existence in the galago, which would serve to increase its likely existence in all primates. For V4, we aim to increase our sophistication regarding V4 topography in the macaque.

Specific aim 1: *The establishment and characterization of presumptive V3d in the prosimian galago (*Otolemur garnetti*) using intrinsic signal optical imaging (IOI).*

This work is designed to further characterize the visual representation of galago cortex directly rostral to dorsal V2 (V2d). Examining the retinotopic organization and functional attributes are central to establishing visual areas. Acceptance of V3 in galagos increases the likelihood that V3 exists in all primates. We hypothesize that IOI will support an organization in galagos consistent with the dorsal division of V3 thus supporting its existence in galagos. We plan to test this hypothesis in several ways.

Locate upper and lower visual field representations directly rostral to V2d. We plan to use visual stimuli confined to the upper or lower visual field. Consistent with V3d, we expect only the lower visual field to be present along the rostral border of V2d.

Examine the retinotopy along the rostral border of V2. We expect the retinotopy of V3 to approximate a mirror reversal of V2 across a common horizontal meridian border with the rostral border of V3 representing the vertical meridian.

Orientation selectivity. Studies in other primates suggest that areas directly rostral to V2d are orientation selective. We predict that presumptive V3d in galagos will also show orientation preference.

Specific aim 2: Characterization of foveal V4 in the Macaque using IOI.

The goal of this aim is to improve our understanding of V4 topographic and functional organization. Previous studies have mapped V4 in the macaque but little is known about the topography of feature specific representations within V4. In this aim we target the understudied foveal V4, because of its central role in visual behavior. We suspect that a detailed topographic study of foveal V4 will lead to novel views and help settle a lingering controversy regarding whether V4 is one or two (V4 and V4A) areas. We believe the evidence will support a single V4 with a modular organization similar to V2. We will study various topographic and functional features to test this belief.

IOI characterization of V4 retinotopy in the awake Macaque. The first part of Aim 2 targets the issue of the retinotopic organization in Macaque V4. Although we have a general understanding of V4 organization and properties in Macaques, our recent studies indicate that V4 retinotopy is more complex than previous publications indicate. We hypothesize that IOI will reveal a retinotopic organization with multiple representations of points in visual space not dissimilar from that of V2. First we will establish V4 representation for different features, such as color and orientation. We will then proceed with using isoeccentric rings, isopolar bars, and spots (patches) to determine if there is evidence for individual representations of stimuli for each functional region. These stimuli will be used to characterize the topography of the central 6 degrees of visual representation. We will be particularly interested in any rostral-caudal repetition in the retinotopic organization that is either consistent or inconsistent with a rostral-caudal division of V4 as two areas.

Characterization of cortical magnification factors. In the second part of Aim 2 we turn our attention to the cortical magnification in V4. It is known that there are different cortical magnification factors at different visual eccentricities. There is also evidence that cortical magnification can differ significantly for isopolar vs. isoeccentric representations (anisotropic representation). Based on previous studies showing that representation of multiple features leads to anisotropic representation, we hypothesize that V4 may have a high degree of anisotropy in cortical representation. Quantification of the allocation of cortex to feature-specific representations will be done by imaging spots, bars, and ring stimuli containing color or achromatic content. Methods will be developed to evaluate cortical magnification of discontinuous, patchy representations. If our hypothesis in Aim 2a is supported, we will attempt to determine if differences in the cortical magnification and anisotropy exist between different functional modules.

Characterization of size preference. In the third part of Aim 2, we investigate possible effects of cortical response due to stimulus size. It is well known that responses of V4 cells are strongly suppressed by large stimuli, indicating the presence of suppressive surrounds in the receptive fields. However, it is not known at the population level what the optimal spot size is and how this varies with eccentricity or whether the population surround differs between surface and contour representations. We hypothesize that the surround of the orientation system (which encodes contours) would be more suppressive than that of the color/luminance system (which encodes surfaces). We will present patches of various size and features (color or orientation) and quantify the size of the cortical response as well as the signal time courses. Preferences regarding the size of

uniform stimuli on a population level will help us understand if the suppressive influence of large stimuli on single neurons is inherited on a larger scale.

Characterization of spatial frequency preferences. In the fourth and final part of Aim 2, we look at possible effects of cortical response due to spatial frequency. Given that inputs to color and orientation domains are likely to be from thin and pale stripes in V2, we would like to know whether the color and orientation domains have different spatial frequency preference. We hypothesize that color and luminance domains, which subserve surface feature representation, have lower spatial frequency preference than orientation domains, which subserve object contour representation. We will use patches with oriented gratings (color and achromatic) with various spatial frequencies to assess this subaim. Studying the interaction of spatial frequency with features such as orientation and color selectivity allow us to learn more about how feature segregations propagates through different visual areas.

References

- Adams DL, Zeki S. 2001. Functional organization of macaque V3 for stereoscopic depth. *J Neurophysiol* 86(5):2195-2203.
- Allman J, Campbell CB, McGuinness E. 1979. The dorsal third tier area in *Galago senegalensis*. *Brain Res* 179(2):355-361.
- Allman JM, Kaas JH. 1975. The dorsomedial cortical visual area: a third tier area in the occipital lobe of the owl monkey (*Aotus trivirgatus*). *Brain Res* 100(3):473-487.
- Allman JM, Kaas JH. 1976. Representation of the visual field on the medial wall of occipital-parietal cortex in the owl monkey. *Science* 191(4227):572-575.
- Baizer JS. 1982. Receptive field properties of V3 neurons in monkey. *Invest Ophthalmol Vis Sci* 23(1):87-95.
- Blasdel GG, Fitzpatrick D. 1984. Physiological organization of layer 4 in macaque striate cortex. *The Journal of neuroscience : the official journal of the Society for Neuroscience* 4(3):880-895.
- Bonhoeffer T, Grinvald A. 1996. Optical Imaging based on intrinsic signals: the methodology. In: Toga AW, Mazziotta JC, editors. *Brain Mapping: the methods*: Academic Press. p 55-97.
- Brewer AA, Liu J, Wade AR, Wandell BA. 2005. Visual field maps and stimulus selectivity in human ventral occipital cortex. *Nature neuroscience* 8(8):1102-1109.
- Brewer AA, Press WA, Logothetis NK, Wandell BA. 2002. Visual areas in macaque cortex measured using functional magnetic resonance imaging. *J Neurosci* 22(23):10416-10426.
- Burkhalter A, Felleman DJ, Newsome WT, Van Essen DC. 1986. Anatomical and physiological asymmetries related to visual areas V3 and VP in macaque extrastriate cortex. *Vision Res* 26(1):63-80.

- Burkhalter A, Van Essen DC. 1986. Processing of color, form and disparity information in visual areas VP and V2 of ventral extrastriate cortex in the macaque monkey. *J Neurosci* 6(8):2327-2351.
- Chen LM, Friedman RM, Roe AW. 2005. Optical imaging of SI topography in anesthetized and awake squirrel monkeys. *J Neurosci* 25(33):7648-7659.
- Chen LM, Friedman RM, Roe AW. 2009. Optical imaging of digit topography in individual awake and anesthetized squirrel monkeys. *Exp Brain Res* 196(3):393-401.
- Chen LM, Turner GH, Friedman RM, Zhang N, Gore JC, Roe AW, Avison MJ. 2007. High-resolution maps of real and illusory tactile activation in primary somatosensory cortex in individual monkeys with functional magnetic resonance imaging and optical imaging. *The Journal of neuroscience : the official journal of the Society for Neuroscience* 27(34):9181-9191.
- Cohen LB. 1973. Changes in neuron structure during action potential propagation and synaptic transmission. *Physiol Rev* 53(2):373-418.
- Condo GJ, Casagrande VA. 1990. Organization of cytochrome oxidase staining in the visual cortex of nocturnal primates (*Galago crassicaudatus* and *Galago senegalensis*): I. Adult patterns. *J Comp Neurol* 293(4):632-645.
- Connor CE. 2003. Active vision and visual activation in area V4. *Neuron* 40(6):1056-1058.
- Conway BR, Moeller S, Tsao DY. 2007. Specialized color modules in macaque extrastriate cortex. *Neuron* 56(3):560-573.
- Cowey A, Campana G, Walsh V, Vaina LM. 2006. The role of human extra-striate visual areas V5/MT and V2/V3 in the perception of the direction of global motion: a transcranial magnetic stimulation study. *Exp Brain Res* 171(4):558-562.
- Cragg BG. 1969. The topography of the afferent projections in the circumstriate visual cortex of the monkey studied by the Nauta method. *Vision Res* 9(7):733-747.

- De Weerd P, Desimone R, Ungerleider LG. 1996. Cue-dependent deficits in grating orientation discrimination after V4 lesions in macaques. *Visual neuroscience* 13(3):529-538.
- De Weerd P, Peralta MR, 3rd, Desimone R, Ungerleider LG. 1999. Loss of attentional stimulus selection after extrastriate cortical lesions in macaques. *Nature neuroscience* 2(8):753-758.
- Devor A, Dunn AK, Andermann ML, Ulbert I, Boas DA, Dale AM. 2003. Coupling of total hemoglobin concentration, oxygenation, and neural activity in rat somatosensory cortex. *Neuron* 39(2):353-359.
- DeYoe EA, Carman GJ, Bandettini P, Glickman S, Wieser J, Cox R, Miller D, Neitz J. 1996. Mapping striate and extrastriate visual areas in human cerebral cortex. *Proc Natl Acad Sci U S A* 93(6):2382-2386.
- Engel SA, Glover GH, Wandell BA. 1997. Retinotopic organization in human visual cortex and the spatial precision of functional MRI. *Cereb Cortex* 7(2):181-192.
- Essen DC, Zeki SM. 1978. The topographic organization of rhesus monkey prestriate cortex. *The Journal of physiology* 277:193-226.
- Felleman DJ, Burkhalter A, Van Essen DC. 1997a. Cortical connections of areas V3 and VP of macaque monkey extrastriate visual cortex. *J Comp Neurol* 379(1):21-47.
- Felleman DJ, Van Essen DC. 1987. Receptive field properties of neurons in area V3 of macaque monkey extrastriate cortex. *J Neurophysiol* 57(4):889-920.
- Felleman DJ, Van Essen DC. 1991. Distributed hierarchical processing in the primate cerebral cortex. *Cereb Cortex* 1(1):1-47.
- Felleman DJ, Xiao Y, McClendon E. 1997b. Modular organization of occipito-temporal pathways: cortical connections between visual area 4 and visual area 2 and posterior inferotemporal ventral area in macaque monkeys. *The Journal of neuroscience : the official journal of the Society for Neuroscience* 17(9):3185-3200.
- Fize D, Vanduffel W, Nelissen K, Denys K, Chef d'Hotel C, Faugeras O, Orban GA. 2003. The retinotopic organization of primate dorsal V4 and surrounding areas: A

- functional magnetic resonance imaging study in awake monkeys. *The Journal of neuroscience : the official journal of the Society for Neuroscience* 23(19):7395-7406.
- Frostig RD, Lieke EE, Ts'o DY, Grinvald A. 1990. Cortical functional architecture and local coupling between neuronal activity and the microcirculation revealed by in vivo high-resolution optical imaging of intrinsic signals. *Proceedings of the National Academy of Sciences of the United States of America* 87(16):6082-6086.
- Gattass R, Sousa AP, Gross CG. 1988. Visuotopic organization and extent of V3 and V4 of the macaque. *J Neurosci* 8(6):1831-1845.
- Gegenfurtner KR, Kiper DC, Levitt JB. 1997. Functional properties of neurons in macaque area V3. *J Neurophysiol* 77(4):1906-1923.
- Ghose GM, Ts'o DY. 1997. Form processing modules in primate area V4. *J Neurophysiol* 77(4):2191-2196.
- Goddard E, Mannion DJ, McDonald JS, Solomon SG, Clifford CW. 2011. Color responsiveness argues against a dorsal component of human V4. *J Vis* 11(4).
- Grinvald A, Lieke E, Frostig RD, Gilbert CD, Wiesel TN. 1986. Functional architecture of cortex revealed by optical imaging of intrinsic signals. *Nature* 324(6095):361-364.
- Hansen KA, Kay KN, Gallant JL. 2007. Topographic organization in and near human visual area V4. *The Journal of neuroscience : the official journal of the Society for Neuroscience* 27(44):11896-11911.
- Hegde J, Van Essen DC. 2005. Stimulus dependence of disparity coding in primate visual area V4. *Journal of neurophysiology* 93(1):620-626.
- Heywood CA, Cowey A. 1987. On the role of cortical area V4 in the discrimination of hue and pattern in macaque monkeys. *The Journal of neuroscience : the official journal of the Society for Neuroscience* 7(9):2601-2617.

- Heywood CA, Gadotti A, Cowey A. 1992. Cortical area V4 and its role in the perception of color. *The Journal of neuroscience : the official journal of the Society for Neuroscience* 12(10):4056-4065.
- Hillman EM. 2007. Optical brain imaging in vivo: techniques and applications from animal to man. *J Biomed Opt* 12(5):051402.
- Hinkle DA, Connor CE. 2001. Disparity tuning in macaque area V4. *Neuroreport* 12(2):365-369.
- Hinkle DA, Connor CE. 2002. Three-dimensional orientation tuning in macaque area V4. *Nat Neurosci* 5(7):665-670.
- Hinkle DA, Connor CE. 2005. Quantitative characterization of disparity tuning in ventral pathway area V4. *J Neurophysiol* 94(4):2726-2737.
- Hubel DH, Livingstone MS. 1987. Segregation of form, color, and stereopsis in primate area 18. *The Journal of neuroscience : the official journal of the Society for Neuroscience* 7(11):3378-3415.
- Hubel DH, Wiesel TN. 1974. Sequence regularity and geometry of orientation columns in the monkey striate cortex. *The Journal of comparative neurology* 158(3):267-293.
- Issa NP, Trepel C, Stryker MP. 2000. Spatial frequency maps in cat visual cortex. *The Journal of neuroscience : the official journal of the Society for Neuroscience* 20(22):8504-8514.
- Jeffs J, Federer F, Ichida JM, Angelucci A. 2012. High-Resolution Mapping of Anatomical Connections in Marmoset Extrastriate Cortex Reveals a Complete Representation of the Visual Field Bordering Dorsal V2. *Cereb Cortex* [Epub ahead of print].
- Kaas JH. 1982. The Segregation of Function in the Nervous System: Why Do sensory Systems Have So Many Subdivisions? In: Neff WP, editor. *Contributions To Sensory Physiology*. New York: Academic Press, Inc. p 201-240.
- Kaas JH, Lyon DC. 2001. Visual cortex organization in primates: theories of V3 and adjoining visual areas. *Prog Brain Res* 134:285-295.

- Kalatsky VA, Polley DB, Merzenich MM, Schreiner CE, Stryker MP. 2005. Fine functional organization of auditory cortex revealed by Fourier optical imaging. *Proceedings of the National Academy of Sciences of the United States of America* 102(37):13325-13330.
- Kaskan PM, Lu HD, Dillenburger BC, Kaas JH, Roe AW. 2009. The organization of orientation-selective, luminance-change and binocular-preference domains in the second (V2) and third (V3) visual areas of New World owl monkeys as revealed by intrinsic signal optical imaging. *Cereb Cortex* 19(6):1394-1407.
- Kotake Y, Morimoto H, Okazaki Y, Fujita I, Tamura H. 2009. Organization of color-selective neurons in macaque visual area V4. *Journal of neurophysiology* 102(1):15-27.
- Li B, Freeman RD. 2007. High-resolution neurometabolic coupling in the lateral geniculate nucleus. *The Journal of neuroscience : the official journal of the Society for Neuroscience* 27(38):10223-10229.
- Lu HD, Chen G, Tanigawa H, Roe AW. 2010. A motion direction map in macaque V2. *Neuron* 68(5):1002-1013.
- Lu HD, Roe AW. 2007. Optical imaging of contrast response in Macaque monkey V1 and V2. *Cereb Cortex* 17(11):2675-2695.
- Lu HD, Roe AW. 2008. Functional organization of color domains in V1 and V2 of macaque monkey revealed by optical imaging. *Cereb Cortex* 18(3):516-533.
- Lui LL, Bourne JA, Rosa MG. 2006. Functional response properties of neurons in the dorsomedial visual area of New World monkeys (*Callithrix jacchus*). *Cereb Cortex* 16(2):162-177.
- Lyon DC, Connolly JD. 2012. The case for primate V3. *Proc Biol Sci* 279(1729):625-633.
- Lyon DC, Kaas JH. 2001. Connectional and architectonic evidence for dorsal and ventral V3, and dorsomedial area in marmoset monkeys. *J Neurosci* 21(1):249-261.

- Lyon DC, Kaas JH. 2002a. Connectional evidence for dorsal and ventral V3, and other extrastriate areas in the prosimian primate, *Galago garnettii*. *Brain Behav Evol* 59(3):114-129.
- Lyon DC, Kaas JH. 2002b. Evidence for a modified V3 with dorsal and ventral halves in macaque monkeys. *Neuron* 33(3):453-461.
- Lyon DC, Kaas JH. 2002c. Evidence from V1 connections for both dorsal and ventral subdivisions of V3 in three species of New World monkeys. *J Comp Neurol* 449(3):281-297.
- Lyon DC, Xu X, Casagrande VA, Stefansic JD, Shima D, Kaas JH. 2002. Optical imaging reveals retinotopic organization of dorsal V3 in New World owl monkeys. *Proc Natl Acad Sci U S A* 99(24):15735-15742.
- Maunsell JH, van Essen DC. 1983. The connections of the middle temporal visual area (MT) and their relationship to a cortical hierarchy in the macaque monkey. *The Journal of neuroscience : the official journal of the Society for Neuroscience* 3(12):2563-2586.
- Merigan WH, Pham HA. 1998. V4 lesions in macaques affect both single- and multiple-viewpoint shape discriminations. *Visual neuroscience* 15(2):359-367.
- Motter BC. 2009. Central V4 receptive fields are scaled by the V1 cortical magnification and correspond to a constant-sized sampling of the V1 surface. *J Neurosci* 29(18):5749-5757.
- Newsome WT, Maunsell JH, Van Essen DC. 1986. Ventral posterior visual area of the macaque: visual topography and areal boundaries. *J Comp Neurol* 252(2):139-153.
- Nishida S, Sasaki Y, Murakami I, Watanabe T, Tootell RB. 2003. Neuroimaging of direction-selective mechanisms for second-order motion. *J Neurophysiol* 90(5):3242-3254.
- Offenhauser N, Thomsen K, Caesar K, Lauritzen M. 2005. Activity-induced tissue oxygenation changes in rat cerebellar cortex: interplay of postsynaptic activation and blood flow. *The Journal of physiology* 565(Pt 1):279-294.

- Okazawa G, Goda N, Komatsu H. 2012. Selective responses to specular surfaces in the macaque visual cortex revealed by fMRI. *Neuroimage*.
- Pasupathy A, Connor CE. 1999. Responses to contour features in macaque area V4. *J Neurophysiol* 82(5):2490-2502.
- Pasupathy A, Connor CE. 2001. Shape representation in area V4: position-specific tuning for boundary conformation. *J Neurophysiol* 86(5):2505-2519.
- Pasupathy A, Connor CE. 2002. Population coding of shape in area V4. *Nat Neurosci* 5(12):1332-1338.
- Poggio GF, Gonzalez F, Krause F. 1988. Stereoscopic mechanisms in monkey visual cortex: binocular correlation and disparity selectivity. *J Neurosci* 8(12):4531-4550.
- Ponce CR, Lomber SG, Born RT. 2008. Integrating motion and depth via parallel pathways. *Nat Neurosci* 11(2):216-223.
- Press WA, Brewer AA, Dougherty RF, Wade AR, Wandell BA. 2001. Visual areas and spatial summation in human visual cortex. *Vision Res* 41(10-11):1321-1332.
- Reppas JB, Niyogi S, Dale AM, Sereno MI, Tootell RB. 1997. Representation of motion boundaries in retinotopic human visual cortical areas. *Nature* 388(6638):175-179.
- Roe AW, Chelazzi L, Connor CE, Conway BR, Fujita I, Gallant JL, Lu H, Vanduffel W. 2012. Toward a unified theory of visual area V4. *Neuron* 74(1):12-29.
- Roe AW, Chen LM. 2008. High-resolution fMRI maps of cortical activation in nonhuman primates: correlation with intrinsic signal optical images. *Ilar J* 49(1):116-123.
- Roe AW, Ts'o DY. 1995. Visual topography in primate V2: multiple representation across functional stripes. *J Neurosci* 15(5 Pt 2):3689-3715.
- Rosa MG, Casagrande VA, Preuss T, Kaas JH. 1997. Visual field representation in striate and prestriate cortices of a prosimian primate (*Galago garnettii*). *J Neurophysiol* 77(6):3193-3217.

- Rosa MG, Manger PR. 2005. Clarifying homologies in the mammalian cerebral cortex: the case of the third visual area (V3). *Clin Exp Pharmacol Physiol* 32(5-6):327-339.
- Rosa MG, Palmer SM, Gamberini M, Tweedale R, Pinon MC, Bourne JA. 2005. Resolving the organization of the New World monkey third visual complex: the dorsal extrastriate cortex of the marmoset (*Callithrix jacchus*). *J Comp Neurol* 483(2):164-191.
- Rosa MG, Pinon MC, Gattass R, Sousa AP. 2000. "Third tier" ventral extrastriate cortex in the New World monkey, *Cebus apella*. *Exp Brain Res* 132(3):287-305.
- Rosa MG, Schmid LM. 1995. Visual areas in the dorsal and medial extrastriate cortices of the marmoset. *J Comp Neurol* 359(2):272-299.
- Rosa MG, Tweedale R. 2000. Visual areas in lateral and ventral extrastriate cortices of the marmoset monkey. *J Comp Neurol* 422(4):621-651.
- Rosa MG, Tweedale R. 2001. The dorsomedial visual areas in New World and Old World monkeys: homology and function. *Eur J Neurosci* 13(3):421-427.
- Schiller PH. 1993. The effects of V4 and middle temporal (MT) area lesions on visual performance in the rhesus monkey. *Visual neuroscience* 10(4):717-746.
- Schummers J, Yu H, Sur M. 2008. Tuned responses of astrocytes and their influence on hemodynamic signals in the visual cortex. *Science* 320(5883):1638-1643.
- Sereno MI, Dale AM, Reppas JB, Kwong KK, Belliveau JW, Brady TJ, Rosen BR, Tootell RB. 1995. Borders of multiple visual areas in humans revealed by functional magnetic resonance imaging. *Science* 268(5212):889-893.
- Smith AT, Greenlee MW, Singh KD, Kraemer FM, Hennig J. 1998. The processing of first- and second-order motion in human visual cortex assessed by functional magnetic resonance imaging (fMRI). *J Neurosci* 18(10):3816-3830.
- Stepniewska I, Collins CE, Kaas JH. 2005. Reappraisal of DL/V4 boundaries based on connectivity patterns of dorsolateral visual cortex in macaques. *Cereb Cortex* 15(6):809-822.

- Tanigawa H, Lu HD, Roe AW. 2010. Functional organization for color and orientation in macaque V4. *Nat Neurosci* 13(12):1542-1548.
- Thompson JK, Peterson MR, Freeman RD. 2003. Single-neuron activity and tissue oxygenation in the cerebral cortex. *Science* 299(5609):1070-1072.
- Tootell RB, Hadjikhani N. 2001. Where is 'dorsal V4' in human visual cortex? Retinotopic, topographic and functional evidence. *Cerebral cortex* 11(4):298-311.
- Tootell RB, Mendola JD, Hadjikhani NK, Ledden PJ, Liu AK, Reppas JB, Sereno MI, Dale AM. 1997. Functional analysis of V3A and related areas in human visual cortex. *J Neurosci* 17(18):7060-7078.
- Tootell RB, Nelissen K, Vanduffel W, Orban GA. 2004. Search for color 'center(s)' in macaque visual cortex. *Cerebral cortex* 14(4):353-363.
- Tsytsarev V, Pope D, Pumbo E, Garver W. 2010. Intrinsic optical imaging of directional selectivity in rat barrel cortex: application of a multidirectional magnetic whisker stimulator. *Journal of neuroscience methods* 189(1):80-83.
- Ungerleider LG, Galkin TW, Desimone R, Gattass R. 2008. Cortical connections of area V4 in the macaque. *Cereb Cortex* 18(3):477-499.
- Wade AR, Brewer AA, Rieger JW, Wandell BA. 2002. Functional measurements of human ventral occipital cortex: retinotopy and colour. *Philos Trans R Soc Lond B Biol Sci* 357(1424):963-973.
- Walsh V, Butler SR, Carden D, Kulikowski JJ. 1992. The effects of V4 lesions on the visual abilities of macaques: shape discrimination. *Behav Brain Res* 50(1-2):115-126.
- Walsh V, Carden D, Butler SR, Kulikowski JJ. 1993. The effects of V4 lesions on the visual abilities of macaques: hue discrimination and colour constancy. *Behav Brain Res* 53(1-2):51-62.
- Wandell BA, Brewer AA, Dougherty RF. 2005. Visual field map clusters in human cortex. *Philosophical transactions of the Royal Society of London Series B, Biological sciences* 360(1456):693-707.

- Wong-Riley M. 1979. Changes in the visual system of monocularly sutured or enucleated cats demonstrable with cytochrome oxidase histochemistry. *Brain Res* 171(1):11-28.
- Xiao Y, Zych A, Felleman DJ. 1999. Segregation and convergence of functionally defined V2 thin stripe and interstripe compartment projections to area V4 of macaques. *Cerebral cortex* 9(8):792-804.
- Xu X, Bosking W, Sary G, Stefansic J, Shima D, Casagrande V. 2004a. Functional organization of visual cortex in the owl monkey. *J Neurosci* 24(28):6237-6247.
- Xu X, Collins CE, Kaskan PM, Khaytin I, Kaas JH, Casagrande VA. 2004b. Optical imaging of visually evoked responses in prosimian primates reveals conserved features of the middle temporal visual area. *Proc Natl Acad Sci U S A* 101(8):2566-2571.
- Youakim M, Bender DB, Baizer JS. 2001. Vertical meridian representation on the prelunate gyrus in area V4 of macaque. *Brain Res* 56(2):93-100.
- Zeki S. 1983. The distribution of wavelength and orientation selective cells in different areas of monkey visual cortex. *Proc R Soc Lond B Biol Sci* 217(1209):449-470.
- Zeki S. 2003. Improbable areas in the visual brain. *Trends Neurosci* 26(1):23-26.
- Zeki S, Shipp S. 1989. Modular Connections between Areas V2 and V4 of Macaque Monkey Visual Cortex. *The European journal of neuroscience* 1(5):494-506.
- Zeki SM. 1969. Representation of central visual fields in prestriate cortex of monkey. *Brain Res* 14(2):271-291.
- Zeki SM. 1971. Cortical projections from two prestriate areas in the monkey. *Brain Res* 34(1):19-35.
- Zeki SM. 1973. Colour coding in rhesus monkey prestriate cortex. *Brain research* 53(2):422-427.
- Zeki SM. 1978. Uniformity and diversity of structure and function in rhesus monkey prestriate visual cortex. *J Physiol* 277:273-290.

CHAPTER II

INTRINSIC SIGNAL OPTICAL IMAGING EVIDENCE FOR DORSAL V3 IN THE PROSIMIAN GALAGO (*OTOLEMUR GARNETTI*)

Abstract

Currently, we lack consensus regarding the organization along the anterior border of dorsomedial V2 in primates. Previous studies suggest that this region could either be DM (dorsomedial area), characterized by both an upper and a lower visual field representation, or the dorsal aspect of area V3, which only contains a lower visual field representation. We examined these proposals using optical imaging of intrinsic signals to investigate this region in the prosimian galago (*Otolemur garnetti*). Galagos represent the prosimian radiation of surviving primates; cortical areas that bear strong resemblances across members of primates provide a strong argument for their early origin and conserved existence. Based on our mapping of horizontal and vertical meridian representations, visuotopy, and orientation preference, we find a clear lower field representation anterior to dorsal V2 but no evidence of any upper field representation. We also show statistical differences in orientation preference patches between V2 and V3. We additionally supplement our imaging results with electrode array data that reveal differences in the average spatial frequency preference, average temporal frequency preference, and sizes of the receptive fields between V1, V2, and V3. The lack of upper visual field representation along with the differences between the neighboring visual areas clearly distinguish the region anterior to dorsal V2 from earlier visual areas and

argue against a DM that lies along the dorsomedial border of V2. We submit that the region of cortex in question is the dorsal aspect of V3 thus strengthening the possibility that V3 is conserved among primates.

Introduction

While general agreement that at least visual areas V1, V2, and MT (Fig. 1A) exist in all primates (Felleman and Van Essen, 1991; Krubitzer and Kaas, 1990; Lyon and Kaas, 2001), it seems surprising that area V3 is not on this list. Early evidence from connection patterns (Cragg, 1969; Zeki, 1969) and microelectrode mapping (Gattass et al., 1988) argued for the existence of a V3, in at least macaque monkeys, while other early results seemed to challenge this view as microelectrode recordings (Allman and Kaas, 1975; Krubitzer and Kaas, 1993) and connection patterns (Krubitzer and Kaas, 1989) indicated that there were representations of the upper visual field in cortex adjacent to or near the representation of the lower visual field in dorsomedial V2. Allman and Kaas (1975) proposed that a dorsomedial visual area (DM), representing both the upper and lower visual quadrants, formed part of the rostral border of dorsomedial V2 (Fig. 1B). Various forms of a proposal where DM borders dorsal V2 have persisted in the literature (e.g., Allman et al., 1979; Beck and Kaas, 1998a; b; Krubitzer and Kaas, 1993; Rosa et al., 1997; Rosa et al., 2009; Rosa et al., 2005; Rosa et al., 2000; Rosa and Schmid, 1995; Rosa and Tweedale, 2000; 2005). More recently, Lyon and Kaas provided further descriptions of the connection patterns of V1 with extrastriate cortex in prosimian galagos (Lyon and Kaas, 2002a), four species of New World monkeys (Lyon and Kaas, 2001; 2002c), and in Old World macaques (Lyon and Kaas, 2002b) that supported the

conclusion that a narrow dorsal V3, representing the lower visual quadrant, does exist between dorsal V2 and a more rostral DM (Fig. 1C). These results are strengthened by optical imaging evidence for dorsal V3 in New World owl monkeys (Lyon et al., 2002), fMRI evidence in macaques (Brewer et al., 2002; Schmid et al., 2009; Tehovnik et al., 2006; Tolias et al., 2005), and fMRI evidence in humans (DeYoe et al., 1996; Engel et al., 1997; Nishida et al., 2003; Reppas et al., 1997; Smith et al., 1998; Tootell et al., 1997; Wade et al., 2002).

In the present report, we provide additional evidence that a dorsal V3 lies along the rostral border of dorsal V2 in prosimian galagos. Our additional evidence is of two types. Primarily we used optical imaging of intrinsic signal to measure visually evoked cortical activity of dorsal V1, dorsal V2, and rostrally adjoining visual cortex (Fig. 1A). The evoked pattern of activity allowed us to identify V1 and V2, and demonstrate activity along the rostral border of dorsal V2 that was evoked by stimulating the lower visual quadrant. Additionally, we recorded from neurons across the width of dorsal V1 into V2 and presumptive V3 with a 100 electrode array. The recordings demonstrate that neurons in cortex just rostral to V2 had larger receptive fields than neurons in V1 and V2, and that these receptive fields were in the lower visual quadrant as expected for V3. Our experiments were within prosimian galagos as these primates have few cortical fissures, and thus the dorsal V1-V2-V3-DM region was accessible on the dorsal surface of the brain for optical imaging and the placement of the 100 electrode array. In addition, galagos represent the prosimian radiation, one of the major surviving branches of primate evolution, and features of cortical organization that exist across members of the early

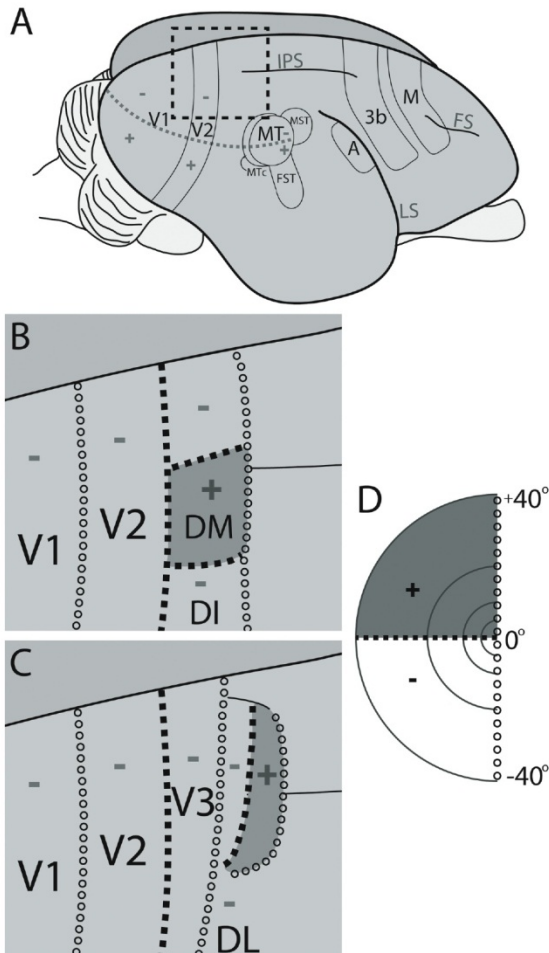


Figure 2- 1. **V3 vs. DM.**

Two possible organizations of visual areas in galagos are depicted. (A) Galago brain and depiction of some cortical areas. (B) DM proposal: region anterior to V2 contains a full visual field representation that includes both lower and upper visual field. (C) V3 proposal: region anterior to V2 is V3 and represents only ventral visual field. DL: dorsolateral area, DI: dorsointermediate area, MT: middle temporal area. MST: middle superior temporal area, FST: fundus of superior temporal sulcus, MTc: MT crescent, A: auditory cortex, M: motor cortex, FS: frontal sulcus, LS: lateral sulcus, IPS: intraparietal sulcus. Upper visual field (+), lower visual field (-), solid lines: vertical meridian, dotted lines: horizontal meridian. Scale Bar = 2mm.

branches of primate evolution are those most likely to have been present in the early ancestors of primates (Kaas, 2004).

Materials and Methods

Optical imaging of intrinsic signals (OIS) was used to examine the functional organization of dorsal V1, V2, and V3 in 5 adult galagos (*Otolemur garnetti*). Electrophysiological data were collected in 3 additional galagos. These procedures are similar to those used previously in optical imaging and electrode recording studies of visual cortex in galagos and owl monkeys (DeBruyn et al., 1993; Kaskan et al., 2009; Lyon et al., 2002; Xu et al., 2004; Xu et al., 2005) and signal unit recording (Jermakowicz et al., 2009). All procedures were approved by the Vanderbilt University Institute for Animal Care and Use Committee and were done in accordance with the National Institute of Health guidelines.

Animal Preparation/Surgery

Surgeries were performed under aseptic conditions. All galagos were initially anesthetized with ketamine hydrochloride (8-10mg/kg) and then maintained with isoflurane (1.5-2% in O₂) through an endotracheal tube during surgical procedures. Pupils were dilated using 1% atropine eyedrops. Clear contact lenses (covered with 3mm artificial pupils) were used to place the retina conjugate plane 28.5 cm away for imaging studies and 57 cm away for electrode recording studies. The optic disc and *area centralis* were plotted using a reversible ophthalmoscope or by back reflection of the retinal blood vessel pattern from the surface of the tapetum (Xu et al., 2005).

Anesthesia was maintained by propofol (2,6-di-isopropylphenol; induction: 3 mg/kg induction; maintenance: 4-10 mg/kg/hr intravenous [i.v.]). During electrode recording studies, NO₂ (NO₂: 75%, O₂: 23.5%, and CO₂: 1.5%) was also used to maintain a stable anesthetic plane. Isoflurane was kept on standby to supplement if necessary. Paralysis was induced and maintained with vecuronium bromide mixed in 5% dextrose lactated Ringer's solution (0.15-0.6 mg/kg/hr intravenous [i.v.]). The anesthetic plane of the animal was monitored by electroencephalogram during imaging experiments. Heart rate, CO₂ tidal volume, and body temperature were continuously monitored throughout all experimental procedures. We regularly verified the location of the optic disc and *area centralis* throughout each experiment. An incision was placed along the midline of the scalp and a craniotomy performed to reveal dorsal V1, V2, and proposed V3. The brain was stabilized using 3-4% agar with a glass cover slip for imaging studies and 1% agar for electrode array studies. We used the intraparietal sulcus as a landmark to help us locate the most likely region where V3 (or DM) would exist along the V2 border to position our imaging window. In cases where the 100 electrode array was inserted, a large craniotomy was performed over the visual cortex centered on the representation of the *area centralis* around V2 (Xu et al., 2005).

Optical Imaging

Images were collected by an Imager 3001 with VDAQ/NT data acquisition software (Optical Imaging, Germantown, NY). We collected intrinsic signal optical imaging data under 632 nm illumination. Images were acquired at 4 Hz for 4-8 sec per stimulus condition (giving 16-24 frames per condition). Twenty to fifty trials were collected for each stimulus set (one block). The camera acquisition parameters were set to an image

matrix of 512x512 with an 8x8 mm² field-of-view, which yielded a 15.625 μm² in-plane resolution.

Visual Stimuli for Optical Imaging. High contrast square-wave gratings were created using custom software written in Matlab (Mathworks, Natick, MA) directing a VSG stimulus system (Cambridge Research Systems, Rochester, U.K.). The gratings were presented in one of four orientations (0°, 45°, 90°, and 135°) on a 40 cm x 30 cm (displayable Width by Height) monitor in a randomly interleaved fashion. Gratings (spatial frequency 0.1-0.5 c/deg., drift velocity 2 Hz, duty cycle 20%) were drifted along the axis perpendicular to the grating orientation (in both directions). For topographic mapping, stimuli were presented to the contralateral eye with a simple cover for the ipsilateral eye or by using electromechanical shutters synchronized to the timing of stimulus presentation and image acquisition.

Coarse maps of visuotopy were made with restricted versions of the orientation gratings (either rectangular or square windows) that were presented in various locations in the visual field. The location of the center of the contralateral *area centralis* guided our placement of the stimuli. Heights for the rectangular windows ranged between 4-26 deg. (see Figs. 4-9) with the widths spanning the screen. We typically started with the larger stimuli (20°) and then progressively used more restricted heights. The goal of presenting stimuli within rectangular windows was to help us isolate the horizontal meridian in order to better distinguish the upper and lower visual field transition. The contralateral *area centralis* was replotted prior to each imaging run to check stability of eye position. To better examine the progression of the horizontal meridian (representing the anterior V2 border and possible border dividing upper and lower visual quadrants of DM) and

vertical meridian (representing the V1/V2 border and the anterior border of V3 or DM), we dedicated a case to presenting $10^\circ \times 10^\circ$ square windowed stimuli (either 0° or 90° gratings, spatial frequency = 0.1 c/deg., drift velocity = 2 Hz, duty cycle = 20%) moved in 5° steps along each meridian.

Electrode Recordings

A 4 mm x 4 mm 100-electrode Cyberkinetics (Salt Lake City, UT) array was inserted pneumatically to a depth of about 600 μm at a location corresponding to the representation of the *area centralis* in V2 (Xu et al., 2005) and covering portions of V1, V2 and proposed V3. The array was then covered with 1% agar to prevent dehydration. Receptive field location and orientation preference for each cell were determined initially using a manually controlled bar of light projected simultaneously on a tangent screen and plotting table (see DeBruyn et al., 1993).

Receptive Field Plotting and Visual Stimulation for Electrode Recordings. A 21-inch Sony Trinitron monitor with refresh rate set to 120 Hz was used to present drifting sine wave gratings. These were first presented prior to receptive field mapping to estimate locations and preferred orientations of all neurons. Eighteen two-second trials of sine wave gratings varying in orientation (0 - 170° in 10° increments, 18 total) and with parameters preferred by galago visual cortex neurons, temporal frequency (TF): 2.0 Hz, spatial frequency (SF): 0.5 c/deg., Contrast: 0.6; (DeBruyn et al., 1993), and a grey-screen blank were presented on an 18° aperture. The drifting sine wave gratings were also used to study the neurons' spatial and temporal frequency tuning properties. To measure SF tuning, 30 two-second trials of drifting gratings (TF: 2.0 Hz, Contrast: 0.60) varying in SF (0.2 - 2.0 c/deg. in 0.2 c/deg. increments, 10 total) and orientation (0 - 150° in 30°

increments, 6 total) were presented with a blank. To measure TF tuning, 30 two-second trials of drifting gratings (SF: 0.5 c/deg., Contrast: 0.60) varying in TF (0.5–5.0 Hz in 10 Hz increments, 10 total) and orientation (0-150° in 30° increments, 6 total) were presented with a blank.

Receptive fields were plotted for all neurons that, within the 18 two-second trials of drifting orientations (see above), had clear orientation tuning with response at the preferred orientation at least twice that compared to the orthogonal orientation. Then by varying the orientation and length of a manually controlled bar of light projected simultaneously on the tangent screen and plotting table we plotted each receptive field (see DeBruyn et al., 1993). These plots, which showed each receptive field relative to the *areae centralii* of each eye, were then used to determine the location and size of the receptive fields.

Data Analysis of Optical Images

Activation maps. Both *single-condition maps* and *difference maps* were calculated (see Lu and Roe, 2007). Single condition maps were either blank (isoluminant gray screen) subtracted maps or first-frame (1-2 frames prior to stimulus onset) subtraction maps (frames 5-16/24 summed for better signal-to-noise). In subtraction maps, light and dark values represent preference for one condition or the other and mid-gray values indicate equal, or no, preference for either condition. Orientation preference maps are difference maps constructed by subtracting orthogonal conditions of orientation gratings. Maps were clipped (1-2 standard deviation(s) from the mean of the pixel distribution) and normalized to an 8-bit range. Large blood vessels were often masked to remove large signal artifact from contributing to the final clipping. In some cases, maps were low pass

filtered with a Gaussian or median filter (5-8 pixels squared in size) and/or high pass filtered with a median filter (150-200 pixels squared in size).

T-maps. Significance of pixel activation was calculated by comparing images (either single condition vs. blank or two orthogonal orientation grating conditions). T-maps were calculated by conducting t-tests on a pixel-by-pixel basis using Matlab. T-maps were visualized by creating binary maps where pixels with p-values reaching a threshold value (typically either $p < 0.01$ or $p < 0.05$) were assigned a value of one (white) and those failing to reach criterion were assigned a value of zero (black). Activation areas consisting of only a few pixels were eliminated. Significant pixels along blood vessels or along the edge of the imaging window, which are typically considered artifact due to ambiguity, were also eliminated.

Analysis of Orientation Patch Sizes. To measure patch sizes, we used t-maps generated from orientation preference maps (either 45° - 135° or 90° - 180°). We should point out that this measurement is distinctly different from measuring the typical iso-orientation domain (e.g., Xu et al., 2004). Patch sizes were measured because we noticed that throughout our orientation preference maps there were consistent qualitative differences in patch sizes between neighboring visual areas and we wanted to see if this difference between the neighboring visual areas was quantifiable. We chose t-maps with equal p-values thresholds for all comparisons between visual areas (both across experiments and within a single experiment). To determine a patch size, we imported the t-map image into Adobe Photoshop and used the wand tool to select individual patches for a pixel count. We then took the provided number and multiplied it by area of a single pixel to determine its total area. Some selections appeared to be multiple patches that

were connected by one or two pixels. In those cases we eliminated the connection and counted them as separate patches. Orientation patch sizes from neighboring visual areas (V1 against V2 and V2 against V3) were compared using an unpaired two-tailed t-test.

Histological Procedures

After data collection, galagos were deeply anesthetized and then given an overdose of sodium pentobarbital, and perfused transcardially with salinated 0.1 M phosphate buffer followed by 2% paraformaldehyde in 0.1 M phosphate buffer and, in some cases this was followed by 2% paraphormaldehyde with 10% sucrose in 0.1 M phosphate buffer. The brain was removed and the cortex was separated from underlying brain structures and flattened as described in Krubitzer and Kaas (1990). The cortex was cut on a freezing microtome tangent to the pial surface. The cortex was cut either at a consistent thickness of 52 μm for electrophysiological cases or was cut at a thickness of 80 μm to preserve surface vasculature for the most superficial sections, and then cut at a thickness of 40 μm for the remainder of the cortical thickness for imaging cases. Sections were then processed for cytochrome oxidase (CO) (Wong-Riley, 1979). CO stains allowed us to visualize the V1/V2 border since CO blobs terminate at the anterior border of V1. Optical images were aligned to superficial CO sections using the surface blood vessel patterns. This alignment was facilitated with images from 568 nm illumination that highlighted surface vessel patterns collected for every *in vivo* imaging field-of-view used. Subsequent, deeper, CO sections were aligned with surface sections using the radial blood vessels (vasculature running perpendicular to the plane of the brain sections). Electrode locations were reconstructed from holes aligned across through the serial 52

µm sections to determine their locations relative to the borders of V1, V2, and proposed V3.

Results

Overview

We examined the representation of the visual field of dorsal V1, V2, and presumptive V3 in galagos. Using rectangular and square visual stimuli, we present findings of cortical response, as measured by OIS, to (1) large upper and lower visual field stimuli, (2) restricted band stimuli, and (3) restricted square stimuli along the HM and VM. We also present electrophysiological array recordings from V1, V2, and 2 mm into our presumptive V3. In order to minimize possible contribution from eye drift, we repeatedly remapped the location of the area centralis. In both OIS and electrophysiological recordings, we found no evidence of an upper visual field representation along the dorsomedial border of V2. We describe qualitative and quantitative differences in the orientation maps between V1, V2, and V3. Estimation from imaging data of the V2/V3 border anterior to the V1/V2 border and the anterior V3 border suggests lengths ranging between 2-2.5 mm and 1-2.5 mm respectively, consistent with the anterior-posterior extents of V2 (max ~3mm) and V3 (max ~2.5mm) previously reported in galagos (Collins et al., 2001; Lyon and Kaas, 2002a).

Alignment of cytochrome oxidase stained sections and optical images

Each experiment began with orientation mapping. As shown in Fig. 2 (case 08-61), the surface vasculature revealed by CO (Fig. 2A, dashed black lines) aligned with the

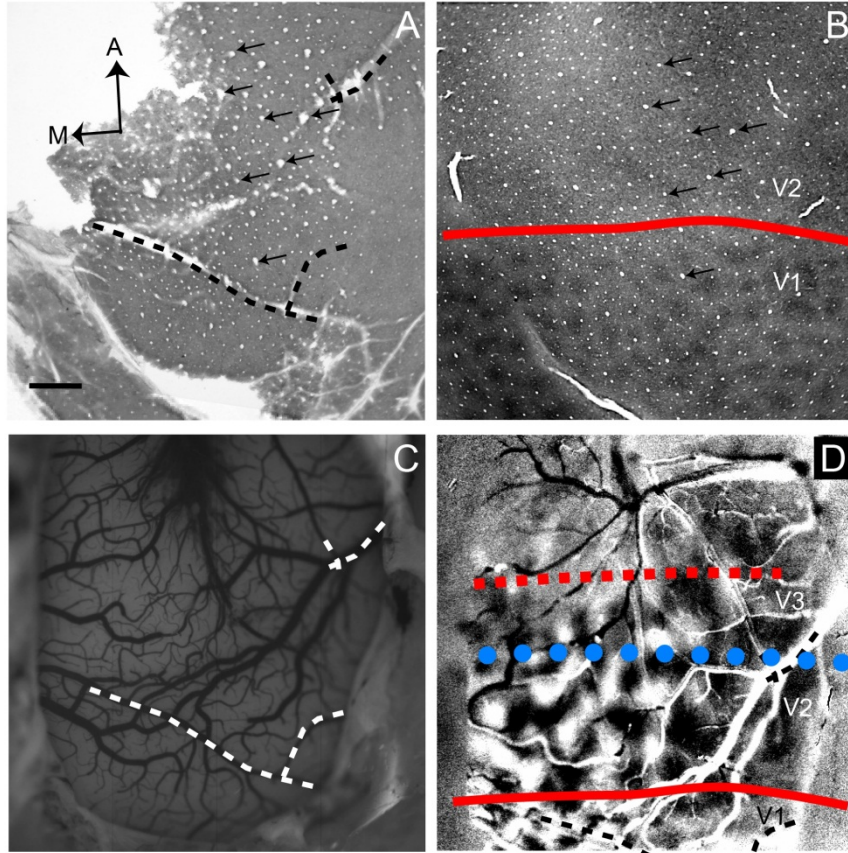


Figure 2- 2. **Alignment of histological tissue and optical images (Case 08-61).** We used CO stained sections to identify the location of the V1/V2 border. (A) A flattened superficial CO section revealing vasculature both perpendicular (holes) and parallel to the flattened surface. (B) A deeper flattened section reveals the characteristic CO blobs of V1, which terminate at the V1/V2 border (solid red line). The two sections (A and B) are aligned with the vessel patterns perpendicular to the imaging plane (arrows). (C) To align CO stains and our optical images, an *in vivo* blood vessel pattern was acquired under green light (see Materials and Methods). The dashed lines delineate sample vessels used to align with surface vasculature in the CO section (dashed black lines in panel A). (D) Optical imaging overlying V1, V2, and V3 (field-of-view is shifted from that in C, see dotted yellow lines). V1/V2 border is then overlain on field-of-view. Dotted blue line: approximate V2/V3 border. Dashed red line: approximate anterior border of V3. Scale bar = 1mm. A: anterior. M: medial.

imaged blood vessel map (Fig. 2C, dashed yellow lines). In Fig. 2B, a deeper CO section reveals the V1/V2 border (solid red line) due to CO blobs in V1 and lack of CO blobs in V2. The CO section in Fig. 2B was then aligned with the superficial CO section in Fig. 2A based on alignment of radial blood vessel patterns (arrows in Fig. 2A and Fig. 2B). The V1/V2 border defined by CO staining is consistent with that revealed in the orientation preference map (0° - 90° in Fig. 2D), as V2 previously has quantitatively been shown to contain larger orientation domains than V1 (Xu et al. 2005) (also see Fig. 13 and Table 1). We illustrate another example in Fig. 3. As in the previous case, the V1/V2 border as shown using CO staining (Fig. 3B, solid red line) is in good agreement with the V1/V2 border revealed by orientation mapping (Fig. 3D). In all subsequent figures, the V1/V2 border was determined as described for Figs. 1 and 2. However, the locations of the presumptive V2/V3 and anterior V3 borders are estimates based on a combination of evidence from imaging experiments.

Lower vs. Upper Visual Field Representation

According to current proposals, DM has both upper and lower visual field representations, where parts of both hemifields share a border with dorsal V2 (see Fig. 1B). In our imaging experiments, oriented drifting gratings presented in the lower visual field strongly activate orientation patch regions in dorsal V1, V2, and regions directly anterior to V2 while the presentation of such gratings in the upper visual field does not (tested in 2 cases).

Figure 4 depicts data from subject 08-61 (same as Fig. 2). In response to lower visual field stimulation (Fig. 4A), orientation difference maps were obtained in V1 and V2 (Fig. 4B, t-map shown in Fig. 4C), revealing the V1/V2 border (solid red line), the anterior V2

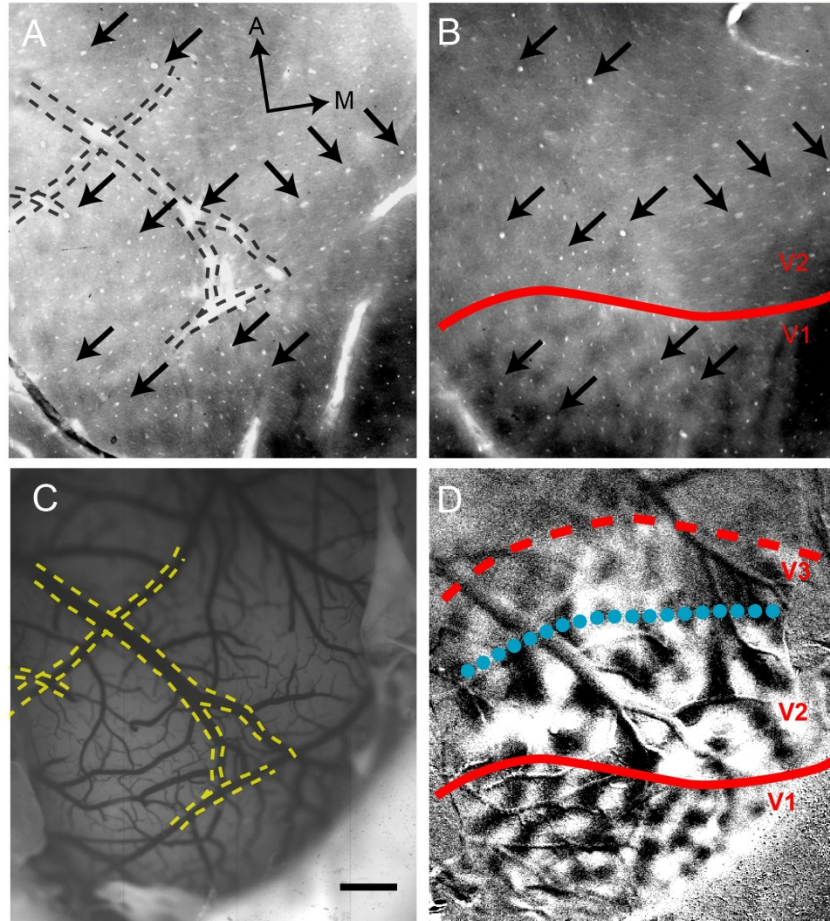


Figure 2- 3. **Alignment of histological tissue and optical images (Case 08-11).** This is another example of aligning a CO defined V1/V2 border to an OIS map. The V1/V2 border defined by the CO blobs overlies region of orientation patch size change. We quantify this difference later (see Figs. 12 and 13). (A) A superficial CO section containing surface vasculature. (B) A deeper section revealing the characteristic CO blobs of V1 which terminate at the V1/V2 border (solid red line). The two sections (A and B) are aligned with vessel patterns (arrows). (C) An *in vivo* blood vessel pattern acquired under green light (see Materials and Methods). Dashed yellow lines delineate sample vessels used to align with surface vasculature shown (dashed black lines in A). (D) Orientation map in V1, V2, and area anterior to V2. Dotted blue line: approximate V2/V3 border. Dashed red line: approximate anterior border of V3. Scale bar = 1mm. A: anterior. M: medial.

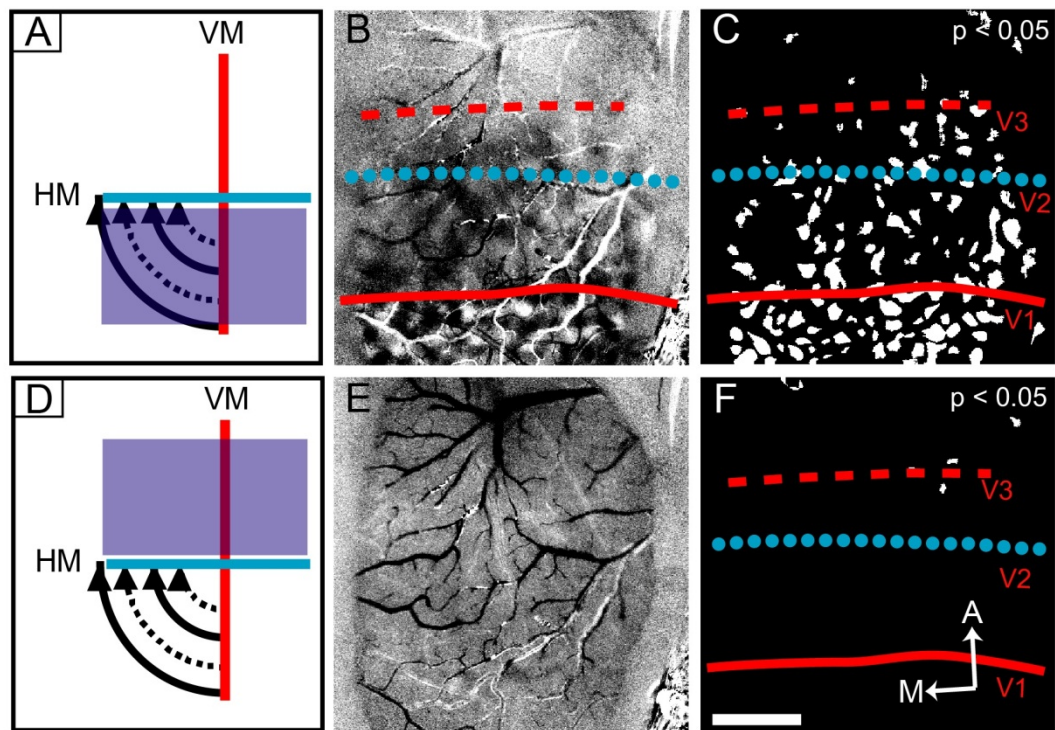


Figure 2- 4. **Lack of upper visual field representation anterior to V2 (Case 08-61).** Here we present two large rectangular stimuli that were 10° apart. In each we presented square wave gratings (see text). The diagrams of stimuli are for illustration purposes only and are not to scale. One stimulus is found in the lower visual field (A) and another in the upper visual field (D). In contrast to lower visual field stimulation, we found no compelling evidence for upper visual field representation along the V2 border. (A) Stimulus location confined to the lower visual field (26° in height). 0° and 90° were presented. (B) The resultant 8-bit gray scale orientation preference map to panel A. (C) We created a t-map (see Materials and Methods) for the orientation preference map shown in B ($p < 0.05$). (D) Stimulus location confined to the upper visual field (24° in height) with the same stimulus parameters as in the lower visual field confined version (A). (E) The resultant 8-bit gray scale orientation preference map to panel D. (F) As we did for the lower visual field confined map, we created a t-map from orientation preference map shown in E ($p < 0.05$). Solid red line: V1/V2 border. Dotted blue line: anterior V2 border. Dashed red line: approximate anterior border of V3. These borders are estimated based on retinotopic mapping and orientation preference maps. Scale bar = 2mm. A: anterior. M: medial.

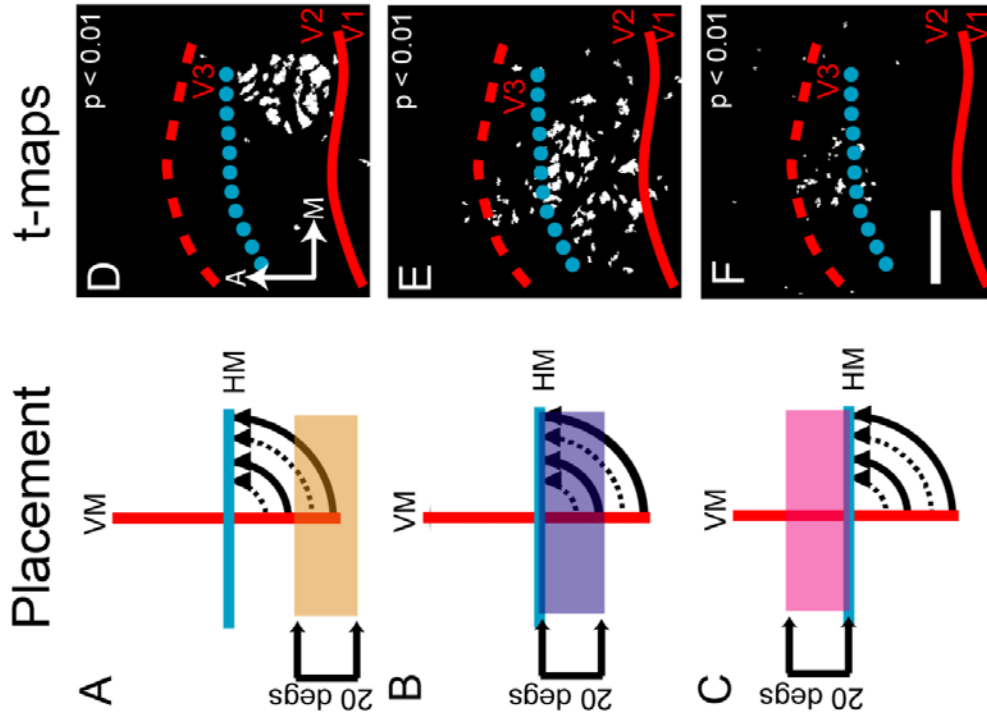
border (dotted blue line), and presumptive V3 spanning approximately 2 mm anterior to V2 (anterior border indicated by the dashed red line). In contrast to lower field stimulation, upper field stimulation (Fig. 4D) resulted in no significant activation in V1, V2, or presumptive V3 (Fig. 4E, t-map shown in Fig. 4F). We considered the possibility that the region anterior to V2 was too weakly activated or is less orientation selective than V1 and V2. A weakness in response or orientation preference could lead to the lack of observed activity in both gray scale maps and t-maps. However examination of the t-maps at a less restrictive p-value ($p < 0.1$) revealed no additional activation (result not shown), suggesting the lack of activation anterior to V2 is not a consequence of inappropriate thresholding. The results indicate that V1, V2, and presumptive V3 region were all clearly activated by drifting gratings of different orientations when presented to the lower visual field, but not the upper visual field. The lack of evidence for an upper visual field representation favors the V3 interpretation anterior to dorsal V2.

Mapping with rectangular windows

We also examined retinotopic organization of these visual areas using rectangular windows presenting oriented moving gratings. We will refer to these stimuli as bar stimuli. We conducted these experiments with 20° (2 cases), 8° (3 cases), and 4° (1 case) bar stimuli. For these experiments we determined the location of the contralateral area centralis using a reversible ophthalmoscope and then placed the bar stimuli parallel to the HM (see Materials and Methods).

20 degree bar stimuli mapping. Figure 5 illustrates an experiment (case 08-11) where 20° bar stimuli were used. Three bar stimuli (20° in height and spanning the full width of the monitor, thus crossing the vertical meridian) were placed in different locations 20-40

Figure 2-5. Retinotopic mapping with 20 degree bar stimuli (Case 08-11).
 In general, we expect a medial to lateral movement as the bars move from more peripheral locations to more foveal locations. (A-C) The relative stimulus (displaying 45° or 135° orientation gratings) locations for 20° height bars in the left column and the resulting t-maps ($p < 0.01$) are shown in the right column (D-F). As in Fig. 4, the diagrams of stimulus position are purely for illustration purposes and are not to scale. Note that in (C), the upper visual field stimulus shows very little activation. The pattern anterior to V2 in panel F overlaps with that in panel E, consistent with our interpretation that this is due to HM activation. Solid red line: V1/V2 border, same as Fig. 3. Dotted blue line: approximate anterior V2 border based on HM mapping. Dashed red line: approximate anterior border of V3. Scale bar = 2mm. A: anterior. M: medial.

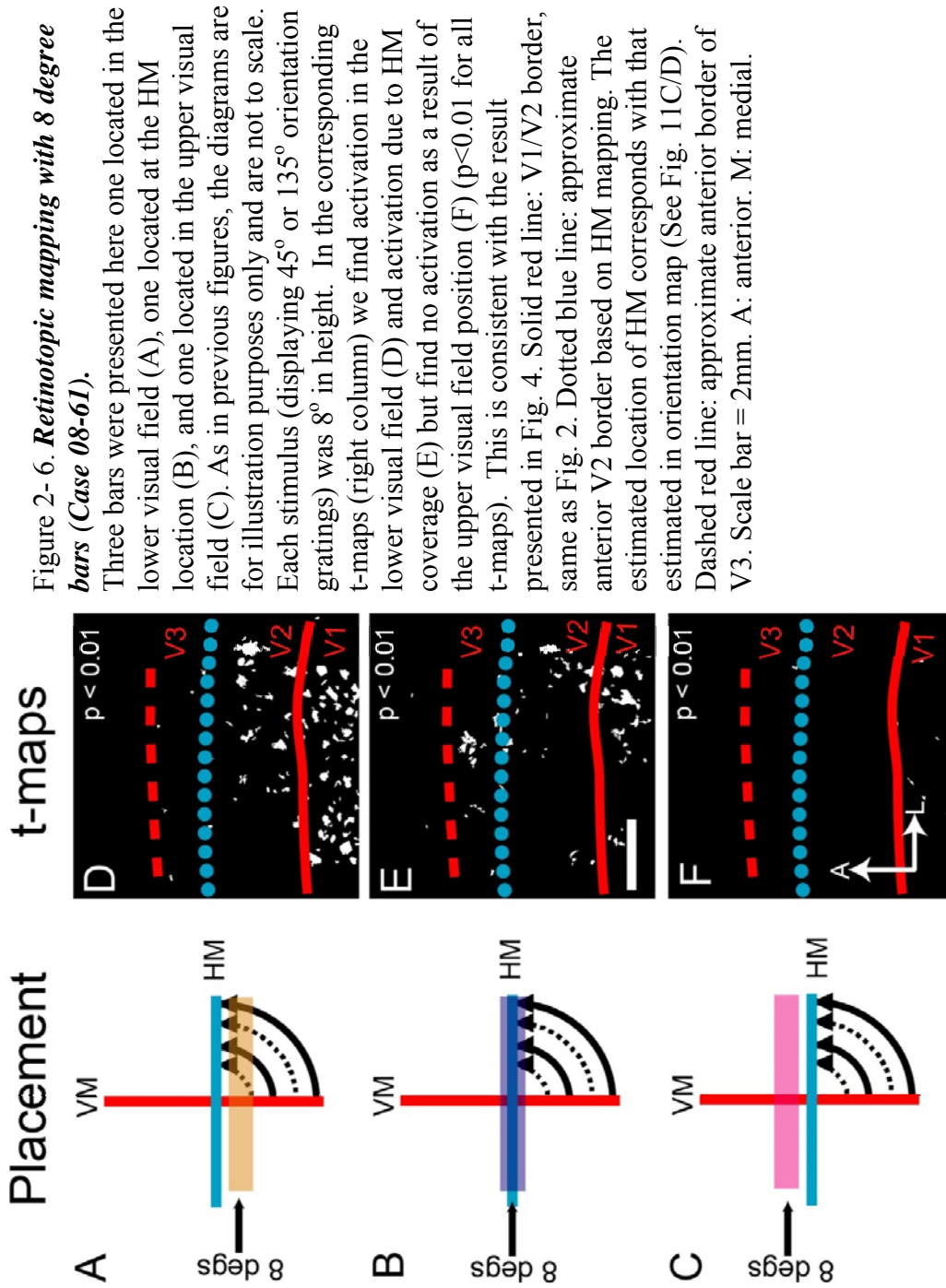


deg. below the HM (Fig. 5A), 0-20 deg. below the HM (Fig. 5B), and 0-20 deg. above the HM (Fig. 5C). In Fig. 5, the V1/V2 border (solid red line) is determined from CO staining, while HM (dotted blue line) and the anterior V3 border (dashed red line) was based on information gained from Figs. 5, 7, and 11A/B.

Within V2, we observed that as the stimulus shifted from Fig. 5A to Fig. 5B, the cortical activation shifted from medial (Fig. 5D) to lateral (Fig. 5E). The middle bar stimulus (Fig. 5B) also revealed activation in V3; this activation spanned both the V1/V2 and the V2/V3 border, consistent with stimulation of a portion of the VM and HM, respectively. The stimulus located in the upper visual field (Fig. 5C) produced little activation in V2 and some activation in V3 (Fig. 5F). The activation observed in V3 is similar between Fig 5E and Fig. 5F. The similarity is likely because the stimuli placement in both 5B and 5C interact with the HM, not due to upper visual field representation.

Although based on this case alone, we cannot exclude the possibility that the activation, anterior to V2 in Fig. 5F, is due to upper field activation. However, we consider this unlikely based on (1) the weakness of activation in Fig 5F compared to the robust activation in Figs. 5D/E (not changed by changing t-map threshold), (2) the likelihood that the similar activation in presumptive V3 is due to common HM stimulation (Fig. 5B/E and Fig. 5C/F), and (3) our results from other cases (Figs. 4, 6, and 9).

8 degree bar stimulus mapping. Results for a second experiment (Case 08-61) support the interpretation presented in Fig. 4 where cortex immediately rostral to V2 shows clear lower, but not upper, visual field activation. Figure 6A-C shows the three 8° height bar



stimuli: one confined to lower visual field (Fig. 6A), one spanning the HM (Fig. 6B), and one confined to upper visual field (Fig. 6C). The restricted lower field stimulations elicited clear activation in V1 and V2 (Fig. 6D). The stimulus spanning the HM elicited more lateral regions of V1 and V2, consistent with representation of central vision. It also produced activation in V3 and along the V2/V3 border (dotted blue line of Fig. 6E). Most importantly, the upper field stimulus (Fig. 6C) produced no activation in V1, V2, or the region anterior to V2 (Fig. 6F). The location of the presumptive V2/V3 border, as determined from HM stimulus mapping, was about 2-2.5 mm anterior to the V1/V2 border. The results for Figs. 4 and 6 show a distinct lack of upper visual field representation, making it unlikely that the activation in Fig. 5F contains an upper visual field component.

4 degree bar stimulus mapping. In a third experiment, we used smaller 4° bar stimuli to try to increase our precision (Fig. 7A-C, case 08-11 same case as Fig 5 but slightly different field-of-view). This is the only case where maps from 4° bar stimuli were obtained. As observed in the t-maps ($p < 0.01$, Fig. 7D and Fig. 7E), significant activation was observed within V2 with the pattern of activation shifting towards the V2/V3 border as the stimulus shifted upward toward the HM (Fig. 7A to 7B to 7C). The stimulus that overlies the HM (Fig. 7C) elicited activation largely at the V2/V3 border (dotted blue line of Fig. 7D-F).

Mapping with square windows

In one case (Case 10-10), we used restricted 10° x 10° windows presenting oriented gratings (0° or 90°) moved in 5° steps along the HM (Fig. 8) and the VM (Fig. 9). Figure 8A1-E1 illustrates visual stimulus positions progressively moved from central to

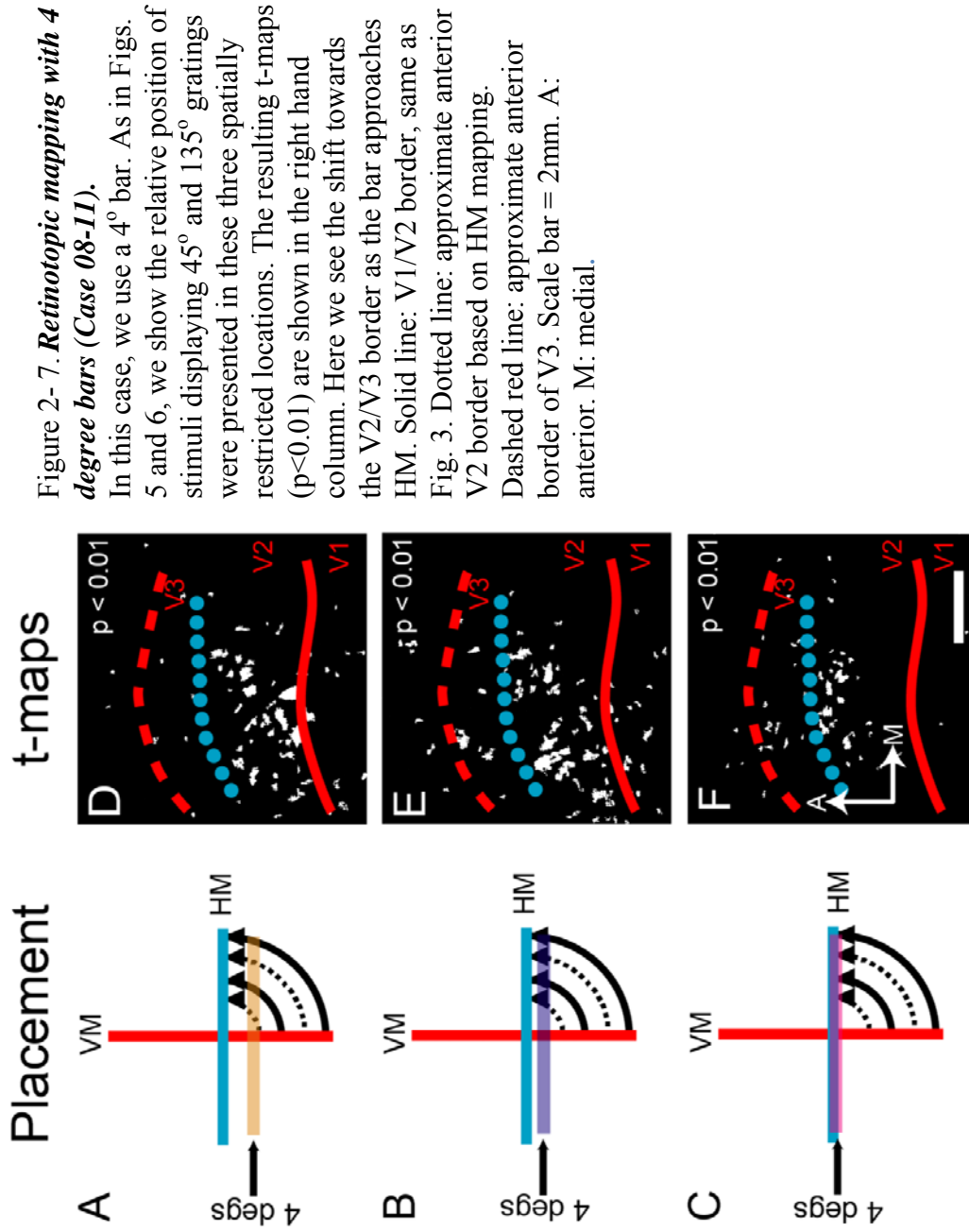


Figure 2- 7. *Retinotopic mapping with 4 degree bars (Case 08-11).*

In this case, we use a 4° bar. As in Figs. 5 and 6, we show the relative position of stimuli displaying 45° and 135° gratings were presented in these three spatially restricted locations. The resulting t-maps ($p < 0.01$) are shown in the right hand column. Here we see the shift towards the V2/V3 border as the bar approaches HM. Solid line: V1/V2 border, same as HM. Dotted line: approximate anterior V2 border based on HM mapping. Dashed red line: approximate anterior border of V3. Scale bar = 2mm. A: anterior. M: medial.

peripheral locations. As shown by the activation maps in gray scale (Fig. 8A2-E2) and in t-map (Fig. 8A3-E3) form, the activation pattern (from the single condition gray scale maps and t-maps) shifts from lateral (Fig. 8A2/3) to medial (Fig. 8E2/3) in V2 (between solid red line and dotted blue line) along the representation of the horizontal meridian (dotted blue line). The blue dotted line was placed based on images in Figs. 8C2/3-E2/3 and extrapolated medially. Note that the largest area of cortical activation in V1, V2, and V3 is seen with centrally located stimuli (Fig. 8A3-B3) and declines with more eccentric stimuli (Fig. 8C3-E3).

We used the same mapping procedure along the VM. Figure 9 provides further evidence (displayed as single conditions maps) that the cortex immediately anterior to V2 is not responsive to upper visual field stimulus but is responsive to the same stimuli in the lower visual field. As the visual stimulus moved from peripheral (lower field, Fig. 9A1) to central locations (Fig. 9F1, stimulus locations shown in Fig. 9A1-K1), the activation (single condition maps shown in Fig. 9A2-K2 and t-maps shown in Fig. 9A3-K3) traveled from medial (Fig. 9A2/A3) to lateral (Fig. 9F2/F3) along cortex, providing an estimate of the location of the VM representation at both the V1/V2 (solid red line) and the anterior V3 (dashed red line) borders. Interestingly, we also see another VM activation anterior to V2 along the lateral margin of our imaged cortex which we think is likely DL (V4). The pattern is easily seen in Fig. 9A3-C3 just lateral to the blue dotted and red dashed lines. At the HM/VM intersection (Fig. 9F1), we see activation laterally in V1, V2, and V3. Note that the central-most stimulus (Fig. 9F1) is very similar to that seen in Fig 8A1. Importantly, no significant activation is observed in response to upper field stimuli (Figs 9G-9K).

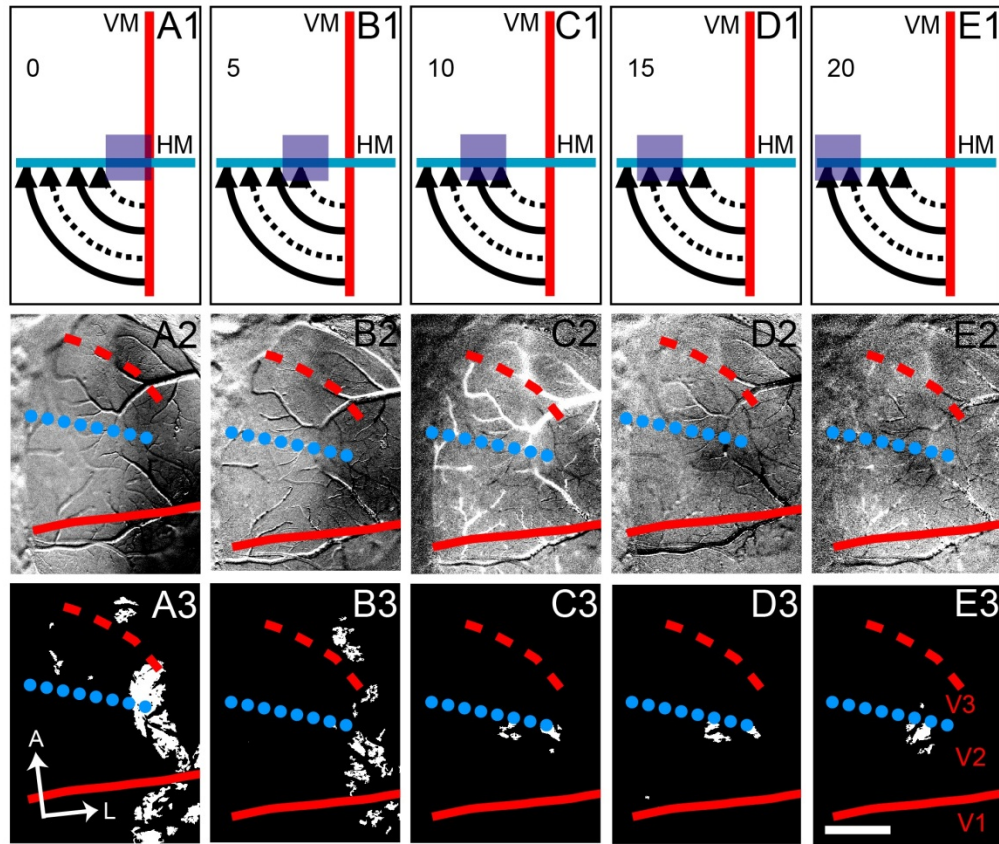


Figure 2- 8. *HM mapping with 10 degree square windows (Case 10-10)*. Here we used 10° square windowed stimuli along the HM. Illustration of the relative positions of the squares are found in the first row (A1-E1). The stimuli start at the area centralis and move in 5° increments into the periphery. Here we used single condition maps (see Materials and Methods) to visualize the cortical representation. The second row (A2-E2), are the familiar 8-bit gray scale images. The third row (A3-E3) shows the corresponding t-maps ($p < 0.01$). See text for additional detail. Solid red line: V1/V2 border. Dotted blue line: V2/V3 border based on this HM mapping. Dashed line: presumptive anterior V3 border, estimated from VM mapping shown in Fig 9. Scale bar = 2mm. A: anterior. L: lateral.

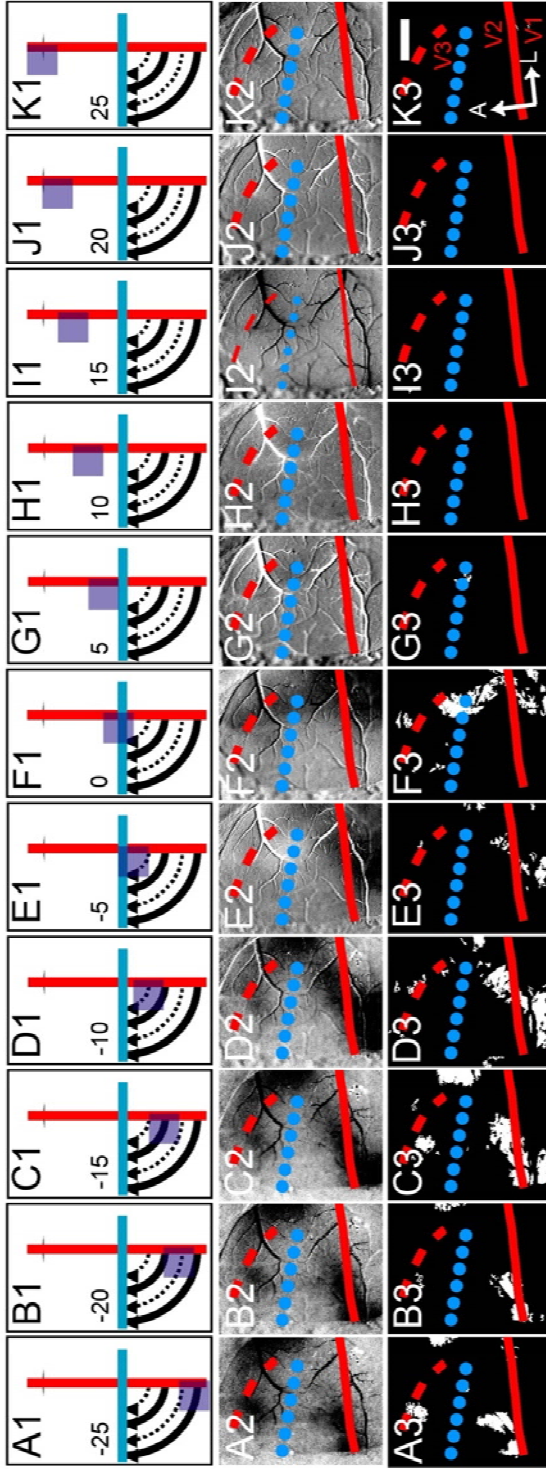


Figure 2-9. *VM mapping with 10 degree square windows (Case 10-10).*

Again we used 10° square stimuli but along the VM. We began in the lower visual field and moved well into the upper visual field. This progression is illustrated in the first row (A1-K1). As in Fig. 8, the squares moved in 5° increments. The corresponding single conditions 8-bit gray scale maps are shown in the second row (A2-K2) and the corresponding t-maps ($p < 0.01$) are presented in the third row (A3-K3). There are strong activation patterns from lower visual field activation (A-E) but not upper field activation (G-K columns). Dashed red line: presumptive anterior V3 border, estimated from this mapping. Dotted blue line: V2/V3 border based on HM mapping from Fig. 8. Scale bar = 2mm. A: anterior. L: lateral.

Electrophysiology

To further investigate the organization of the cortex in the region of presumptive V3, we recorded from three galagos with a 4 mm x 4 mm 100-electrode Cyberkinetics array placed over a location similar to our imaged area. A total of 175 well-isolated single units were recorded from V1, V2, and presumptive V3. Figure 10 summarizes results from case 07-12. V1 neurons were distinguished by their location within the CO blob region (Fig. 10A). V2 neurons were located in a band of cortex corresponding to the known width of V2 just rostral to V1. The receptive fields of V2 neurons were consistently larger than those for V1 neurons, data that are consistent with the larger orientation domains demonstrated with optical imaging within V2 (see Xu et al.2005). As shown in Fig. 10B, the presumptive V3 neurons were distinguished by considerably larger receptive fields than V2 neurons (mean \pm SE; V2: 12.3 ± 2.5 deg.², V3: 138 ± 22 deg.²; $p \leq 0.05$; student t-test). All presumptive V3 neurons were recorded at a distance of 1.5 mm or greater, anterior to the edge of the V1 CO blobs. This classification yielded 69 V1 neurons, 51 V2 neurons and 55 V3 neurons. Additionally, clear differences existed between the average preferred spatial frequency ($p \leq 0.05$, ANOVA; mean \pm SE; V1: 0.607 ± 0.024 c/deg., V2: 0.547 ± 0.03 c/deg., V3: 0.431 ± 0.038 c/deg.; Fig. 10C) and the average preferred temporal frequency ($p \leq 0.05$, ANOVA; mean \pm SE; V1: 1.84 ± 0.10 Hz, V2: 2.32 ± 0.11 Hz, V3: 2.49 ± 0.13 Hz; Fig. 10D) of the neurons divided into these groups, further indicating that neurons with these receptive field properties came from different visual areas. V1 neurons preferred the highest spatial and lowest temporal frequencies while the presumptive V3 neurons preferred the lowest spatial and highest temporal frequencies.

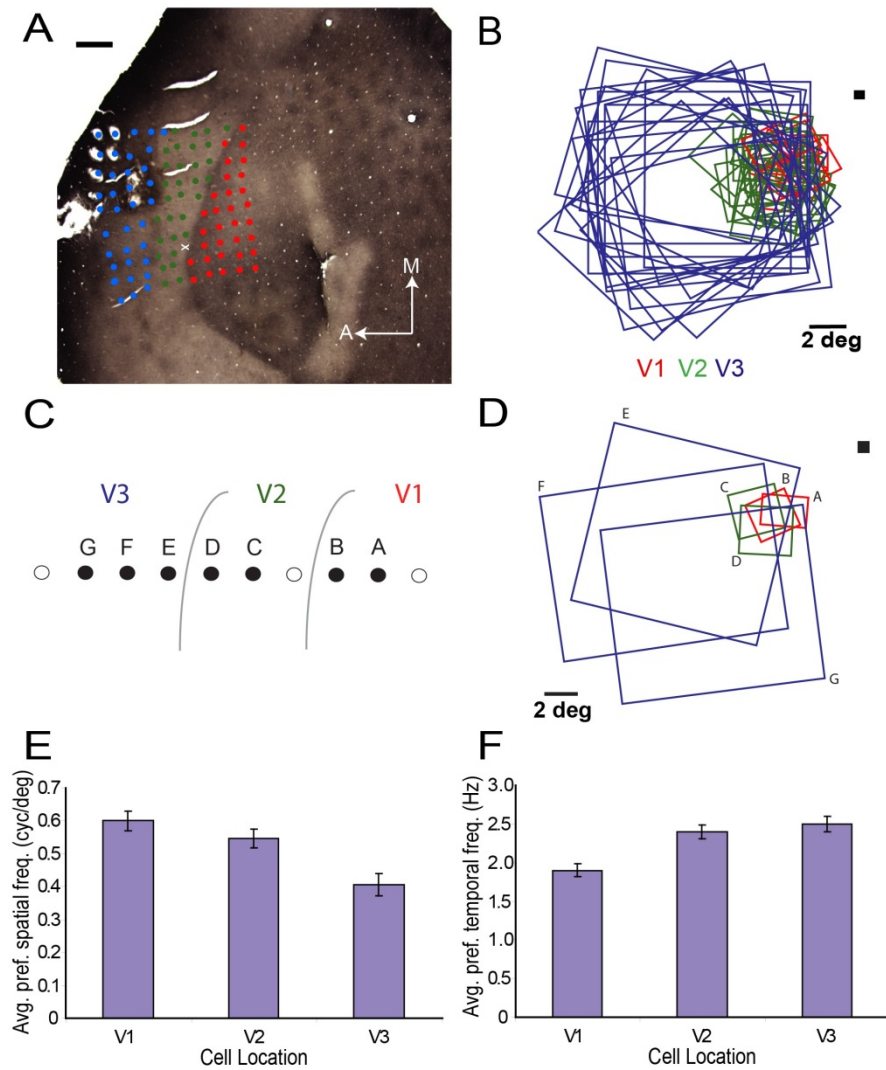


Figure 2- 10. ***Electrode array recording data.***

(A) CO-stained section of visual cortex after removal of the array. The V1/V2 border was determined using CO staining to mark CO blobs in area V1. Red dots: V1 electrodes, Green dots: V2 electrodes, Blue dots: V3 electrodes. Scale bar = 1 mm. A: anterior; D: dorsal. (B) Receptive fields of 56 V1, V2, and V3 neurons. The V2/V3 border was determined by dramatic change in receptive field sizes. Scale bar = 2°. Red: V1, Green: V2, Blue: V3. (C) Average spatial frequency preference of the 56 neurons from this case. (D) Average temporal frequency preference of the 56 neurons from this case.

Most importantly, consistent with a V3 interpretation, all of the proposed V3 receptive field centers fell within the lower visual field (see Fig 10B, black square). The retinotopic distributions of V1, V2 and V3 receptive fields observed in case 07-12 are representative of all three cases (Fig. 10B). In these cases, the V3 receptive fields extended from the HM to 10-15° below the horizontal meridian, overlapping nearly all of the dorsal V1 and V2 receptive fields. Although some of the V3 receptive fields impinge on the upper field representation, the receptive field centers are clearly in the lower field. Moreover, as seen from the imaging evidence (Figs 4-9) any such impingement on the upper field reveals no associated cortical activation. The large receptive field sizes and scatter also help explain why a clear retinotopic progression is challenging to obtain in galagos.

Orientation patch sizes in V1, V2, and V3

Another way to differentiate areas is based on differences in functional organization and patch size. We found both qualitative and quantitative differences in orientation structure between V2 and V3. Figure 11 shows orientation preference maps from 2 cases (Fig 11AB and 11CD) in which the V2/V3 borders (dotted blue lines) were estimated by the available OIS data described above. Orientation maps in V2 appear continuous, consistent with previous observations (Xu et al., 2005). However, V3 reveals a discontinuous or banded appearance (Fig 11B and 11D). This discontinuous appearance in V3 is also evident in Fig. 4C, 5E, and 6E. This is reminiscent of previous descriptions in owl monkey V3 (Kaskan et al., 2009; Xu et al., 2004). We did not conduct additional studies to determine what bearing on retinotopic maps the banding causes. We did attempt other stimulus features (such as moving random dots (Lu et al., 2010) and large field luminance modulation (Kaskan et al., 2009)) to see if we could elicit responses other

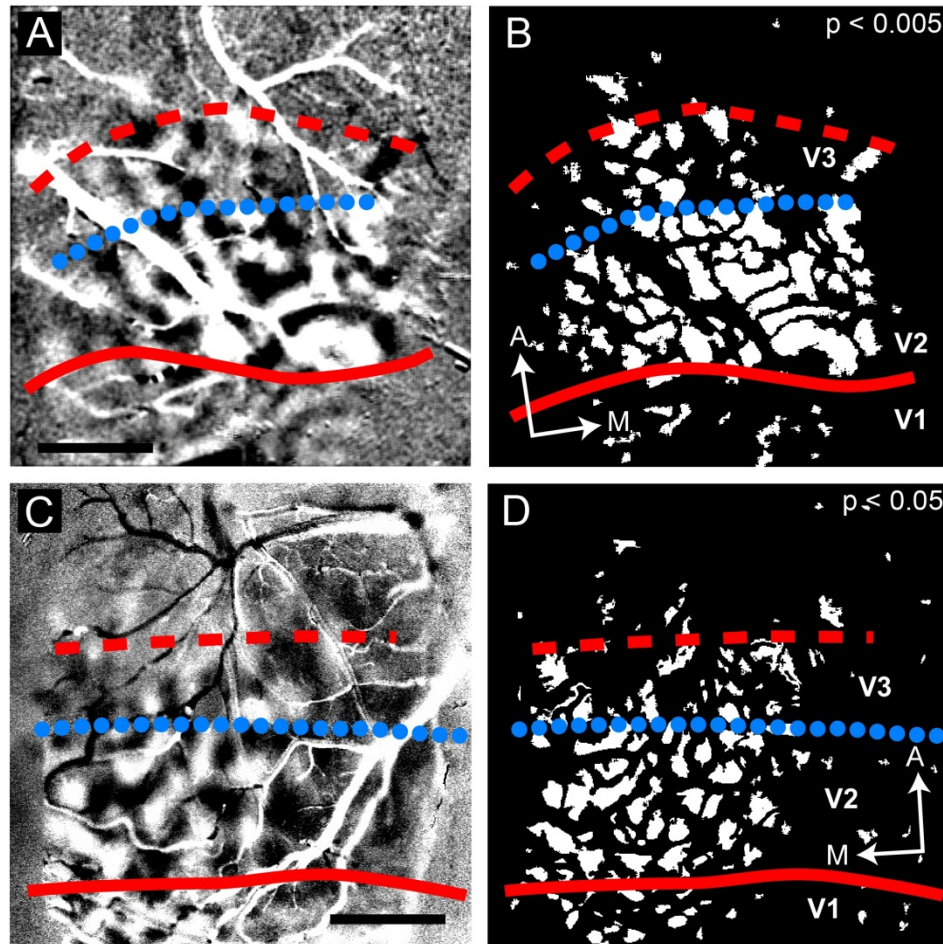


Figure 2- 11. *Orientation preference maps are not continuous along the anterior border of V2 (Cases 08-11/08-61).*

We show two example cases where there are regions that lack of signal to the orientation gratings. One possibility is this exhibits banding of orientation selective regions in V3 (see text for additional possibilities). A-B: orientation and t-maps, respectively, from case 08-11 (0° - 90°). C-D: orientation and t-maps, respectively, from case 08-61 (0° - 90°). In contrast, Area V2 lacks evidence of banding. In both cases, the locations of areal borders based on banding differences between areas agrees well with the defined borders histologically and retinotopic mapping using OIS. Solid red line: V1/V2 border. Dotted blue line: V2/V3 border. Dashed red line: estimated anterior V3 border. Scale bar = 2mm. A: anterior. M: medial.

than orientation selectivity or possible complementary structure; however, these stimuli did not reveal any significant cortical responses.

Throughout our images a qualitative assessment of orientation preference patches are noticeably different between neighboring visual areas. Because we noticed this difference in the orientation difference maps, we investigated the difference in this form. Figure 12 (case 08-49) illustrates our procedure for measuring orientation patch sizes in V2 and V3. Since we did not want to make any a priori assumption about the location of the V2/V3 border, we developed an iterative procedure, which identified a border between two regions of significantly different patch sizes ($p < 0.05$). To do this, we used 1 mm wide zones (shaded rectangles in Fig. 12E) anterior to the V1/V2 border and measured patch sizes (based on t-maps of orientation difference maps) in each of these zones. We repeated this procedure, shifting the two zones in 0.25 mm increments from near the V1/V2 border through the V3 region. Through this procedure, we identified the border location, which yielded the maximal difference in patch sizes (the smallest p-value). We also tested smaller 0.1 mm increments but found little difference in the final location. The blue dotted line in Fig. 12F reflects the position determined for this case. There is no retinotopic mapping associated with this line; the blue dotted line simply marks the location dividing regions of orientation patch size difference. Its position is an approximation of where the V2/V3 border lies. We also examined patch size distributions based on qualitative estimation of V2/V3 borders and found no difference in resulting distributions.

Figure 13 shows the distributions of orientation patch sizes in V1 ($n = 187$), V2 ($n = 157$), and V3 ($n = 79$) pooled from 4 cases for 10 total difference maps (3 cases

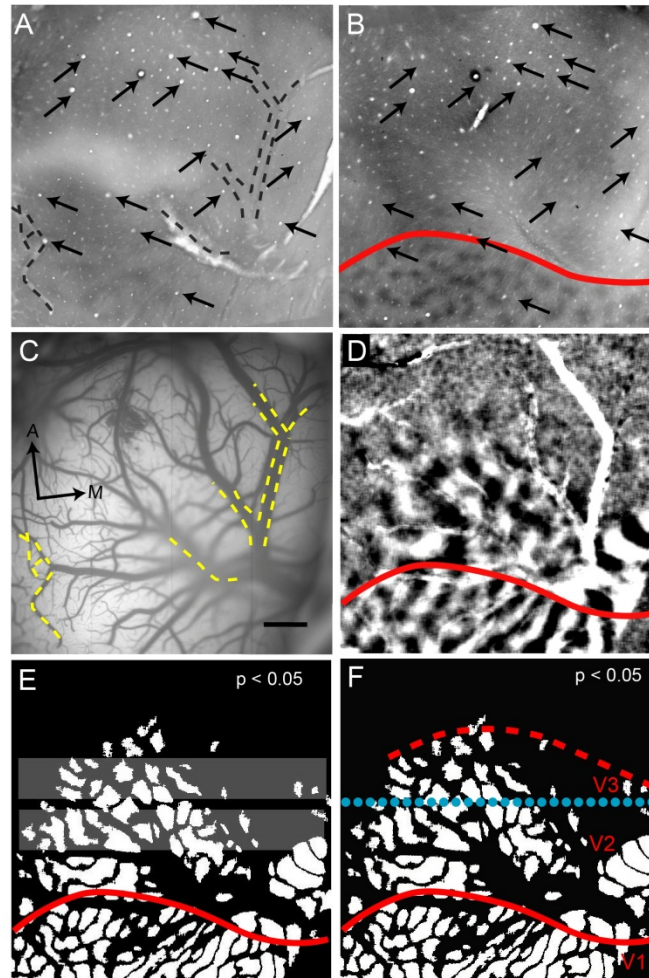


Figure 2- 12. **Procedure for orientation preference patch size determination (Case 08-49).**

In many of the orientation preference maps, it appeared that there were three distinct populations of orientation patch sizes. (A) A superficial CO section containing surface vasculature. (B) A deeper section revealing the characteristic CO blobs of V1 which terminate at the V1/V2 border (solid red line). (C) An *in vivo* blood vessel pattern acquired under green light (see Materials and Methods). Dashed red lines in A and C delineate sample vessels used to align with surface vasculature shown. (D) Orientation map in V1, V2, and area anterior to V2. As in Figs. 3 and 4, we used this information (A-D) to place the CO blob defined V1/V2 border onto our imaging maps. (E-F) T-map ($p < 0.05$) of the orientation preference map shown in panel D. We determined those samples using two sample regions (the superimposed light gray rectangles 1mm in height). The bars were moved in an iterative fashion to arrive at this final location (see text). Only those patches lying within a single sample region were selected for measurement. Solid red line: V1/V2 border. Dotted blue line: estimated V2/V3 border. Dashed red line: estimated anterior V3 border. Scale bar = 1mm. A: anterior. M: medial.

Histogram of Patch Size

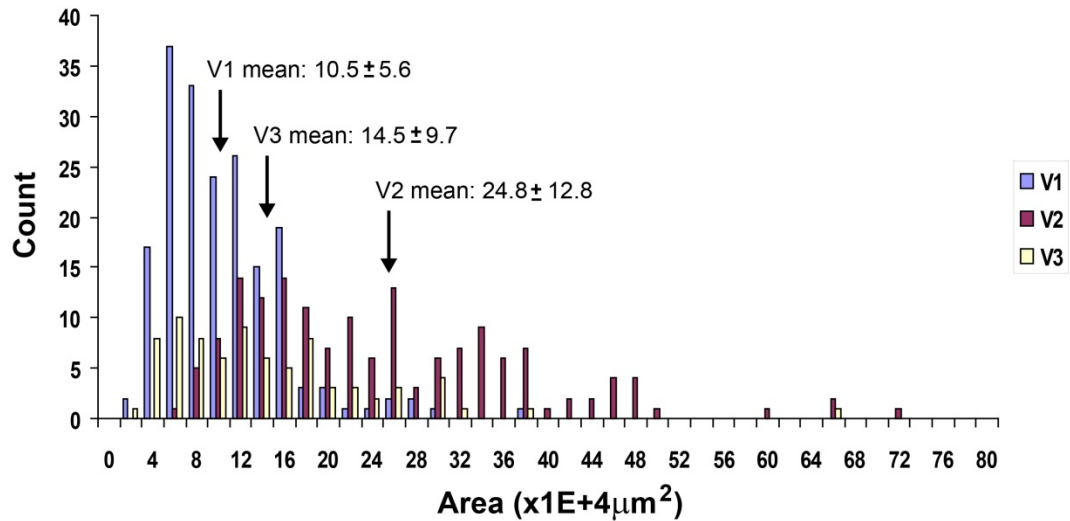


Figure 2- 13. *Distribution of orientation preference patch sizes in V1, V2, and V3.* Patches from orientation maps for V1, V2, and V3 were measured using t-maps at a threshold of $p < 0.05$. The distribution shown is pooled data from 4 cases. Borders for V1, V2, and V3 were chosen based on all available combinations of histological and OIS data. T-tests were performed in pairs: V1 vs. V2 and V2 vs. V3. All were found to be significantly different ($p < 0.01$ for all three comparisons). V1 patches: $n=187$; V2 patches: $n=157$; V3 patches: $n=79$.

contributed 1 hemisphere and 1 case contributed both hemispheres). For each hemisphere, we measured patches for 2 maps within orientation preference t-map of orthogonal conditions (45°-135° and 90°-180°). The patch sizes in V1 were taken from the region of cortex characterized by V1 cytochrome oxidase staining. Those in V2 and V3 were taken via the process described above. Means and standard deviations are indicated. The same p-values were used for all t-maps. We did not remove outliers and included all values. Removing outliers (greater than 2 standard deviations) did improve our statistics, but did not change the location of borders. We used t-tests to compare patch sizes in V1 vs. V2 and V2 vs. V3. All comparisons were significantly different (all $p < 0.005$). The differences between V1 and V2 and between V2 and V3 were significant within each case as well as across cases (Table 1). Surprisingly, V3 did not possess the largest orientation preference patch sizes, but is intermediate in patch size between V1 and V2.

Case	V1 (mean \pm sd)	V2 (mean \pm sd)	V3 (mean \pm sd)	V1 vs. V2	V2 vs. V3
08-07	10.1 \pm 4.9 μm^2	25.5 \pm 14.4 μm^2	16.4 \pm 12.9 μm^2	< 0.005	< 0.005
08-11	9.3 \pm 3.5 μm^2	30.6 \pm 12.8 μm^2	15.3 \pm 6.7 μm^2	< 0.005	< 0.005
08-49	14.8 \pm 8.0 μm^2	27.0 \pm 8.0 μm^2	11.1 \pm 9.2 μm^2	< 0.005	< 0.005
08-61	10.4 \pm 5.4 μm^2	18.4 \pm 7.7 μm^2	9.0 \pm 6.0 μm^2	< 0.005	< 0.005
ALL	10.5 \pm 5.6 μm^2	24.8 \pm 12.8 μm^2	14.5 \pm 9.7 μm^2	< 0.005	< 0.005

Table 2- 1. ***Orientation patch calculations for three visual areas.***

The mean and standard deviations of measured patches sizes for 4 individual cases and collectively for V1, V2, and V3 are provided. The p-values for the comparisons V1 vs. V2 and V2 vs. V3 are shown.

Discussion

Summary

In this study, we used OIS and electrophysiology to examine the cortical representation anterior to area V2 in prosimian galagos. We find little evidence for an upper field representation in this region, suggesting that, in galagos, the cortex anterior to V2 is area V3 and not area DM. Using OIS we studied 6 hemispheres in 5 galagos. The main OIS findings were: (1) lack of upper field activation anterior to V2, (2) VM representation at the V1/V2 border and the anterior V3 border, (3) one HM representation dividing V2 and V3, (4) lateral to medial shift in cortical activation with greater stimulus eccentricity, consistent with previous mapping studies, (5) a V2/V3 border 1.5-2.5 mm anterior to the V1/V2 border and an anterior V3 border 1-2.5 mm further anterior, consistent with the anterior-posterior extents of V2 (max ~3mm) and V3 (max ~2.5mm) reported previously in galagos (Collins et al., 2001; Lyon and Kaas, 2002a), (6) distinctions between V1, V2, and V3 by orientation preference patch size, and (7) possible banding structure in V3. In addition to our OIS findings, we provide receptive field mapping data, in three additional galagos, from multielectrode array recording, illustrating three distinct pools of receptive field sizes, average spatial frequency preference, and average temporal frequency preference in V1, V2, and V3, none of which exhibited an upper field representation, consistent with the OIS data. These findings thus suggest the region anterior to V2 is area V3 and provide no compelling evidence for a DM representation.

Experimental considerations

In this study, we found no evidence for an upper visual field representation in the region anterior to V2. This is curious given reports of an upper visual field representation bordering V2 (e.g., Allman et al., 1979; Beck and Kaas, 1998a; b; Krubitzer and Kaas, 1993; Rosa et al., 1997; Rosa et al., 2009; Rosa et al., 2005; Rosa et al., 2000; Rosa and Schmid, 1995; Rosa and Tweedale, 2000; 2005). Here, we discuss experimental considerations.

One possibility is that the lack of upper field response was due to general ineffectiveness of the stimuli presented. However, this seems unlikely. Using the same experimental conditions, we consistently elicited clear activation throughout the imaging field-of-view with lower visual field stimuli. To examine whether the upper visual field representation is present but weaker, we assessed the activation maps at lower p-value thresholds but still failed to find upper field activation. In contrast, stimuli falling on the HM or in the lower visual field demonstrate clear activation (see Figs. 2-9). Consistent results were obtained with full field, rectangular, and square windowed stimuli, indicating that the lack of activation is not due to stimulus size or configuration. Additionally, under similar anesthesia protocols, these same stimuli elicited clear electrophysiological mapping of receptive fields (Fig. 10) in the lower visual field but not the upper visual field.

It is also unlikely that our imaging field-of-view or electrophysiology array failed to include the area of interest. Our imaging field-of-view was quite large (8 mm x 8 mm) and included not only V1 and V2, but also the additional several millimeters anterior to V2. We also confirmed histologically that the electrophysiology array spanned several

millimeters anterior to the V1/V2 border. With respect to mediolateral extent, our field-of-view extended from medial to fairly lateral (foveal) regions of cortex. We also used the intraparietal sulcus as an anatomical landmark (see Materials and Methods), and are sure that our sampling areas included the relevant cortex in question near the anterior border of dorsal V2

Another potential source of error is in our estimate of the *area centralis* location. This could lead to the false assignment of upper visual field representation to the lower field. However, we find this unlikely as we repeatedly measured the *area centralis* location prior to each imaging run and due to our paralytic the position was very stable throughout experimentation. We also tested locations well into the upper visual field and found no upper field representation. Additionally, the estimated locations of the horizontal and vertical meridian were consistent across experiments and consistent with the size of V2 from previous studies. Thus, despite significant effort, we were unable to find any evidence for an upper field representation anterior to V2.

Consistent with dorsal V3

Optical imaging evidence in owl monkeys (Kaskan et al., 2009; Lyon et al., 2002; Xu et al., 2004) and some tracer studies in New World monkeys (Lyon and Kaas, 2001; 2002c) support the interpretation that dorsal V3 (depicted in Fig. 1C) lies along the rostral border of dorsomedial V2. However there continues to be electrophysiology and some tracer studies supporting the presence of DM (depicted in Fig. 1C) along V2, instead of dorsal V3 (Jeffs et al., 2009; Lui et al., 2006; Rosa et al., 2009; Rosa et al., 2005; Rosa et al., 2000; Rosa and Schmid, 1995; Rosa and Tweedale, 2000; 2001; 2005). In prosimians, early electrode recording and anatomical studies also suggest the

representation of the upper visual field directly along the anterior border of dorsal V2 (Allman et al., 1979; Beck and Kaas, 1998b; Newsome and Allman, 1980; Rosa et al., 1997). However a reinvestigation of the connection patterns in galagos, using tracers placed in V1, supported the existence of a V3 in prosimians (Lyon and Kaas, 2002a). The ability for Lyon and Kaas to detect V3 using tracer studies in a variety of primates (2001; 2002a, b, c) is partly due to strategy. By making targeted injections of refined tracers into V1, Lyon and Kaas were able to clearly confine injections into a single visual area.

The combined optical imaging and electrophysiological evidence in this study was extremely important considering that a significant part of the interpretational division lies along methodological lines. Electrode recordings have tended to favor a DM interpretation (e.g., Rosa et al., 2009; Rosa and Tweedale, 2000). However, given the large size of receptive fields anterior to V2, single penetration electrophysiological mapping may not provide sufficient density or positional certainty to map reversals. The use of fixed arrays of microelectrodes alleviates much of the positional ambiguity. The difficulty of interpretation is highlighted by Lyon and Connelly (2012) in their argument for V3 in primates, where they demonstrate that electrophysiology data previously published in favor of DM can easily be re-interpreted to support the existence of V3.

Based on the retinotopic data provided in Figs. 5-9, a mirror reflection between V2 and V3 is only an approximation. Another reported aspect of the DM hypotheses is the existence of a HM representation perpendicular to the HM along the anterior border of dorsal V2 (see Fig. 1B). However, the evidence presented provides no support for such a HM representation.

Functional Organization

We confirm previous reports of orientation selective responses anterior to dorsal V2 in the presumptive area V3 of galagos (Jermakowicz et al., 2009). We also demonstrate the ability to distinguish V1, V2, and V3 based on their relative orientation preference patch sizes (see Figs. 12 and 13) and the sizes of individually mapped receptive fields (see Fig. 10). Consistent with previous studies on iso-orientation domains in owl monkeys (Xu et al., 2004) and in galagos (Xu et al., 2005), we find orientation patch sizes in V2 are larger than those in V1. Surprisingly, orientation patch sizes appear to be smaller in V3 than in V2 in the galago. This is in contrast to iso-orientation domains in the owl monkeys which are larger in V3 than in V1 or V2 (Xu et al., 2004). However this relationship could change if we were to calculate the relationships between iso-orientation domains rather than patches. Iso-orientation comparisons in owl monkeys (Xu et al., 2004), showed the V2 and V3 iso-orientation distinction to be small and not significantly different. Ultimately we chose not to pursue iso-orientation measures since we were interested in a quantifiable difference. It would be more interesting to see if in other primates, where the differences in iso-orientation domain sizes are not statistically significant, became distinctly different populations when using orientation patches from simple difference maps instead. Being able to distinguish visual areas using difference maps of orientation preference would allow for quick assessment of visual area borders without explicit visuotopic mapping which would be advantageous for several applications. We highlight two interesting points using our simplified differentiation. First, the qualitative difference between the neighboring visual areas is quantifiable (Figs. 12 and 13). Second, the

locations for these borders are similar in location to those found by more traditional mapping.

Consistent with a previous study (Xu et al., 2004), V2 in galagos lacks any band-like structure, unlike that in the macaque (Lu and Roe, 2007; 2008; Roe and Ts'o, 1995), owl monkey (Kaskan et al., 2009; Xu et al., 2004), or marmoset (Federer et al., 2009; McLoughlin and Schiessl, 2006; Roe et al., 2005) where there is a clear presence of a band-like appearance, associated with high and low orientation selectivity. We found orientation maps that appear band-like in galago V3 (Fig. 11). This is reminiscent to the bands described in owl monkey V3 (Kaskan et al., 2009; Xu et al., 2004).

We report the first evidence of possible banding in presumptive V3 in galagos. To investigate the possibility that the regions between the orientation bands may have different stimulus preference, we used other stimuli (e.g. moving dot stimuli, full field luminance modulation) but did not observe activation to these stimuli. Alternatively, patches of V3 may become unresponsive under our particular mapping conditions. One interesting possibility to consider is that the gaps between the bands represent an intrusion of another visual area into the proposed V3 region. If present, our study suggests its functional properties would be asymmetrical to the proposed V3. Previously, Rosa et al. (2005 see Fig 17B) considered such a model but dismissed it because of its complexity. Our data do not eliminate this possibility.

Conclusion

V3 can be found in a variety of primate species based on V1 connections and architectural features (Lyon and Kaas, 2001; 2002a; b; c). From the current study and in

previous studies, optical imaging of intrinsic signal has provided functional evidence for dorsal V3 in prosimian and New World primates (Kaskan et al., 2009; Lyon et al., 2002; Xu et al., 2004). Electrode recordings anterior to V2 also suggest the existence of V3 in macaques (Adams and Zeki, 2001; Baizer, 1982; Felleman and Van Essen, 1987; Gattass et al., 1988; Poggio et al., 1988; Zeki, 1978a; b). Human (DeYoe et al., 1996; Engel et al., 1997; Nishida et al., 2003; Reppas et al., 1997; Smith et al., 1998; Tootell et al., 1997; Wade et al., 2002) and macaque fMRI (Brewer et al., 2002; Schmid et al., 2009; Tehovnik et al., 2006; Tolias et al., 2005) studies also appear more consistent with a V3 interpretation.

In this study, we provide the first OIS data regarding the visuotopy of the cortical area anterior to V2 in galagos and confirm that receptive fields in this zone are much larger than in either V1 or V2. We also present the first OIS evidence for orientation preference maps in galago V3, demonstrate differences in orientation patch sizes in V1, V2, and V3, and suggest possible band-like functional architecture within V3. Finally, the lack of detectable upper visual field representation suggests this area is more consistent with V3, not DM, and argues in favor of the inclusion of V3 as a common visual area among primates.

Acknowledgements We thank, Lisa Chu, Julia Mavity-Hudson, Alyssa Zuehl, Dr. Robert Friedman, and Dr. Haidong Lu, for all of their valuable assistance and thoughtful discussions.

References

- Adams DL, Zeki S. 2001. Functional organization of macaque V3 for stereoscopic depth. *J Neurophysiol* 86(5):2195-2203.
- Allman J, Campbell CB, McGuinness E. 1979. The dorsal third tier area in *Galago senegalensis*. *Brain Res* 179(2):355-361.
- Allman JM, Kaas JH. 1975. The dorsomedial cortical visual area: a third tier area in the occipital lobe of the owl monkey (*Aotus trivirgatus*). *Brain Res* 100(3):473-487.
- Baizer JS. 1982. Receptive field properties of V3 neurons in monkey. *Invest Ophthalmol Vis Sci* 23(1):87-95.
- Beck PD, Kaas JH. 1998a. Cortical connections of the dorsomedial visual area in new world owl monkeys (*Aotus trivirgatus*) and squirrel monkeys (*Saimiri sciureus*). *J Comp Neurol* 400(1):18-34.
- Beck PD, Kaas JH. 1998b. Cortical connections of the dorsomedial visual area in prosimian primates. *J Comp Neurol* 398(2):162-178.
- Brewer AA, Press WA, Logothetis NK, Wandell BA. 2002. Visual areas in macaque cortex measured using functional magnetic resonance imaging. *J Neurosci* 22(23):10416-10426.
- Collins CE, Stepniewska I, Kaas JH. 2001. Topographic patterns of v2 cortical connections in a prosimian primate (*Galago garnetti*). *J Comp Neurol* 431(2):155-167.
- Cragg BG. 1969. The topography of the afferent projections in the circumstriate visual cortex of the monkey studied by the Nauta method. *Vision Res* 9(7):733-747.
- DeBruyn EJ, Casagrande VA, Beck PD, Bonds AB. 1993. Visual resolution and sensitivity of single cells in the primary visual cortex (V1) of a nocturnal primate (bush baby): correlations with cortical layers and cytochrome oxidase patterns. *J Neurophysiol* 69(1):3-18.
- DeYoe EA, Carman GJ, Bandettini P, Glickman S, Wieser J, Cox R, Miller D, Neitz J. 1996. Mapping striate and extrastriate visual areas in human cerebral cortex. *Proc Natl Acad Sci U S A* 93(6):2382-2386.
- Engel SA, Glover GH, Wandell BA. 1997. Retinotopic organization in human visual cortex and the spatial precision of functional MRI. *Cereb Cortex* 7(2):181-192.

- Federer F, Ichida JM, Jeffs J, Schiessl I, McLoughlin N, Angelucci A. 2009. Four projection streams from primate V1 to the cytochrome oxidase stripes of V2. *J Neurosci* 29(49):15455-15471.
- Felleman DJ, Van Essen DC. 1987. Receptive field properties of neurons in area V3 of macaque monkey extrastriate cortex. *J Neurophysiol* 57(4):889-920.
- Felleman DJ, Van Essen DC. 1991. Distributed hierarchical processing in the primate cerebral cortex. *Cereb Cortex* 1(1):1-47.
- Gattass R, Sousa AP, Gross CG. 1988. Visuotopic organization and extent of V3 and V4 of the macaque. *J Neurosci* 8(6):1831-1845.
- Jeffs J, Federer F, Angelucci A. Anatomical evidence for an area DM, but not V3, bordering dorsal V2 in the marmoset; 2009 October 17-21; Chicago, IL.
- Jermakowicz WJ, Chen X, Khaytin I, Bonds AB, Casagrande VA. 2009. Relationship between spontaneous and evoked spike-time correlations in primate visual cortex. *J Neurophysiol* 101(5):2279-2289.
- Kaas JH. 2004. Neuroanatomy is needed to define the "organs" of the brain. *Cortex* 40(1):207-208.
- Kaskan PM, Lu HD, Dillenburger BC, Kaas JH, Roe AW. 2009. The organization of orientation-selective, luminance-change and binocular-preference domains in the second (V2) and third (V3) visual areas of New World owl monkeys as revealed by intrinsic signal optical imaging. *Cereb Cortex* 19(6):1394-1407.
- Krubitzer LA, Kaas JH. 1989. Cortical integration of parallel pathways in the visual system of primates. *Brain Res* 478(1):161-165.
- Krubitzer LA, Kaas JH. 1990. Cortical connections of MT in four species of primates: areal, modular, and retinotopic patterns. *Vis Neurosci* 5(2):165-204.
- Krubitzer LA, Kaas JH. 1993. The dorsomedial visual area of owl monkeys: connections, myeloarchitecture, and homologies in other primates. *J Comp Neurol* 334(4):497-528.
- Lu HD, Chen G, Tanigawa H, Roe AW. 2010. A motion direction map in macaque V2. *Neuron* 68(5):1002-1013.
- Lu HD, Roe AW. 2007. Optical imaging of contrast response in Macaque monkey V1 and V2. *Cereb Cortex* 17(11):2675-2695.
- Lu HD, Roe AW. 2008. Functional organization of color domains in V1 and V2 of macaque monkey revealed by optical imaging. *Cereb Cortex* 18(3):516-533.

- Lui LL, Bourne JA, Rosa MG. 2006. Functional response properties of neurons in the dorsomedial visual area of New World monkeys (*Callithrix jacchus*). *Cereb Cortex* 16(2):162-177.
- Lyon DC, Connolly JD. 2012. The case for primate V3. *Proc Biol Sci* 279(1729):625-633.
- Lyon DC, Kaas JH. 2001. Connectional and architectonic evidence for dorsal and ventral V3, and dorsomedial area in marmoset monkeys. *J Neurosci* 21(1):249-261.
- Lyon DC, Kaas JH. 2002a. Connectional evidence for dorsal and ventral V3, and other extrastriate areas in the prosimian primate, *Galago garnetti*. *Brain Behav Evol* 59(3):114-129.
- Lyon DC, Kaas JH. 2002b. Evidence for a modified V3 with dorsal and ventral halves in macaque monkeys. *Neuron* 33(3):453-461.
- Lyon DC, Kaas JH. 2002c. Evidence from V1 connections for both dorsal and ventral subdivisions of V3 in three species of New World monkeys. *J Comp Neurol* 449(3):281-297.
- Lyon DC, Xu X, Casagrande VA, Stefansic JD, Shima D, Kaas JH. 2002. Optical imaging reveals retinotopic organization of dorsal V3 in New World owl monkeys. *Proc Natl Acad Sci U S A* 99(24):15735-15742.
- McLoughlin N, Schiessl I. 2006. Orientation selectivity in the common marmoset (*Callithrix jacchus*): the periodicity of orientation columns in V1 and V2. *Neuroimage* 31(1):76-85.
- Newsome WT, Allman JM. 1980. Interhemispheric connections of visual cortex in the owl monkey, *Aotus trivirgatus*, and the bushbaby, *Galago senegalensis*. *J Comp Neurol* 194(1):209-233.
- Nishida S, Sasaki Y, Murakami I, Watanabe T, Tootell RB. 2003. Neuroimaging of direction-selective mechanisms for second-order motion. *J Neurophysiol* 90(5):3242-3254.
- Poggio GF, Gonzalez F, Krause F. 1988. Stereoscopic mechanisms in monkey visual cortex: binocular correlation and disparity selectivity. *J Neurosci* 8(12):4531-4550.
- Reppas JB, Niyogi S, Dale AM, Sereno MI, Tootell RB. 1997. Representation of motion boundaries in retinotopic human visual cortical areas. *Nature* 388(6638):175-179.

- Roe AW, Fritsches K, Pettigrew JD. 2005. Optical imaging of functional organization of V1 and V2 in marmoset visual cortex. *Anat Rec A Discov Mol Cell Evol Biol* 287(2):1213-1225.
- Roe AW, Ts'o DY. 1995. Visual topography in primate V2: multiple representation across functional stripes. *J Neurosci* 15(5 Pt 2):3689-3715.
- Rosa MG, Casagrande VA, Preuss T, Kaas JH. 1997. Visual field representation in striate and prestriate cortices of a prosimian primate (*Galago garnetti*). *J Neurophysiol* 77(6):3193-3217.
- Rosa MG, Palmer SM, Gamberini M, Burman KJ, Yu HH, Reser DH, Bourne JA, Tweedale R, Galletti C. 2009. Connections of the dorsomedial visual area: pathways for early integration of dorsal and ventral streams in extrastriate cortex. *J Neurosci* 29(14):4548-4563.
- Rosa MG, Palmer SM, Gamberini M, Tweedale R, Pinon MC, Bourne JA. 2005. Resolving the organization of the New World monkey third visual complex: the dorsal extrastriate cortex of the marmoset (*Callithrix jacchus*). *J Comp Neurol* 483(2):164-191.
- Rosa MG, Pinon MC, Gattass R, Sousa AP. 2000. "Third tier" ventral extrastriate cortex in the New World monkey, *Cebus apella*. *Exp Brain Res* 132(3):287-305.
- Rosa MG, Schmid LM. 1995. Visual areas in the dorsal and medial extrastriate cortices of the marmoset. *J Comp Neurol* 359(2):272-299.
- Rosa MG, Tweedale R. 2000. Visual areas in lateral and ventral extrastriate cortices of the marmoset monkey. *J Comp Neurol* 422(4):621-651.
- Rosa MG, Tweedale R. 2001. The dorsomedial visual areas in New World and Old World monkeys: homology and function. *Eur J Neurosci* 13(3):421-427.
- Rosa MG, Tweedale R. 2005. Brain maps, great and small: lessons from comparative studies of primate visual cortical organization. *Philos Trans R Soc Lond B Biol Sci* 360(1456):665-691.
- Schmid MC, Panagiotaropoulos T, Augath MA, Logothetis NK, Smirnakis SM. 2009. Visually driven activation in macaque areas V2 and V3 without input from the primary visual cortex. *PLoS One* 4(5):e5527.
- Smith AT, Greenlee MW, Singh KD, Kraemer FM, Hennig J. 1998. The processing of first- and second-order motion in human visual cortex assessed by functional magnetic resonance imaging (fMRI). *J Neurosci* 18(10):3816-3830.

- Tehovnik EJ, Tolias AS, Sultan F, Slocum WM, Logothetis NK. 2006. Direct and indirect activation of cortical neurons by electrical microstimulation. *J Neurophysiol* 96(2):512-521.
- Tolias AS, Sultan F, Augath M, Oeltermann A, Tehovnik EJ, Schiller PH, Logothetis NK. 2005. Mapping cortical activity elicited with electrical microstimulation using fMRI in the macaque. *Neuron* 48(6):901-911.
- Tootell RB, Mendola JD, Hadjikhani NK, Ledden PJ, Liu AK, Reppas JB, Sereno MI, Dale AM. 1997. Functional analysis of V3A and related areas in human visual cortex. *J Neurosci* 17(18):7060-7078.
- Wade AR, Brewer AA, Rieger JW, Wandell BA. 2002. Functional measurements of human ventral occipital cortex: retinotopy and colour. *Philos Trans R Soc Lond B Biol Sci* 357(1424):963-973.
- Wong-Riley M. 1979. Changes in the visual system of monocularly sutured or enucleated cats demonstrable with cytochrome oxidase histochemistry. *Brain Res* 171(1):11-28.
- Xu X, Bosking W, Sary G, Stefansic J, Shima D, Casagrande V. 2004. Functional organization of visual cortex in the owl monkey. *J Neurosci* 24(28):6237-6247.
- Xu X, Bosking WH, White LE, Fitzpatrick D, Casagrande VA. 2005. Functional organization of visual cortex in the prosimian bush baby revealed by optical imaging of intrinsic signals. *J Neurophysiol* 94(4):2748-2762.
- Zeki SM. 1969. Representation of central visual fields in prestriate cortex of monkey. *Brain Res* 14(2):271-291.
- Zeki SM. 1978a. The third visual complex of rhesus monkey prestriate cortex. *J Physiol* 277:245-272.
- Zeki SM. 1978b. Uniformity and diversity of structure and function in rhesus monkey prestriate visual cortex. *J Physiol* 277:273-290.

CHAPTER III

THE INFLUENCE OF MODULARITY ON V4 VISUAL TOPOGRAPHY

Abstract

The visuotopic representation of visual areas is often modeled as a smooth continuous representation without disruption. However it is known that there are duplicate representations of the visual field in V1 between ocular dominance columns and repeated representations between V2 stripes. Using intrinsic signal optical imaging, we assessed the visuotopic relationship for bands of color and orientation modules in V4. As previously reported, we show representation of the visual field specific to each modality (color and orientation). Because the areas of activation we observe in V4 are not a single point, we calculate the centers of mass for the representation of each visual stimulus. with the center of mass values we calculated the cortical magnification factors (CMF) for each modality and found the CMFs for bands of color and orientation modules to be nearly identical both within and between the two subjects (color band power coefficient: -0.866 Subject L; -0.859 Subject J / orientation band power coefficient : -0.951 Subject L; -0.951 Subject J). These results show that the multiple visuotopic mapping strategy in areas like V1 and V2 also appear to be utilized in V4.

Introduction

Recently, the use of intrinsic signal optical imaging (IOI) revealed bands of color and orientation modules in V4 (Tanigawa et al., 2010). This finding is consistent with and extends previous evidence from IOI (Ghose and Ts'o, 1997), anatomical tracer studies (Felleman et al., 1997b; Xiao et al., 1999; Zeki and Shipp, 1989), and fMRI studies (Conway et al., 2007). Acceptance of a modality-specific organization introduces the question of how much cortical territory is devoted to each modality, an issue that can be addressed by examining modality-specific cortical magnification.

Cortical magnification has long been recognized as an important metric of a visual area (Daniel and Whitteridge, 1961; Hubel and Wiesel, 1974b; LeVay et al., 1985; Motter, 2009; Rosa and Schmid, 1995; Tootell et al., 1982; Van Essen et al., 1984; Xu et al., 2005). In V1, visuotopic repeats are found between ocular dominance columns (Blasdel and Fitzpatrick, 1984; Hubel and Wiesel, 1974a). In V2, there is multiple representation of the same visual space that occurs between V2 stripes (Roe and Ts'o, 1995; Shipp and Zeki, 2002). There is also evidence from IOI for the modality specific representation of the visual field in V4 (Tanigawa et al., 2010). These re-representations of visual space in among OD columns and in V2 stripes results in similar cortical magnification factors (CMF). It is in our interest to determine if a similar relationship occurs in V4 as it would strengthen the possibility that the coalescence of functional properties with visual topographic re-representations is a significant trait among visual areas.

Using IOI, we examine the topography of bands of color and orientation modules in V4. Similar to a previous report (Tanigawa et al., 2010), we identify band specific

representations of the visual field. In the current study we extend this observation by calculating the center of mass of each visual stimulus to assess the visuotopic progression on cortex. With the center of mass positions we then calculate the CMF values between the color and orientation modules and found them to be nearly identical both within and between the two subjects.

Material and methods

Intrinsic signal optical imaging (IOI) was used to map V4 topography in 2 adult rhesus macaques. All procedures are approved by the Vanderbilt University Institute for Animal Care and Use Committee and are in accordance with the National Institute of Health guidelines.

Animal preparation

Prior to imaging, two adult rhesus monkeys (*Macaca mulatta*, 5 and 8 kg, respectively) under sterile surgical conditions were anesthetized and a headpost placed. After training on a fixation task, a chronic nylon imaging chamber (Roe, 2007) was placed over dorsal V4 under sterile surgical conditions. Native dura in the chamber was replaced with a clear artificial dura (Tecoflex, Thermedics Polymer Products). The chamber was sealed with a nylon cap and opened under sterile conditions for image acquisition. The chamber was located on the right hemisphere of one monkey (Subject L) and on the left hemisphere of another (Subject J).

Optical imaging in awake, fixating animal

Subjects were trained to sit calmly and fixate on a single spot (0.15°) displayed on a CRT monitor positioned 118 or 140 cm away. An infrared eye tracker (RK-801, ISCAN, or

iView X, SensoMotoric Instruments) monitored the subject's eye position. Animals were trained to fixate continuously within a fixation window radius of less than 0.75° for 4 sec (the duration of image acquisition). A drop of juice was given for each successful trial. Once animals achieved a consistent success rate of 90%, the chamber was implanted, and the image acquisition phase began following a recovery period and brief retraining. Images were collected by an Imager 3001 system (Optical Imaging, Germantown, NY) which included the VDAQ/NT data acquisition software and the 1M60P Dalsa CCD camera. Images of surface vessel patterns were collected for every imaging session. Image frames were collected under 630 nm illumination at 4 Hz. The image matrix was set to 512x512 and the lens combination provided a field of view of 8 mm x 8 mm. Image acquisition included a 0.5 second pre-stimulus period, followed by a 3.5 second stimulus presentation period. Each experiment contained 4–16 stimulus conditions and one blank condition (no stimulus except fixation point); each condition was repeated 40–100 times, pseudo-randomly interleaved with an inter-trial interval of 2 - 12 sec. The length of inter-stimulus interval did not affect our findings (see Tanigawa et al., 2010, supplementary Fig. 6). Only trials with successful fixation throughout the duration of the imaging interval were analyzed. We report on 25 total imaging sessions from a data set gathered from imaging each subject every other day for several months.

Visual stimuli

Visual stimuli were created using VSG 2/5 or ViSaGe hardware and software (Cambridge Research Systems) and presented on a CRT monitor gamma corrected using a photometer (Minolta Chroma Meter CS-100, Ramsey). Stimuli consisted of circular patches (1° diameter), iso-eccentric arcs (0.1° width), and iso-polar bars (0.1° width) on a

uniform gray background. These stimuli contained squarewave or sinewave red/green or black/white oriented drifting gratings. Full screen versions of the drifting gratings were also presented. Optimal stimulus parameters were qualitatively assessed by iterative visual assessment of the image quality. Gratings were set to 1 or 2 cycles per degree, and drift rates of 0.5 or $1^\circ \cdot \text{s}^{-1}$, and orientations of 0° , 45° , 90° , or 135° . Drifting direction was randomized on every trial. Gratings had an average luminance of $26.8 \text{ cd} \cdot \text{m}^{-2}$, identical to the background luminance.

Data analysis

Image frames were analyzed offline using custom software written in MATLAB (Mathworks, Natick, MA). Prior to image analysis, we performed a correlation based rigid registration of all imaging frames within trials of interest. After registration, single condition maps, differential condition maps, and t-maps were generated. We have previously described the calculation of such maps and describe them briefly here (see Lu and Roe, 2007; Tanigawa et al., 2010).

Single condition and difference maps. For all maps, we first removed global non stimulus-specific signals (see Tanigawa et al., 2010). This was done by convolving individual imaging frames with a $1.875 \text{ mm} \times 1.875 \text{ mm}$ to $3.125 \text{ mm} \times 3.125 \text{ mm}$ median filter and subtracting it from the original unfiltered frame. For single condition maps, image frames were then averaged over time points 1.25 sec – 4 sec and the average of the pre-stimulus period (initial 0.5 sec) subtracted. For difference maps, pairs of single condition maps were then subtracted (ex: two color conditions, orthogonal orientations, or a single condition against a blank condition). For visualization purposes, we converted

the 12-bit single-condition maps into to 8-bit gray images and custom set the upper and lower bounds (typically 1-2 standard deviations of the mean).

t-map (binary map of activation). To verify observations based on difference maps, we tested for significance of activation by performing t-test comparisons between conditions on a pixel-by-pixel basis (Tsunoda et al., 2001). We assigned significant pixels (those meeting or exceeding threshold level of $p < 0.001$) the value 1 (white) and the value 0 (black) for pixels that did not reach significance. Images were low (median filter $187.5 \mu\text{m} \times 187.5 \mu\text{m}$ median filter) and high pass filtered ($1.875 \text{ mm} \times 1.875 \text{ mm}$ median filter) prior to pixelwise t-testing (Fan et al., 2012; Tanigawa et al., 2010). This resulted in the creation of a binary map that revealed locations of activation reaching a specific threshold. Pixels overlying large vessels and at the chamber edge were excluded from the calculation using ImageJ (Rasband, 1997-2008). To remove possible spurious activations, we eliminated activations that were very small by requiring a size threshold of 100 pixels (one pixel is $15.625 \mu\text{m} \times 15.625 \mu\text{m}$) in total area. We tested several size thresholds and found negligible differences in the final calculations of the center of mass positions for which these images were primarily used (see next subsection). There were instances where continuous regions were connected by a small bridge of one to four pixels. These bridges were eliminated and resulting domains assessed for size sufficiency. We refer to the final binary map as a *t-map*.

Retinotopic position and cortical magnification. To calculate cortical magnification factor (CMF), we considered using both areal and distance approaches. Calculating areal size of activation is subject to choice of threshold levels. We therefore determined CMF based on the spatial separations between areas of cortical activations to stimuli at

different visual field locations. Since activations in V4 are typically patchy due to the presence of multiple functional domains (see Tanigawa et al., 2010), we used the center-of-mass of significantly activated pixels (white pixels in t-map) as our measure of the activation center. We then calculated cortical magnification factor (CMF) by dividing the cortical distance between two centers of activation by the visual distance between stimuli. The reported CMF values were based on neighboring visuotopic positions within an imaging session. Thus, each pair of adjacent locations produced one CMF value. We do not calculate non-adjacent points. We later plot CMF values against eccentricity or polar angle. The CMF value is plotted against the smaller eccentric or polar angle value of the pair used in the calculation.

The visuotopic positions in this study are obtained from a collection of 26 total imaging sessions. For arc stimuli, the positions were spaced 0.25° apart ranging starting from 0.25° to 2.00° eccentricity. For spot stimuli, either 1° spacing (for positions 0.5° - 4°) or 2° spacing (for positions 4° - 18°) was used. Both arc and spot data were used in the CMF vs. eccentricity plots. Iso-polar bars or spot stimuli spaced 22.5° apart were used to evaluate polar representations.

Results

General retinotopic organization of foveal V4

In order to get a sense of the of the general retinotopic organization near foveal V4, we analyzed V4 in response to isoeccentric arcs and isopolar bars irrespective of modality. Figure 1A illustrates the chamber overlying foveal visual cortex in Subject J; the red box outlines the field of view shown in Fig. 1B. Retinotopic activation in V4 is

shown in Fig. 1C1-C5 and Fig. 1D1-D7 row. Figure 1C1-C5 illustrates the activations in V4 in response to different iso-eccentric arc conditions. As eccentricities increase from 0.25° to 0.50° to 0.75° to 1.00° to 1.25° , the focus of activation (Fig. 1C) shifts from ventral to dorsal. As shown in Fig 1D, as iso-polar angles increase from vertical meridian 0° to 22.5° to 45° to 67.5° to horizontal meridian 90° , cortical activation progresses roughly from the posterior to anterior parts of V4. When the bar progresses past the horizontal meridian into the upper visual quadrant, little cortical activation is seen (Fig. 1D6-7), as this activation presumably falls in inferior V4 which is out of the field of view. The general topography appears to have highly overlapping representations for neighboring stimulus representations across eccentricity and over polar angle.

Stability of maps in awake monkey V4

Prior to performing quantitative assessment of the topographic maps, we first assessed the sensitivity of our analytic measure and the stability of cortical activations over different sessions. As described in the methods, we used a center-of-mass method from *t*-maps to assess progressions of cortical activation. The activation center was robust to minimum area criterion, in which activation patches smaller than a certain threshold was eliminated. Comparisons of three minimum area thresholds (Fig. 2B: 100 pixels; Fig. 2C: 200 pixels; Fig. 2D: 400 pixels) reveal that the positions are nearly identical (see colored dots in Fig. 2B-D, dots overlain in Fig. 2A). This is not surprising given that larger domains contribute greater weight to center-of-mass calculation and shows that this calculation is not strongly affected by relatively small alteration. We also found that different statistical *t*-map thresholds with a factor of 10 difference produced very similar activation centers (Fig. 3B and 3C).

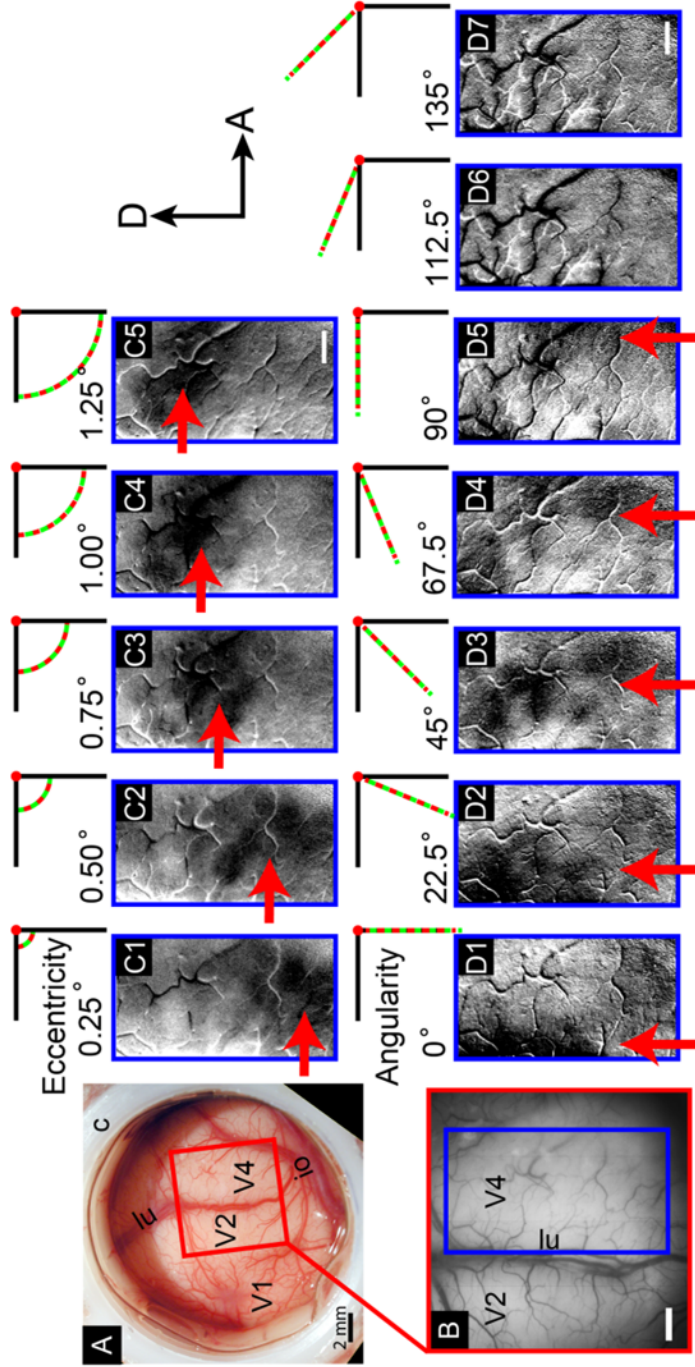


Figure 3- 1. **General retinotopic organization of central V4.**

(A) We show the imaging chamber for Subject L. The blue box approximates the location of the imaging field of view shown in panel B. The blue rectangle is the cropped area the we focus on in the difference maps shown in panels C1-C5 and D1-D7. . Images of isoeccentricity in V4 based on isoeccentric arcs of radius r . C1: $r=0.25^\circ$, C2: $r=0.50^\circ$, C3: $r=0.75^\circ$, C4: $r=1.00^\circ$, C5: $r=1.25^\circ$ and images based on isoangular bars in V4 . D1: $\Delta=0^\circ$, D2: $\Delta=22.5^\circ$, D3: $\Delta=45^\circ$, D4: $\Delta=67.5^\circ$, D5: $\Delta=90^\circ$. Data showing eccentricity and angularity are from different imaging sessions. Images are difference images of stimulus condition (arc, bar widths 0.1°) minus full field stimulus of identical parameters. Red arrows highlight the changing positions on cortex based on the changing visual stimulus eccentricity (C1-C5) of polar angle (D1-D7). Here it is possible to appreciate the general progression along the ventral-to-dorsal (increasing eccentricity) and posterior-to-anterior (increasing angularity) axes and absence of an upper visual field representation (D6-D7). Scalebar = 1mm. D: dorsal, A: anterior, lu: lunate sulcus.

Figure 4 illustrates examples of map stability for each subject across different sessions. For each subject, we align the images onto a common blood vessel map (taken under 570 nm illumination). For Subject L we present maps with areas of activity outlined acquired on consecutive days from the same 1° spot stimulus at 4.5° eccentricity (Figs. 4A1-A2). Figure 4A3 presents the overlay of the two days revealing high similarity. For Subject J we show maps that were acquired a month apart (Fig. 4B1-B2) as well as the overlay (Fig. 4B3).

Figure 5 illustrates our method for calculating cortical magnification factors. Figure 5B and 5C illustrate t-maps obtained in response to 1° diameter color spot stimuli positioned at 8.0° eccentricity (Fig. 5B) and at 6.0° eccentricity (Fig. 5C). We calculate the center of mass (CoM) for each representation (green dots). Figure 5A shows their relative positions on the vessel map. The distance between these two CoM points is used for the CMF calculation.

An additional concern is the possibility that some activation is not visible, as it may fall within sulci or extend outside the imaged field of view (FOV). This is a limitation of our approach and we address some of its possible influence on our data in the discussion. Despite this concern, we will show that our results are consistent between subjects.

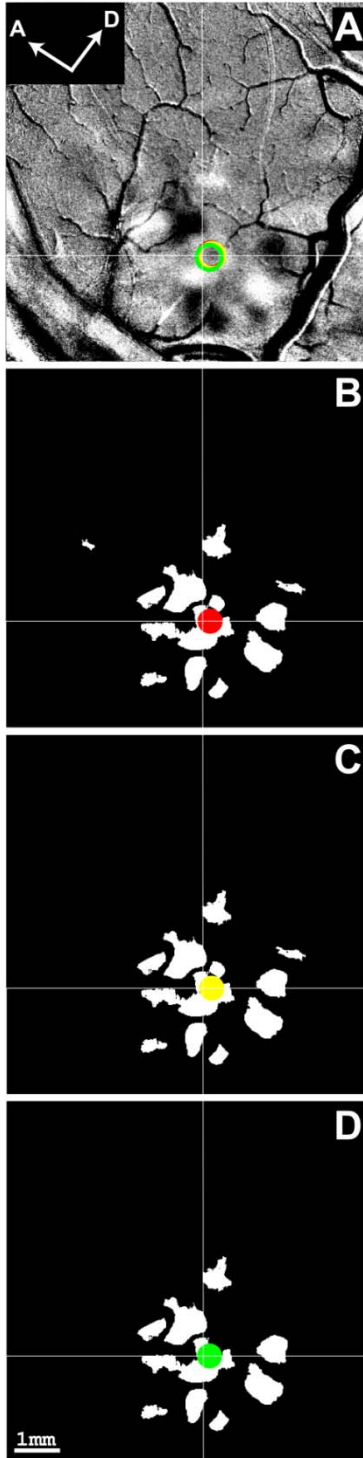


Figure 3- 2. *Stability of center of mass against different area thresholds.*

The alteration to the center of mass for the representation of a spot in V4 based on different area thresholds for removal (Fig. 2B: 100 pixels; Fig. 2C: 200 pixels; Fig. 2D: 400 pixels). The solid spots in Fig. 2B-D show the location of the calculated center-of-mass. These points are overlaid in Fig. 2 A as circles in a gray scale activation map. Note that the positions are nearly identical despite the loss of certain domains as the threshold is increased. The stability of the position demonstrates that the CoM is mainly based on the larger and more clustered domains locations. The spots used in this example are 1° in diameter. D: dorsal, A: anterior.

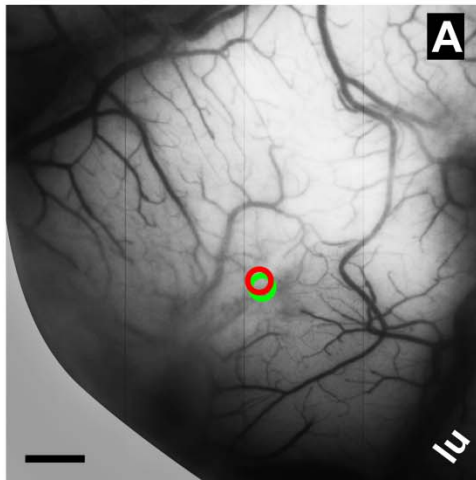
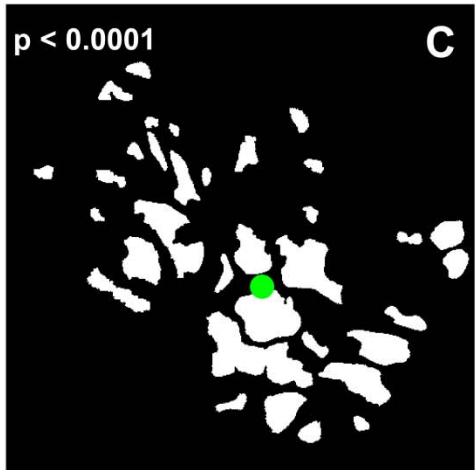
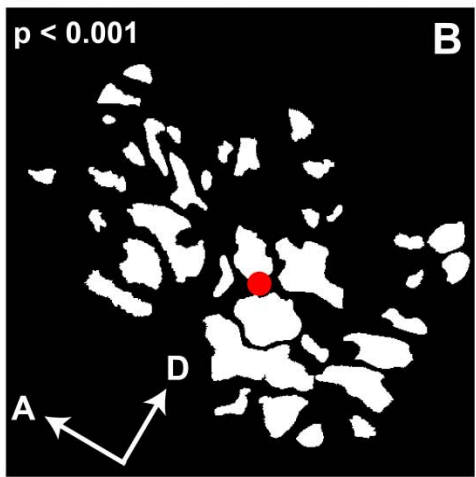


Figure 3- 3. *Stability of center of mass over different p-value thresholds.*

Here we show that within this 10 fold p-value difference (B: $p < 0.001$; C: $p < 0.0001$). The centers of mass are shown as red (B) and green (C) spots for the respective t-maps. The positions are overlaid in the green map (A). The change in the CoM position, like in area threshold in Fig. 2, is negligible. Scalebar = 1 mm. D: dorsal, A: anterior, lu: lunate sulcus.



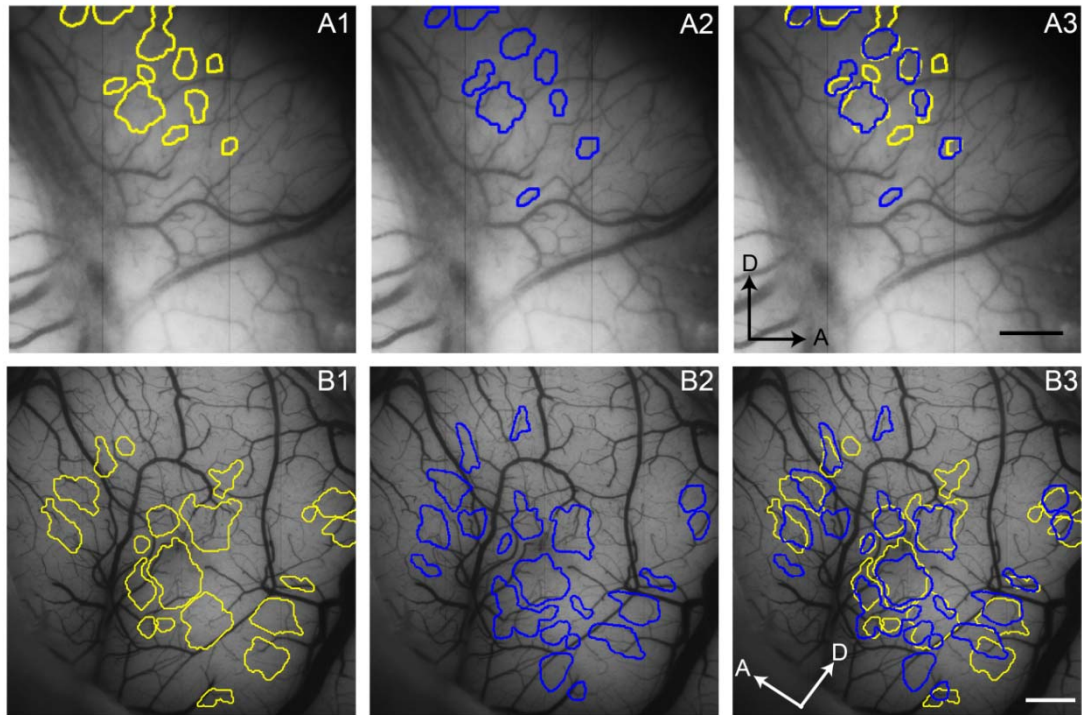


Figure 3- 4. *Stability of maps over time.*

Outlines of color preference domains from t-maps ($p < 0.001$). In row A we show the correlation of two consecutive days of imaging in Subject L, the imaging field of views have been aligned to match based on reference vessel images taken at the start of an imaging session (A1 day 1, A2 day 2, A3 overlay of day 1 and day 2). Row B illustrates t-maps for color preference as well in Subject J. The time difference here is 1 month. These images have also been aligned. Notice that similar to the consecutive day case, there is very little difference between the domain pattern over time. The outlined areas are significant color preference domains from tmaps ($p < 0.001$). The color coding is simply to differentiate between time points. Scalebar = 1 mm. D: dorsal, A: anterior, lu: lunate sulcus.

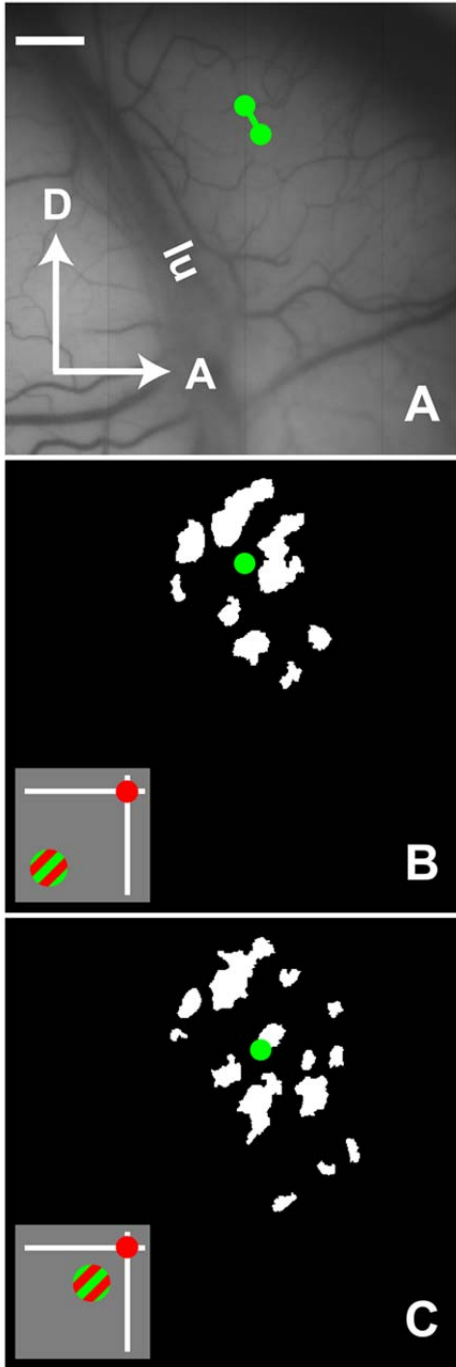


Figure 3- 5. *Center of mass of the representation of two spots in V4. T-maps of color selective regions from two different eccentricities (Fig. 4B-8.0°; Fig. 4C-6.0°).*

The green dots mark the determined center-of-mass (CoM) from each location. Figure 1A shows their relative position on a vessel maps (acquired under 532 nm light) and illustrates the use the straight line distance between the points for CoM calculation. The spots used are 1° in diameter. Bar = 1mm. D: dorsal, A: anterior, lu: lunate sulcus.

Modality-specific retinotopic organization of foveal V4

Figure 6 shows in foveal V4 of Subject L single condition color preference domains (outlined in green) and orientation preference domains (outlined in red) obtained in response to large field stimuli. As shown in Fig. 6A and previously reported (Tanigawa et al., 2010), there is an anterior-posterior bias of orientation preference (more anterior) from the color preference domains (more posterior). The difference is less distinctive in this figure than in the previous report (Tanigawa et al., 2010) because we use a lesser threshold in p-value and threshold value for our calculations. This provides the appearance of more mixture between the two due to relative increases in the domain sizes and the appearance of a few additional smaller domains than previously reported. In Fig. 6B-G we present mapped CoM positions from iso-eccentricities and iso-polar angles of isoluminant color arcs and bars or achromatic arcs and bars. CoM for eccentricities from 0.25° to 2.00° eccentricity was mapped for color (Fig. 6B, blue circles, Fig. 6D red circles) and for orientation (Fig. 6B, blue circles, Fig. 6D green circles) modalities. The two progressions appear to follow paths that are in line with the trajectory of the underlying preference domains (red and green outlines). Thus, it appears that the same visual space is represented once by color domains and again by orientation domains.

With respect to iso-polar angle representation, there is the CoM values show a progression from the vertical meridian (0°) to the horizontal meridian (90°) for both the color domains (Fig. 6E) and orientation domains (Fig. 6F). These color and orientation

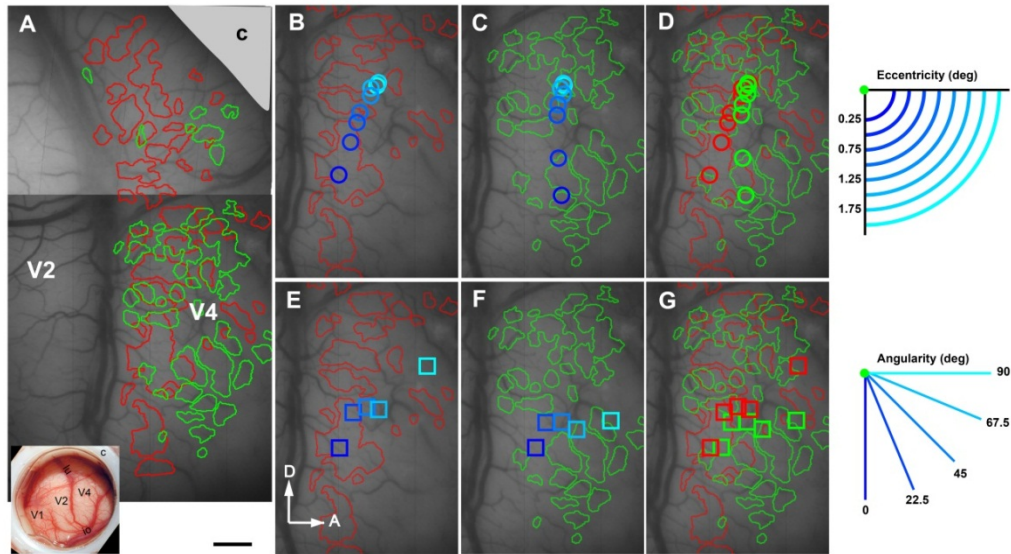


Figure 3- 6. **Center of mass representations of eccentricity and angularity.** Two imaging FOV have been combined with color selective patches (red outlines) and orientation selective patches (green outlines) overlain. In Fig. 6A, we overlay the color selective and orientation selective domains revealed from imaging cases to reveal the general distribution of orientation and color selective domains. Here we use a lower p-value than in a previous report (see text). We then calculated the CoM positions based on the distribution of domains from isoeccentric arcs are color coded in a blue gradient and plotted based on the color preference domains (B) or orientation preference domains (C). We show the overlay of both progression and match by color (red-color selective; green-orientation selective) (D). We show the same analysis for isoangular bars in E-G. Bar = 1mm. D: dorsal, A: anterior, lu: lunate sulcus.

progressions are shown overlain in Fig. 6G. The progression for color domains (red squares in Fig. 6G) show only a slight posterior and dorsal bias in their CoM positions in comparison to the orientation domain CoM positions. The exception is the horizontal meridian (90°) position where we see a departure in the dorsal ventral axis of the two points. The larger space found between the mapped 67.5° to 90° position could also reflect a discontinuity in the visual representation that is better illustrated in Fig. 7.

In Fig. 7, we find a clear example of a discontinuity in the polar angle representation transitioning from 22.5° to 45° to 67.5° for the orientation domains. The squares in Fig. 7A-C are CoM positions calculated for domains associated with the polar positions presented for color domains (red) and orientation domains (green). When we compare the progression of CoM positions from 45° (Fig. 7B) to 67.5° (Fig. 7C), the CoM positions for orientation domains (green squares) clearly have a large shift whereas the CoM shift for color domains (red squares) makes a shift similar to the transition between 22.5° (Fig. 7A) to 45° (Fig. 7B). A similar, but less dramatic increase in distance between polar angles is shown in Fig. 6 between the 67.5° and 90° positions for the color module (anterior two red squares in Fig. 6G) which could also indicate an impending discontinuity. To further illustrate the discontinuity in Fig. 7, we collapse two-dimensional representation of the domains (Figs. 7A-C) along a single axis by summing from top to bottom the significant pixels determined for orientation (green outline) or color (red outline) preference in t-maps ($p < 0.001$) are shown Figs. 7A-C.

By comparing the plots in Fig. 7D-F, the plots clearly show that the orientation domains (green lines) are absent for about a ~ 3 mm extent in Fig. 7E. Additionally there is no significant values found in the plots shown in Fig. 7D (22.5°) and Fig. 7F (67.5°) for

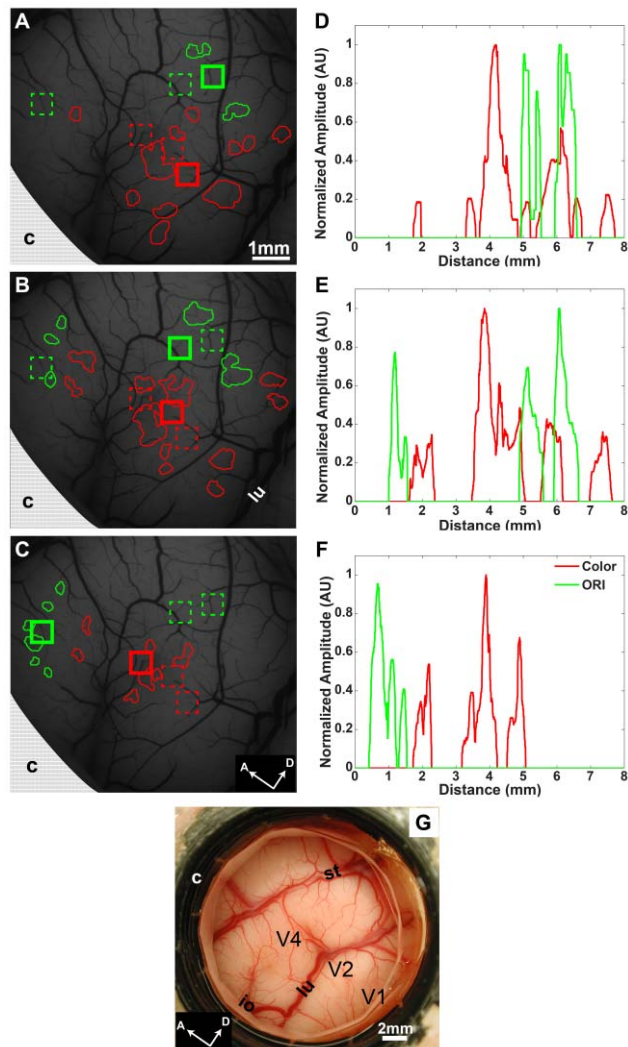


Figure 3- 7. ***Discontinuous representation of angular positions in Subject J.*** (A-C). Color (red) and orientation (green) domain outlines and CoM positions (red and green squares) for bars at 22.5 (A), 45 (B), and 67.5 (C) degree polar positions. The solid line squares denote the current CoM for the image and polar position. The dotted line squares denote the other positions and are placed in each image for reference. D-F. To highlight the gap between the representations of the orientation domains, we collapse the binary versions of the outlined domains that were based on t-maps where the domains are assigned a 1 and the remainder of the images is a 0. We then sum down the columns to arrive at the corresponding plots directly to the right of each image. We also illustrate the effect of the discontinuous representation by showing that at the transition where the discontinuity occurs (45deg to 67.5deg) there is a large increase in the relative distance between the CoM positions. (G) Imaging chamber for Subject J. Bar = 1 mm. D: dorsal, A: anterior, lu: lunate sulcus.

the region where there is a 3mm absence of significant domains in Fig. 7E. This large gap can be attributed to the intervening color module (Fig. 7A-C, red outlines; Fig. 7D-F red lines). Thus within this region of cortex, color domain representation appears to shift continuously, while orientation domain representation exhibits a discontinuity.

Modality-specific cortical magnification

Based on the individual color or orientation modality CoM values, we examined the feature-specific cortical magnification factors (CMF). We aimed to determine if CMF values for the bands of color and orientation modules were similar or different.

In Fig. 8A we plot CMF values calculated based on neighboring polar angle representations for color (red squares) and orientation (green squares) for Subject L. We do the same for eccentricity (Fig. 8B). The CMF vs. eccentricity values from bands of color and orientation modules show trends that are nearly identical for Subject L. For Subject J, we perform the same analysis and find the same relationship between the color and orientation bands. In the CMF vs. polar angle plot for Subject J (Fig. 9A), the increase in the CMF value at 45° is due to the discontinuity (see Fig. 7). In Fig. 10 we compare the curves *between subjects* (purple: Subject J, blue: Subject L), for color modules (Fig. 10A) and for orientation modules (Fig. 10B), the values remain nearly identical. When we compare between CMF and polar angle between subjects (purple: Subject J, blue: Subject L), we find that the major difference come at the CMF for 45° where there is the discontinuity. In Fig. 9 we show the fitted equations. The power coefficient from the linear trend on the regressive log-log plots for orientation is 0.951 for both subjects. It is notable that the R^2 values for fits associated with orientation bands are lower than those associated with color bands. There are two likely contributing factors.

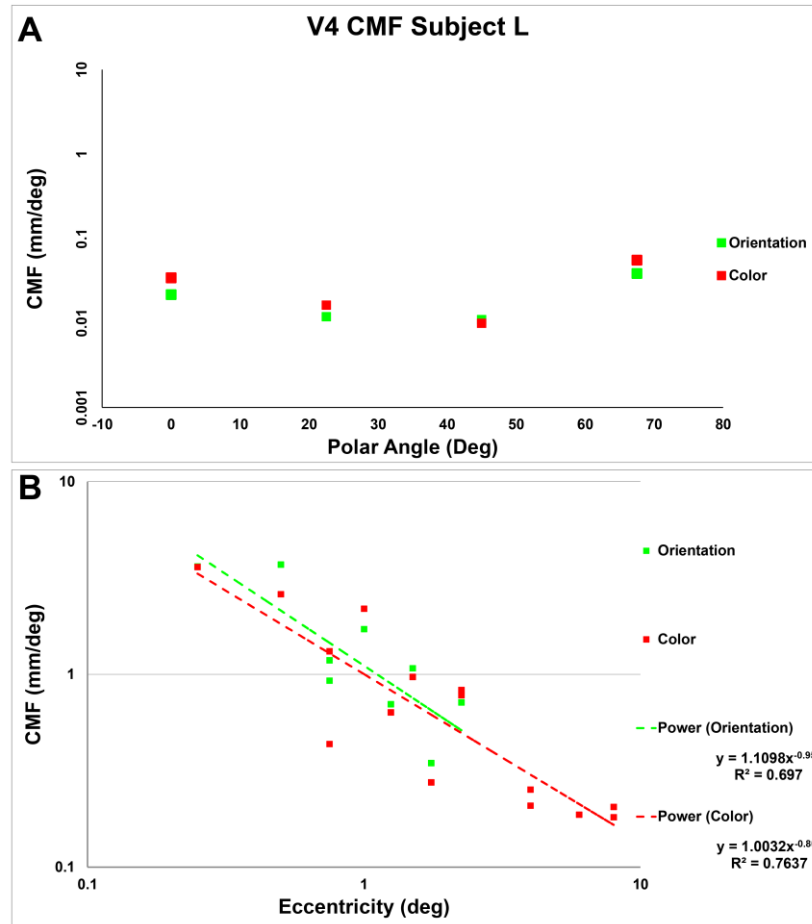


Figure 3- 8. *Modular comparison of cortical magnification for Subject L.*

We calculate and plot CMF as a function of polar angle (A) and eccentricity (B). The resulting curves for color and orientation features are very similar. Figure 8A shows a rather flat line with the ends having slightly greater CMF values. The increases in values could signal partial representation from limited field of view or indications of a discontinuity (see Fig. 6). Red squares: color. Green squares: orientation.

First is that the orientation domains were often revealed nearer to the edge of the imaging windows we used (see green outlines of upper imaging panel of Fig. 6A and green outlines of Fig. 7). Second is, with the exception of the foveal window of Subject L (main imaging panel shown throughout Fig. 6) there tended to be fewer orientation domains revealed. However, despite these challenges, we found highly similar trends for both subjects. For color, the power coefficients are 0.859 (Subject J) and 0.866 (Subject L). Previous reports for macaque V4 power coefficients derived from CMF vs. eccentricity in regressive log-log plots not considering modularity reported a value of 0.9 (Gattass et al., 1988) very similar to the value reported here. The consistency of the power of the curves between the two modules is an indication that these are a part of a single area and also implies that we are likely sampling from a similar parts of cortex.

Discussion

Summary

In this study we investigated the influence of modularity on visual topography of V4 in awake macaques. Using our awake IOI preparation, we are able to evaluate highly central representations of V4. In V4 we find that bands of color and orientation modules with similar CMF relationships. The color and orientation modality specific representation of the visual field that have similar CMF values is analogous to V2 stripes and suggests that such visuotopic relationships are a common strategy used by visual areas to more efficiently process information.

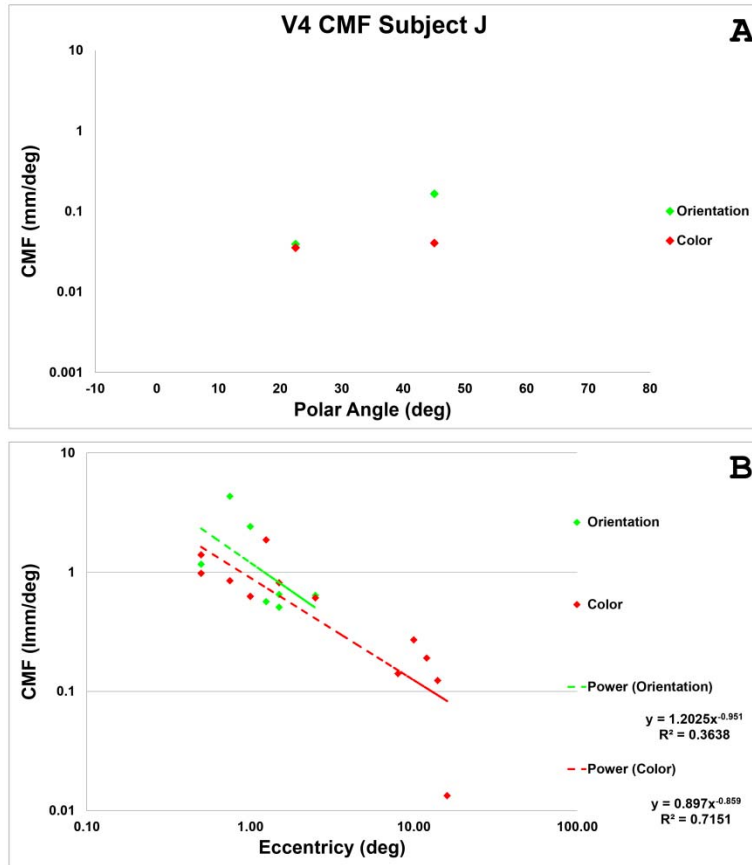


Figure 3- 9. *Modular comparison of cortical magnification for Subject J.*

Similar to Fig. 8 we calculate and plot CMF as a function of polar angle (A) and eccentricity (B). The resulting curves for color and orientation features are very similar just as in Subject L in Fig. 8. Here we only have two points available for the polar angle plot because our imaging window and data set were limited to three samples of polar angles (see Fig. 6). Red diamonds: color. Green diamonds: Orientation.

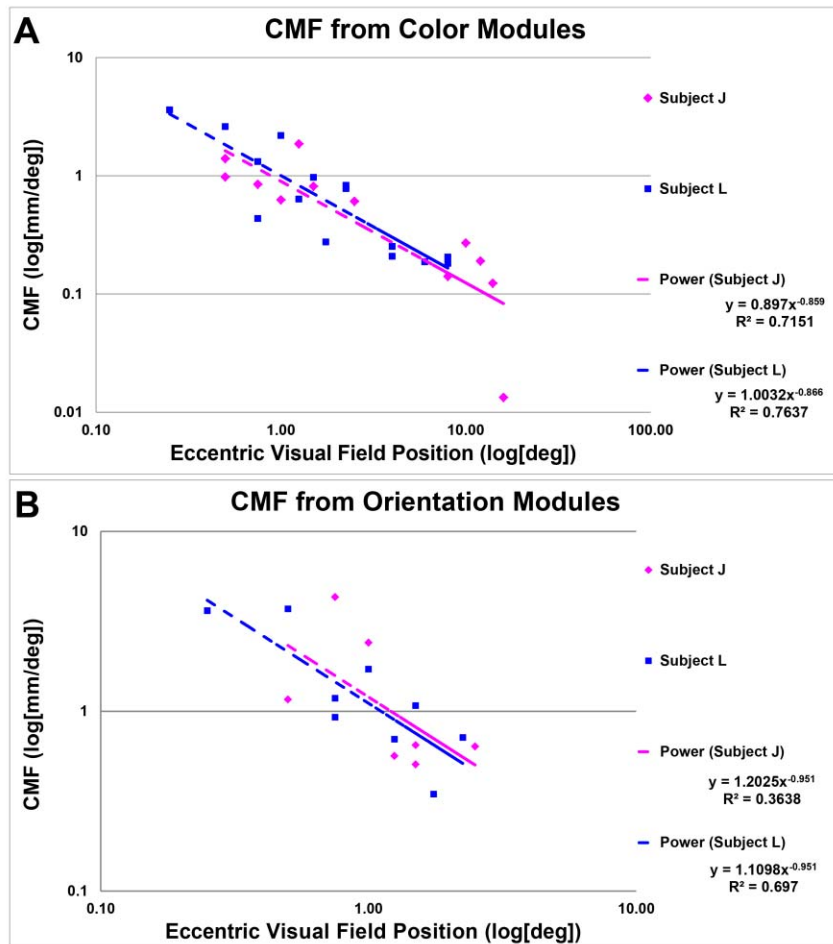


Figure 3- 10. *Comparison of cortical magnification factor vs eccentricity between Subject L and J.*

We compare the CMF vs. eccentricity curves for color (A) and orientation (B). The trends in both plots are nearly identical. The fitted curves related to each subject is displayed directly below the associated legend. Purple diamonds: Subject J. Blue squares: Subject L.

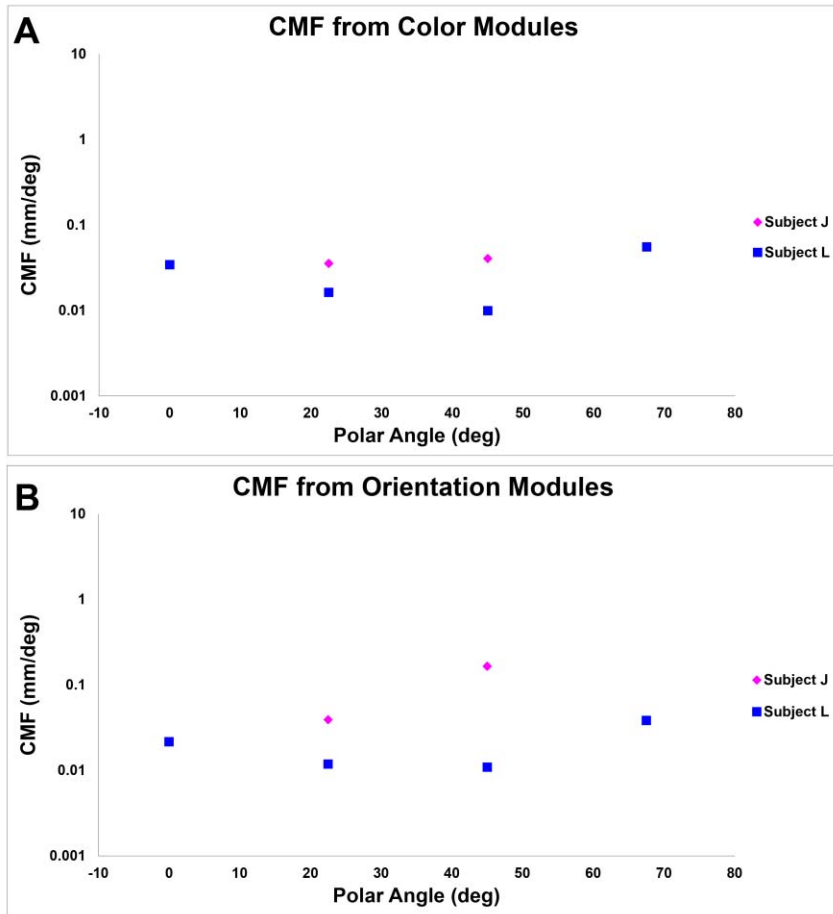


Figure 3- 11. *Comparison of cortical magnification factor vs. polar angle between Subject L and J.*
 We compare the CMF vs. polar angle values for color (A) and orientation (B). The values for the most part fairly flat in both panels but those coming from Subject J is slightly higher for the matching points when compared to Subject L. Purple diamonds: Subject J. Blue squares: Subject L.

Modular level visual field representations in foveal V4

Qualitatively, the representations in Fig. 1 of eccentricity and polar angles in the lower visual field representation of foveal V4 are compatible with previous reports of V4 topography (e.g. Brewer et al., 2002; Fize et al., 2003; Gattass et al., 1988; Kolster et al., 2009; Pinon et al., 1998). Specifically that from posterior to anterior parts of V4, there is a progression of polar representations from the vertical meridian to the horizontal meridian and that in the superior half of V4 that more central visual representations are found more ventrally more peripheral representations are found more dorsally. Our non-modality specific activation maps in Fig. 1 show a patchy substructure, that reflects underlying functional domains structure within V4. V4 was shown to have modular attributes that have definable regions for color and orientation preference (Tanigawa et al., 2010). This is consistent with previous suggestions of V4 modularity using IOI (Ghose and Ts'o, 1997), fMRI (Conway et al., 2007), and anatomical tracers (Felleman et al., 1997a; Xiao et al., 1999; Zeki and Shipp, 1989). In V1 OD columns repeat representation of the visual field (Blasdel and Fitzpatrick, 1984) as do V2 stripes (Roe and Ts'o, 1995). These repeated representations also result in similar CMF values between the respective divisions. The re-representation of visual space in the bands of color and orientation domains in V4 was previously presented in these subjects (see Fig. 4 in Tanigawa et al., 2010). In Fig. 6 and 7 we show color and orientation modality specific representation of visual field positions in V4 as CoM positions.

The nature of the angular coverage potentially makes proper identification of VM and HM representations problematic in foveal V4 in the absence of IOI like information. This could also true of other parts of V4 as well. Our data clearly demonstrate that a given area

of cortex can respond over a wide polar range as well as several degrees of eccentricity and that in some regions there can be 3 mm gaps between neighboring polar representations of the visual field for a single modality (see green outlines and squares of Fig. 7). Although we only report color and orientation feature modules for macaque V4, using IOI, a motion direction map in V4 have also been suggested (Li et al., 2011). Given that the organization of color and orientation domains is at least partially interleaved and not completely segregated in select areas (see Fig. 6 and 7), it would be entirely possible to find more than one partial HM and/or VM representation. However they would not be reversals as is seen between V1 and V2 or V2 and V3. Instead there would be two or more all with similar progression anterior to posterior progression for the vertical to horizontal meridian. This possible confound could have also contributed (although admittedly tenuous) to evidence for anterior-posterior separations of V4, like the proposed V4/V4A division (Stepniewska et al., 2005; Zeki, 1971). It is also possible that such potential uncertainty has contributed to the various proposals regarding V4 extent (e.g. Maguire and Baizer, 1984; Pigarev et al., 2002; Stepniewska et al., 2005; Youakim et al., 2001; Zeki, 1971).

Center of Mass

One of the issues we have addressed throughout this work is a concern of using a center of mass value when we are limited in our FOV. First we point out that despite that concern that we show highly similar measures of CMF in the two subjects as presented in Fig. 9. Another factor that supports our CMF measures is the similarity in the power coefficients found in this study and previous studies (Gattass et al., 1988) in V4. This all implies that despite possible issues due to FOV limitations, our analysis and

interpretation of our OIS images ultimately provides useful and important information regarding properties of V4. This might not be true if we could not evoke strong IOI activation of appropriate cortical locations resulting in consistent t-maps over time (Fig. 3). The robustness of the method is also evidenced by the consistent CoM positions we find (Fig. 2) despite the 5 fold change in minimum pixel area value.

Cortical Magnification of foveal V4

We calculated the CMF for eccentricity and polar angle and plotted their distribution on a log-log plot (Figs. 7-11). The CMF vs. eccentric trends, between the bands of color and orientation modules, are very similar in both Subject L (power coefficient for orientation: 0.951, power coefficient for color: 0.866) and Subject J (power coefficient for orientation: 0.951, power coefficient for color: 0.859). These values are favorable to the power coefficient of 0.9 found previously in macaque V4 (Gattass et al., 1988). It is even more so if we pool the points for color and orientation within each subject and recalculate the linear regression (plot not shown). We find the power coefficient to be 0.9 in Subject L and 0.908 in Subject J when we ignore functional modality. The slightly lower value for the power coefficient associated with the color band might suggest that the value is associated with a neighboring visual area and not a module of V4. However Gattass et al. (1988) reported a power coefficient of 0.74 for V3, considerably lower than the power coefficient reported for color in the current study. Interestingly, the power coefficient for V4 of MT (0.68-0.98) (Fiorani et al., 1989) but we are well away from this region.

While most of our CMF values do fall within the scatter range of previous reports, our final fitted values curve suggests CMF values smaller by a constant scaling factor of 3 to

those reported (Gattass et al., 1988; Pinon et al., 1998). One weaker possibility for the discrepancy is the location of V4 we are sampling tends to provide values on the lower range of CMF values one can expect if we sampled all of V4 using IOI. For instance if it were possible to apply the same IOI method in the lunate, we might find CMF values a few multiples larger bringing the CMF values closer in terms of magnitude. However a logical reason why one part of V4 would produce different CMF values from another, other than sample variance, seems unlikely so we find this possibility more remote. A more analytical reason is the existence of repeated visuotopic positions that are factored into our CoM calculation. In a traditional linear interpolation model of the visuotopic map, repeated visuotopic positions are eliminated. The effect of our including these responses would be the dilution of distances. In terms of a more traditional single global mapping of the visual field to produce CMF measures, we would be closest to reporting a lower bound for the cortical magnification factors in V4.

The visuotopy, measured by CoM, implies a pronounced anisotropy in V4. If we just consider Figure 1, approximately 3.25 mm of cortex, some part of the the entire angular range (0° to 90°) can be found. But to represent 2° of eccentricity, a span of around 4 mm is needed. This observation suggests that there is an anisotropy ratio between CMF for eccentricity and CMF for polar angle of ~ 56 for this area of cortex. If we calculate the CMF value at 0.25° eccentricity using one of the fitted equations for color and the mean values found in Fig. 12, the anisotropy ratio is on the order of ~ 83 . This is a rather large value. One of the issues that could be contributing to this large ratio is the the compression effect we mentioned previously. It is unclear if the compression factor is the same or different between eccentricity and polar angles. Thus a direct comparison may

not be appropriate. However if we assume a direct ratio is acceptable, and determine the anisotropy at 2° eccentricity we find the ratio is ~14-15 depending on which power coefficient we use (see Fig. 10). While not specifically calculated in this manner, using the map presented by Gattass et al. (1988) we can make an estimate. For the 2° iso-eccentricity in the dorsal half of V4 and assuming that there is a full polar representation between the borders of the lunate and superior temporal sulci, which would be reasonable based on our data, then along that path there is up to roughly 8 mm representing 90° of polar angle. Using their equation for CMF and the polar angle CMF of 8 mm/90° we estimate the anisotropy ratio for would be ~18 at this position based on Gattass et al. (1988) indicating that the ratios we are finding are not out of line with previous measurements. The anisotropy suggests that the information along the polar angle component is highly compressed at the central most parts of V4. In V1 anisotropy foveal anisotropy has been measured to be as high as 1.5:1 (Dow et al., 1985; Tootell et al., 1982). More peripherally, V1 anisotropy has been reported as isotropic (Hubel and Freeman, 1977; Hubel and Wiesel, 1977; LeVay et al., 1975). In V2, anisotropy for a single stripe is 2:1 and 6:1 if we ignore stripes (Roe and Ts'o 1995). The increasing levels of anisotropy from V1 to V2 to V4 in central representations of visual areas might suggest integration of information across iso-eccentric positions is a component of visual processing.

By calculating the CoM we presume that multiple parts of cortex respond to a given visual field position and that their contribution is important in the evaluation of local cortical magnification. It is worth noting that for V1, the cortical magnification factor trend for macaques is smaller by a factor of 3.6 when compared to humans (Schira et al.,

2007). However the reported values for CMF as a function of eccentricity between human V4 (Harvey and Dumoulin, 2011), CMF previously reported for macaque V4 (Gattass et al., 1988), and CMF values reported for cebus monkeys (Pinon et al., 1998) are similar. Why there would be this interspecies consistency in V4 and not V1 is an interesting phenomenon. One possibility is that this could simply be a trait of higher order primate visual areas that the cortical area devoted to different modalities converge among primate species. Alternatively, the perceived consistency among various species could be a result of linear interpolation model. This can be understood by reviewing the presented data in this manuscript. Our data shows that polar positions can clearly repeat between bands of color and orientation modules. The factor of 3 difference in our CMF value when compared to previous reports can be explained based on local repeating of visual representations within the bands of orientation and color modules themselves. If the distinct points between locations of V4 visuotopic positions are rather large due to the relative receptive field sizes and scatter, the effect of these factors might be enough to cause a macroscopic view of the visuotopic representation of V4 to appear more similar across species with regard to CMF values.

Conclusion

We show detailed topographic mapping of highly foveal aspects of V4. Using centers of mass points we are able to map the progression of visual field representations and calculate the cortical magnification to assess the cortical territory devoted to each modality. We find that the CMF values for color and orientation modalities in V4 to be nearly identical both within and between the two subjects. This visuotopic relationship

between bands of V4 modules is similar to that found between V2 stripes and V1 OD columns and indicate that such visuotopic relationships are a common strategy used by many, if not all, visual areas to more efficiently process information.

References

- Blasdel GG, Fitzpatrick D. 1984. Physiological organization of layer 4 in macaque striate cortex. *The Journal of neuroscience : the official journal of the Society for Neuroscience* 4(3):880-895.
- Brewer AA, Press WA, Logothetis NK, Wandell BA. 2002. Visual areas in macaque cortex measured using functional magnetic resonance imaging. *J Neurosci* 22(23):10416-10426.
- Conway BR, Moeller S, Tsao DY. 2007. Specialized color modules in macaque extrastriate cortex. *Neuron* 56(3):560-573.
- Daniel PM, Whitteridge D. 1961. The representation of the visual field on the cerebral cortex in monkeys. *The Journal of physiology* 159:203-221.
- Dow BM, Vautin RG, Bauer R. 1985. The mapping of visual space onto foveal striate cortex in the macaque monkey. *The Journal of neuroscience : the official journal of the Society for Neuroscience* 5(4):890-902.
- Fan RH, Baldwin MK, Jermakowicz WJ, Casagrande VA, Kaas JH, Roe AW. 2012. Intrinsic signal optical imaging evidence for dorsal V3 in the prosimian galago (*Otolemur garnettii*). *The Journal of comparative neurology*.
- Felleman DJ, Burkhalter A, Van Essen DC. 1997a. Cortical connections of areas V3 and VP of macaque monkey extrastriate visual cortex. *J Comp Neurol* 379(1):21-47.
- Felleman DJ, Xiao Y, McClendon E. 1997b. Modular organization of occipito-temporal pathways: cortical connections between visual area 4 and visual area 2 and posterior inferotemporal ventral area in macaque monkeys. *The Journal of neuroscience : the official journal of the Society for Neuroscience* 17(9):3185-3200.
- Fiorani M, Jr., Gattass R, Rosa MG, Sousa AP. 1989. Visual area MT in the Cebus monkey: location, visuotopic organization, and variability. *The Journal of comparative neurology* 287(1):98-118.
- Fize D, Vanduffel W, Nelissen K, Denys K, Chef d'Hotel C, Faugeras O, Orban GA. 2003. The retinotopic organization of primate dorsal V4 and surrounding areas: A functional magnetic resonance imaging study in awake monkeys. *The Journal of neuroscience : the official journal of the Society for Neuroscience* 23(19):7395-7406.
- Gattass R, Sousa AP, Gross CG. 1988. Visuotopic organization and extent of V3 and V4 of the macaque. *J Neurosci* 8(6):1831-1845.

- Ghose GM, Ts'o DY. 1997. Form processing modules in primate area V4. *J Neurophysiol* 77(4):2191-2196.
- Harvey BM, Dumoulin SO. 2011. The relationship between cortical magnification factor and population receptive field size in human visual cortex: constancies in cortical architecture. *The Journal of neuroscience : the official journal of the Society for Neuroscience* 31(38):13604-13612.
- Hubel DH, Freeman DC. 1977. Projection into the visual field of ocular dominance columns in macaque monkey. *Brain research* 122(2):336-343.
- Hubel DH, Wiesel TN. 1974a. Sequence regularity and geometry of orientation columns in the monkey striate cortex. *The Journal of comparative neurology* 158(3):267-293.
- Hubel DH, Wiesel TN. 1974b. Uniformity of monkey striate cortex: a parallel relationship between field size, scatter, and magnification factor. *The Journal of comparative neurology* 158(3):295-305.
- Hubel DH, Wiesel TN. 1977. Ferrier lecture. Functional architecture of macaque monkey visual cortex. *Proc R Soc Lond B Biol Sci* 198(1130):1-59.
- Kolster H, Mandeville JB, Arsenault JT, Ekstrom LB, Wald LL, Vanduffel W. 2009. Visual field map clusters in macaque extrastriate visual cortex. *The Journal of neuroscience : the official journal of the Society for Neuroscience* 29(21):7031-7039.
- LeVay S, Connolly M, Houde J, Van Essen DC. 1985. The complete pattern of ocular dominance stripes in the striate cortex and visual field of the macaque monkey. *The Journal of neuroscience : the official journal of the Society for Neuroscience* 5(2):486-501.
- LeVay S, Hubel DH, Wiesel TN. 1975. The pattern of ocular dominance columns in macaque visual cortex revealed by a reduced silver stain. *The Journal of comparative neurology* 159(4):559-576.
- Li P, Chen M, Han C, Zhu S, Xu H, Roe AW, Lu HD. A motion direction map in macaque V4; 2011 November 12 -16, 2011; Washington, DC, USA.
- Lu HD, Roe AW. 2007. Optical imaging of contrast response in Macaque monkey V1 and V2. *Cereb Cortex* 17(11):2675-2695.
- Maguire WM, Baizer JS. 1984. Visuotopic organization of the prelunate gyrus in rhesus monkey. *The Journal of neuroscience : the official journal of the Society for Neuroscience* 4(7):1690-1704.

- Motter BC. 2009. Central V4 receptive fields are scaled by the V1 cortical magnification and correspond to a constant-sized sampling of the V1 surface. *J Neurosci* 29(18):5749-5757.
- Pigarev IN, Nothdurft HC, Kastner S. 2002. Neurons with radial receptive fields in monkey area V4A: evidence of a subdivision of prelunate gyrus based on neuronal response properties. *Experimental brain research Experimentelle Hirnforschung Experimentation cerebrale* 145(2):199-206.
- Pinon MC, Gattass R, Sousa AP. 1998. Area V4 in Cebus monkey: extent and visuotopic organization. *Cerebral cortex* 8(8):685-701.
- Rasband WS. 1997-2008. ImageJ. U S National Institutes of Health <http://rsb.info.nih.gov/ij/>.
- Roe AW. 2007. Long-term optical imaging of intrinsic signals in anesthetized and awake monkeys. *Appl Opt* 46(10):1872-1880.
- Roe AW, Ts'o DY. 1995. Visual topography in primate V2: multiple representation across functional stripes. *J Neurosci* 15(5 Pt 2):3689-3715.
- Rosa MG, Schmid LM. 1995. Magnification factors, receptive field images and point-image size in the superior colliculus of flying foxes: comparison with the primary visual cortex. *Experimental brain research Experimentelle Hirnforschung Experimentation cerebrale* 102(3):551-556.
- Schira MM, Wade AR, Tyler CW. 2007. Two-dimensional mapping of the central and parafoveal visual field to human visual cortex. *Journal of neurophysiology* 97(6):4284-4295.
- Shipp S, Zeki S. 2002. The functional organization of area V2, II: the impact of stripes on visual topography. *Visual neuroscience* 19(2):211-231.
- Stepniewska I, Collins CE, Kaas JH. 2005. Reappraisal of DL/V4 boundaries based on connectivity patterns of dorsolateral visual cortex in macaques. *Cereb Cortex* 15(6):809-822.
- Tanigawa H, Lu HD, Roe AW. 2010. Functional organization for color and orientation in macaque V4. *Nat Neurosci* 13(12):1542-1548.
- Tootell RB, Silverman MS, Switkes E, De Valois RL. 1982. Deoxyglucose analysis of retinotopic organization in primate striate cortex. *Science* 218(4575):902-904.
- Tsunoda K, Yamane Y, Nishizaki M, Tanifuji M. 2001. Complex objects are represented in macaque inferotemporal cortex by the combination of feature columns. *Nature neuroscience* 4(8):832-838.

- Van Essen DC, Newsome WT, Maunsell JH. 1984. The visual field representation in striate cortex of the macaque monkey: asymmetries, anisotropies, and individual variability. *Vision Res* 24(5):429-448.
- Xiao Y, Zych A, Felleman DJ. 1999. Segregation and convergence of functionally defined V2 thin stripe and interstripe compartment projections to area V4 of macaques. *Cerebral cortex* 9(8):792-804.
- Xu X, Bosking WH, White LE, Fitzpatrick D, Casagrande VA. 2005. Functional organization of visual cortex in the prosimian bush baby revealed by optical imaging of intrinsic signals. *J Neurophysiol* 94(4):2748-2762.
- Youakim M, Bender DB, Baizer JS. 2001. Vertical meridian representation on the prelunate gyrus in area V4 of macaque. *Brain Res* 56(2):93-100.
- Zeki S, Shipp S. 1989. Modular Connections between Areas V2 and V4 of Macaque Monkey Visual Cortex. *The European journal of neuroscience* 1(5):494-506.
- Zeki SM. 1971. Cortical projections from two prestriate areas in the monkey. *Brain Res* 34(1):19-35.

CHAPTER IV

SIZE AND SPATIAL FREQUENCY PREFERNCES OF V4 MODULES

Abstract

While there have been studies conducted in V4 establishing preferences to visual stimulus parameters such as stimulus size and spatial frequency, these studies have been conducted with limited information about potential modular organizational features. We address this problem by studying the effect of spot diameter size and spatial frequency within color and orientation preference modules revealed by intrinsic signal optical imaging. For size, we found that surround suppression in orientation domains tended to be greater than color domains in V4. We also report a bimodal distribution in our optical imaging signal to spatial frequency in both color and orientation selective domains of V4. For both domains, and at all eccentricities tested (0.5, 0.75, 4.5°), we find a persistent peak around 1 cycles/° and a second peak that around 12 cycles/° at 0.5° eccentricity and reduces with increasing eccentricity. This bimodal distribution for SF response relvealing an interesting low and high pass frequency processing ability in V4.

Introduction

An accurate depiction of functional preferences is critical to understanding a visual area. While we have characterized a variety of stimulus features in V4 (Desimone and Schein, 1987; Gallant et al., 1993; Gallant et al., 1996; Hegde and Van Essen, 2005; Heywood et al., 1992; Hinkle and Connor, 2001; Pasupathy and Connor, 1999; 2001; 2002; Roe et al., 2012: Review; Zeki, 1973), we have not studied them as they relate to the individual functional modalities in V4.

In V1 and V2, possible variations in functional preferences are aided by known histological divisions. For instance, spatial frequency responses have been demonstrated to be mapped orderly onto V1 (see Harvey and Dumoulin, 2011; Xu et al., 2007; Yu et al., 2005). But there are studies that demonstrate possible differences exist between the blobs and interblob regions (Born and Tootell, 1991; Edwards et al., 1995). The proposed blob and interblob associations with spatial frequency are possible because cytochrome oxidase (CO) staining reveals V1 blobs and interblobs in which are historically used to help differentiate information for color (blob), form (interblob), and disparity (diffusely distributed in layer 4B). These divisions are proposed to continue into the CO definable thin (color processing), pale (form processing), and thick (disparity) stripes of V2 (Livingstone and Hubel, 1988; however see Sincich and Horton, 2005). With the aid of intrinsic signal optical imaging (IOI), the functional associations with CO stripes in V2 can be revealed without the aid of histological staining (Lu and Roe, 2008). While there is no synonymous anatomical marker in V4 that reveals such divisions, IOI can reveal bands of color and orientation modules (Ghose and Ts'o, 1997; Tanigawa et al., 2010). There have been previous reports in V4 regarding stimulus size and spatial frequency

(Desimone and Schein, 1987; Kumano et al., 2008; Pollen et al., 2002; Schein and Desimone, 1990). However, with the ability to distinguish regions of V4 that have clear color or orientation preferences, it would be of significant interest to examine if these functional domains in V4 differ in their response to changing the size or the spatial frequency of a given visual stimulus.

Here we report the effect of stimulus size and SF, based on IOI studies, for color preference domains and orientation preference domains as separate modular entities. We find that the peak change in IOI signal based on stimulus spot diameter does not appear dependent on feature domain however there does appear to be greater depression of IOI signal from orientation domains when compared to color domains at a given eccentricity. We also report that, in general, the color preference domains and orientation domains have similar peak SF at different eccentricities but are not identical with the main difference being the tuning of SF from orientation domains tend to slightly sharper. Finally we find that are spatial frequency data from V4 of both preference domains are best fitted to a bimodal Gaussian, a finding that indicates the possible presence of low and high pass frequency processing units.

Materials and methods

Intrinsic signal optical imaging (IOI) was used to evaluate V4 response to changes in stimulus spot size and grating spatial frequency at various eccentricities in 2 adult rhesus macaques. All procedures are approved by the Vanderbilt University Institute for Animal Care and Use Committee and are in accordance with the National Institute of Health guidelines.

Animal preparation

The procedures for animal preparation have been previously described (Tanigawa et al. 2010). Prior to imaging, two adult rhesus monkeys (*Macaca mulatta*, 5 and 8 kg, respectively) were trained to fixate for the length of an imaging acquisition (4 sec.). Error trials were any trial where the subject did not fixate within the prescribed fixation window (0.75° radius) or mistakenly saccaded to the presented stimulus. After training, the subject was anesthetized and a chronic nylon imaging chamber (Roe, 2007) was placed over dorsal V4 under sterile surgical conditions. Native dura in the chamber was replaced with a clear artificial dura (Tecoflex, Thermedics Polymer Products). The chamber was sealed with a nylon cap and opened under sterile conditions for image acquisition. The chamber was located on the right hemisphere of one monkey (Subject L) and on the left hemisphere of another (Subject J).

Optical imaging in awake, fixating animal

The two macaques subjects were trained to sit calmly and fixate on a single spot (0.15°) displayed on a CRT monitor 118 or 140 cm away. An infrared eye tracker (RK-801, ISCAN, or iView X, SensoMotoric Instruments) monitored the eye position in order to maintain a fixation window radius of less than 0.75° . Error trials were any trial where the subject did not fixate within the prescribed fixation window (0.75° radius) or mistakenly saccaded to the presented stimulus. The macaque subjects were required to fixate continuously for 4 sec (the duration of image acquisition). Positive reinforcement was provided with a drop of juice for a successful trial. Image acquisition began after the macaque subjected achieved a consistent success rate of 90%. Images were collected by an Imager 3001 system (Optical Imaging, Germantown, NY) which included the

VDAQ/NT data acquisition software and the 1M60P Dalsa CCD camera. Surface vessel patterns were collected for every *in vivo* imaging study under 570 nm illumination. We collected IOI data under 630 nm illumination at 4 Hz. The image matrix was set to 512x512 and the lens combination provided a field of view of 8 mm x 8 mm. Image acquisition included a 0.5 sec. pre-stimulus period, followed by 3.5 sec. stimulus presentation period. Each experiment contained 4–16 stimulus conditions and one blank condition (no stimulus except fixation point); each condition was repeated 40–100 times, pseudo-randomly interleaved with an inter-trial interval of 2 - 12 sec. The length of ISI did not affect our findings (see Tanigawa et al., 2010, supplementary Fig. 6). Only trials with successful fixation throughout were analyzed.

Visual stimuli

Visual stimuli were created using VSG 2/5 or ViSaGe (Cambridge Research Systems) and presented on a CRT monitor gamma corrected using a photometer (Minolta Chroma Meter CS-100, Ramsey). Stimuli consisted of circular patches of various diameters typically displaying red/green or black/white oriented drifting square wave or sine wave gratings at various spatial frequencies (SF). To assess the effect of size, we fixed the visual field position and other parameters and only varied the diameter of the stimulus. In 15 imaging cases (8 color preference tests, 7 orientation preference tests), we tested stimulus spot sizes of 0.25, 0.50, 1.00, 2.00, 4.00, 6.00, 8.00, and 10.0° in diameter. For stimulus diameter size comparisons, we tested multiple diameters at various visual field eccentricities of 0.5, 0.75, 2.0, 4.5, and 6.0°. In many of the cases, full screen versions of the stimuli were also presented. Similarly, to examine the effect of SF we fixed the visual field position and other parameters and only varied the SF. In 14

imaging cases (6 color preference tests, 8 orientation preference tests), we tested SF of 0.125, 0.250, 1.00, 2.00, 4.00, 8.00, and 16.0 cycles/° (cpd). To test the effects of SF at different eccentricities, we tested visual field eccentricities of 0.50, 0.75, 4.5, and 8.0°. The SF data are presented two ways. First, the data are analyzed within a single eccentric location. Second, the data are analyzed into two major groups, a “foveal” group, which we define as eccentricities equal to 2° or less, and a “parafoveal” group, which is data composed of eccentricities larger than 2°. The cutoff of 2° was chosen to emphasize the most foveal components of our V4 data. For the 8.0° eccentricity data there is no case where more than 3 different SF values were collected and so is not presented as a separate entity. The stimuli drifting directions was randomized on every trial. Gratings had an average luminance of $26.8 \text{ cd}\cdot\text{m}^{-2}$, identical to the background luminance.

Data analysis

Image frames were analyzed offline using custom software written in MATLAB (Mathworks, Natick, MA). Prior to other analysis, we performed a correlation based rigid registration of the all imaging frames within trials of interest. After registration, single condition maps, differential condition maps, and t-maps were generated. These maps were used to determine locations to assess changes in imaging signal. We have previously described the calculation of such maps and describe them briefly here (see Lu and Roe, 2007; Tanigawa et al., 2010).

Single condition and difference maps. For all maps, we first removed global non stimulus-specific signals (see Tanigawa et al., 2010). This was done by convolving individual imaging frames with a 1.875 mm x 1.875 mm to 3.125 mm x 3.125 mm median filter and subtracting it from the original unfiltered frame. For single condition

maps, image frames were then averaged over time points 1.25 sec – 4 sec and the average of the pre-stimulus period (initial 0.5 sec) subtracted. For difference maps, pairs of single condition maps were then subtracted (ex: two color conditions, orthogonal orientations, or a single condition against a blank condition). For visualization purposes, we converted the 12-bit single-condition maps into to 8-bit gray images and custom set the upper and lower bounds (typically 1-2 standard deviations of the mean).

t-map (binary map of activation). To verify observations based on difference maps, we tested for significance of activation by performing t-test comparisons between conditions on a pixel-by-pixel basis (Tsunoda et al., 2001). We assigned significant pixels (those meeting or exceeding threshold level of $p < 0.01$) the value 1 (white) and the value 0 (black) for pixels that did not reach significance. Images were low (median filter 187.5 μm x 187.5 μm median filter) and high pass filtered (1.875 mm x 1.875 mm median filter) prior to pixelwise t-testing (Fan et al., 2012; Tanigawa et al., 2010), this resulted in the creation of a binary map that revealed locations of activation reaching a specific threshold. Pixels overlying large vessels and at the chamber edge were excluded from the calculation using ImageJ (Rasband, 1997-2008). To partial control for false positive in our t-maps, we eliminated activations that were very small by requiring a size threshold of 100 pixel (one voxel is 15.625 μm x 15.625 μm) in total area. We tested several size thresholds and found negligible differences in the final calculations of the center of mass positions for which these images were primarily used (see next subsection). There were instances where continuous regions were connected by a small bridge of one to four pixels. These bridges were eliminated and resulting domains

assessed for size sufficiency. We refer the final thresholded binary maps simply as *t*-maps.

Domain area. In select cases, we used the *t*-maps to determine the total area covered by the domains. This was a simple procedure of counting the significant pixels (white pixels) in the *t*-maps. We perform the count in ImageJ (Rasband, 1997-2008). We did take an intermediate step of converting the pixel count into millimeters squared by multiplying the pixel count by the area of a voxel (0.0156 mm x 0.0156 mm). However in the presented cases, the data points are normalized by the largest value making the presented data plots unitless.

Determining changes in signal. To assess changes in signal, we used the *t*-maps and to locate the color and orientation selective domains and then selected four circles regions of interests (ROIs), 10 pixel (0.156 mm) diameter. Figure 1 illustrates an example of this process. We provide an example *t*-map (Fig. 1D) and gray scale difference map (Fig. 1E) from an example orientation preference domain maps in Subject L. Signals are determined from 4 selected ROIs (Fig. 1D). The points are determined by creating *t*-maps of orientation or color preference (see description above). Locations are not selected randomly from one single condition for an imaging case. We create outlines of the various *t*-maps over all relevant conditions (all available SF maps or size maps associated with orientation domains of color domains) within an imaging session. From these outlines we look for locations with the most common areas of activation and select 4. With only a few exceptions, we were able to select 4 locations for evaluations over the prescribed ranges. Time courses (Fig. 1A-C) are determined from the camera images as percent change in reflectance (dR/R). We then average the individual time course to

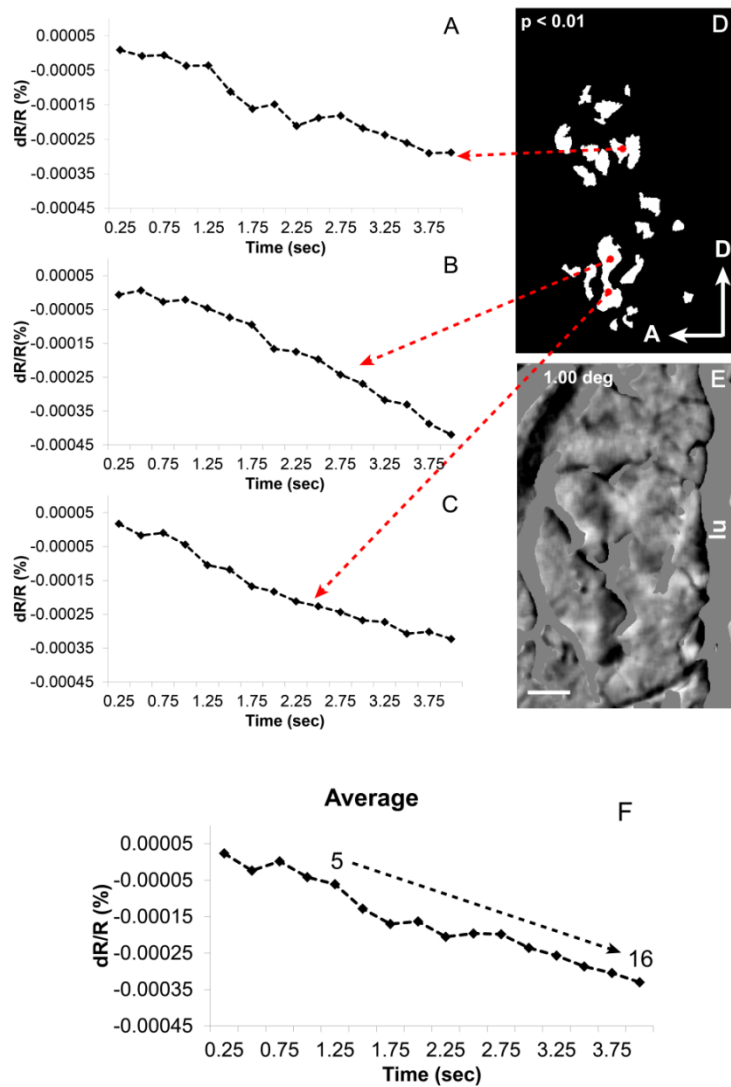


Figure 4- 1. **Extracting time courses.**

Sample time courses (A-C) are determined from sample ROIs (0.156mm [10 pixels] diameter circles) taken from locations deemed significant based on t-maps $p < 0.01$ (D). The corresponding gray scale map from the example t-map is shown (E). For each eccentricity, the sum of time points 1.25sec (Frame 5) to 4sec (Frame 16) are taken (F). The resulting value is then plotted as the amplitude against changing stimulus size diameter or spatial frequency and then fitted to a model (see Figs. 4, 7, and 8). The map is generated from a stimulus spot (1° in diameter) located at 1° eccentricity with a spatial frequency of 2 cycles/ $^\circ$ Scale bar = 2mm. lu = lunate. Axis: A = anterior, D = dorsal.

create a single time course (Fig. 1F). We then sum the time points 1.25-4 seconds (corresponding to imaging frames 5-16). The time courses are generated from the difference of two stimulus conditions (orthogonal orientations or color vs luminance) not based on a single condition against a blank condition. The absolute values of these summed time points become the data points we use as for the fitting presented in subsequent figures (see below) and in the fitting analysis. We scale data from each imaging case to a blank condition (which common to all imaging sessions). For duplicate data points among different imaging cases, we average the point into a single point after blank scaling.

Fitting procedures

Fitting size data. The size data are fitted to a simple second order polynomial using the built in MATLAB (Mathworks, Natick, MA) function *polyfit*. This function solves a least square problem that provides the coefficients of the function:

Equation 1.

$$\frac{dR}{R} = C_1 d^2 + C_2 d + C_3$$

Where, C_1 and C_2 are the coefficients, C_3 is a constant, d is the diameter of the spot stimulus in millimeters and dR/R is the change reflectance in percent. Using the output from *polyfit*, we can evaluate using the MATLAB function *polyval* to evaluate at arbitrary diameters. In this way we can find the theoretical optimal stimulus diameter at a given eccentricity for both color preference and orientation preference domains. We chose a 2nd order polynomial since it is the simplest model that would capture potential differences in the signal size around any peak diameter particularly declines from the theoretical peak size that indicate surround suppression effects.

Fitting spatial frequency data. Spatial frequency data are fitted to bimodal Gaussians of the form:

Equation 2.

$$\frac{dR}{R} = C_1 \frac{1}{\sqrt{2\pi\sigma_1^2}} e^{-(SF-\mu_1)^2/2\sigma_1^2} + C_2 \frac{1}{\sqrt{2\pi\sigma_2^2}} e^{-(SF-\mu_2)^2/2\sigma_2^2}$$

Where, C_1 and C_2 are the coefficients, SF is the spatial frequency in cycles/°, μ_1 and μ_2 are the means (or expectations) for each mode, σ_1 and σ_2 are the deviations, and dR/R is the change reflectance in percent. The data was fitted using non-linear least squares fitting routines in Matlab. For fitting, we set the coefficients (C_1 and C_2), means (μ_1 and μ_2), and standard deviations (σ_1 and σ_2) as free parameters. For unimodal fits we simply eliminate the second term. We used a variety of initialization values in order to avoid local minimums. We chose bimodal Gaussians because original analysis with unimodal Gaussians produced fits that clearly could not appropriately capture the signal profile. We settled on the bimodal Gaussian model because of the drastic qualitative and quantitative improvements. Because there are two modes, we determined the half width and half max (HWHM) and peak values for each mode to get a sense of the relative tuning for the different modalities. The peak amplitudes and HWHM values of a Gaussian can be determined with means and standard deviations, which we find during the fitting routine. All plots are presented normalized to the peak value of the fitted curves.

Results

In this study we took a unique perspective on V4 at various eccentric visual field positions. We studied the effects on IOI signal for changing stimulus size or SF for specific modules in V4. Here we report our findings based on data gathered from orientation and color preference domains in V4.

Optical imaging response of color and orientation preference domains to stimulus size

We first show examples of color preference domains from spot stimuli at 0.5° eccentricity (Fig. 2) and orientation preference domains from spot stimuli at 0.75° eccentricity (Fig. 3). For both the color preference domains in Subject J (Fig. 2) and the orientation preference domains in Subject L (Fig. 3), there is a qualitative change in the t-maps ($p < 0.01$) that imply both features have an “optimal” diameter. The most apparent change in the domain distribution in our color example occurs between Fig. 2G (0.5° in diameter) and Fig. 2H (1.0° in diameter). In the orientation preference example (Fig. 3G-J), there are perceptual differences in the number and distribution of domains at every diameter. In certain imaging cases we had a reasonable dynamic range so we looked at the effect spot stimulus diameter had on the area of domains within those specific imaging cases to get a sense of any potential trends we might expect from signal strength (Fig. 4). At the eccentricities less than 1° , we found that in these selected test cases (less than 0.75° eccentricity for orientation domains and less than 0.5° eccentricity for color domains) the largest area coverage over the tested diameters was for a spot of 1° in diameter (normalize peak values in Fig. 4A). Interestingly, the decline of domain area

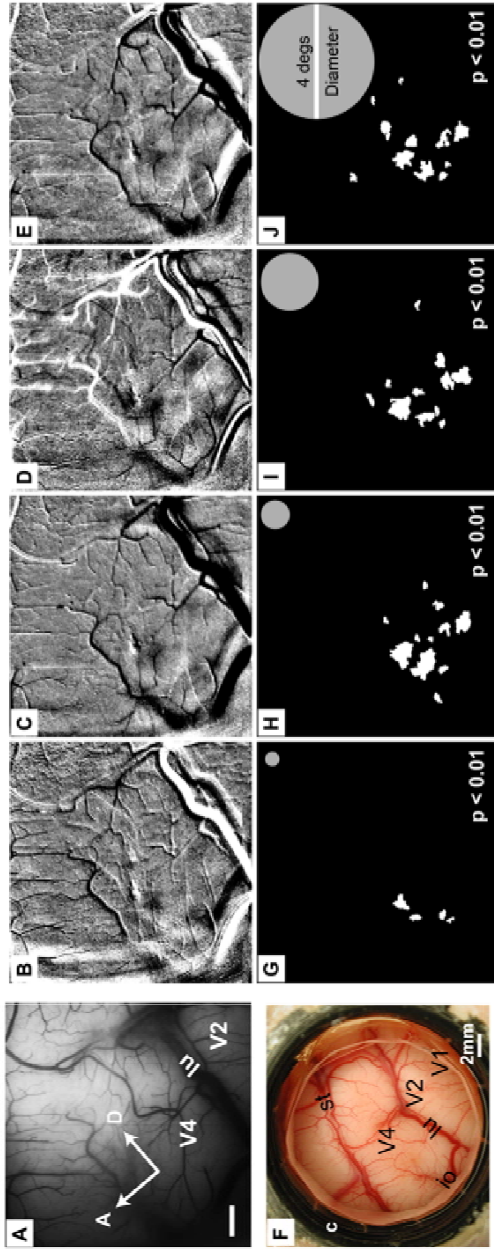


Figure 4- 2. **Example of color domain coverage due to different spot stimulus diameters.** We present an example color domain maps that results from differing spot sizes in V4 of Subject J. Here we illustrate that there is dependence to changing spot diameter in the color modules of V4. (A) 8 mm x8 mm image of cortex taken under green light (570nm). Gray scale difference maps (B-E) (Red/Green-Luminance) and the corresponding t-maps $p < 0.01$ (G-J), 0.5° (B/G), 1.0° (C/H), 2.0° (D/I), 4.0° (E/J). The gray dots in upper right hand corner of panels G-J are relative scales for reference and are not intended to represent true scaling or representation of actual stimuli used. The alteration in total area coverage from revealed domains is best observed between the 0.5° diameter (G) and 1° diameter (H) spot size. Imaging chamber for Subject J (F). Scale bar (1mm) in panel A applies to all but panel F. Eccentric location = 0.5° lu = lunate. Axis: A = anterior, D = dorsal, io = inferior occipital sulcus, st = superior temporal sulcus.

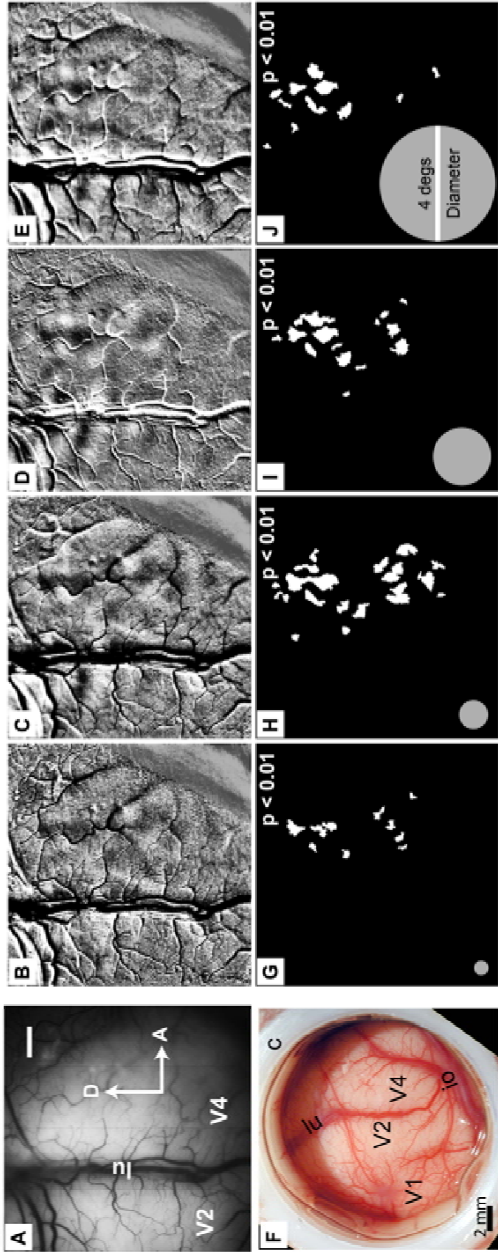


Figure 4-3. Example of orientation domain coverage due to different spot stimulus diameters. We present an example orientation domain maps that results from differing spot sizes in V4 of Subject L. Here we illustrate that there is dependence to changing spot diameter in the orientation modules of V4. (A) 8mm x 8mm image of cortex taken under green light (570nm). Gray scale difference maps (B-E) (Acute-Oblique) and the corresponding t-maps $p < 0.01$ (G-J), 0.5° (B/G), 1.0° (C/H), 2.0° (D/I), 4.0° (E/J). Imaging chamber for Subject L (F). The gray dots in lower right hand corner of panels G-J are relative scales for reference and are not intended to represent true scaling or representation of actual stimuli used. Scale bar (1mm) in panel A applies to all panels except panel F. Eccentric location = 0.75°. lu = lunate. Axis: A = anterior, D = dorsal. io = inferior occipital sulcus. st = superior temporal sulcus.

from increasing diameter from 1° is shallower for the color (green lines) preference domains than the orientation preference domains at this foveal ($<1^\circ$ eccentricity) location. This could simply be due to the 0.25° difference in eccentricity. While we have no orientation preference domain data, at 2° eccentricity, the largest value for total color preference domain area has moved out to 4° in diameter (Fig. 4B), a 4x increase compared to total peak diameter found for area coverage at 0.5° eccentricity. The increasing peak diameter value continuous onto 4.5° eccentricity (Fig. 4C) where the largest value for total color preference domain area for spot stimuli of 6° in diameter. However the trend for color preference domains appears to be broken at 6.0° eccentricity where the largest spot diameter value for total color preference domain area is found for spot stimuli of 4° in diameter. But at the 0.5° and 2.0° eccentric locations, there are clear declines in total area after the largest value of the tested diameters is reached, while at eccentricities of 4.5 and 6.0° , there is no consistent decline from the peak diameter. For orientation domains (blue lines), the largest values for total area at 0.75° eccentricity is for spots of 1° in diameter (Fig. 4A), at 4.5° eccentricity the largest total area value is for spots of 2° in diameter (Fig. 4C), and at 6.0° eccentricity the largest total area value is for spots of 8.0° in diameter. Unlike for color domains, we observed no break in the trend toward larger spot size diameters for increasing eccentricity. While these quantifications of area are interesting and provide some insight we hesitate to place too much emphasis on the meaning of these results since these are all relative changes of total area within our imaging window and likely do not reflect the domain area value that would be attained if we were capable of imaging all of V4 at high resolution simultaneously (see Discussion for more). But the identified areas of significant activation in the example t-maps

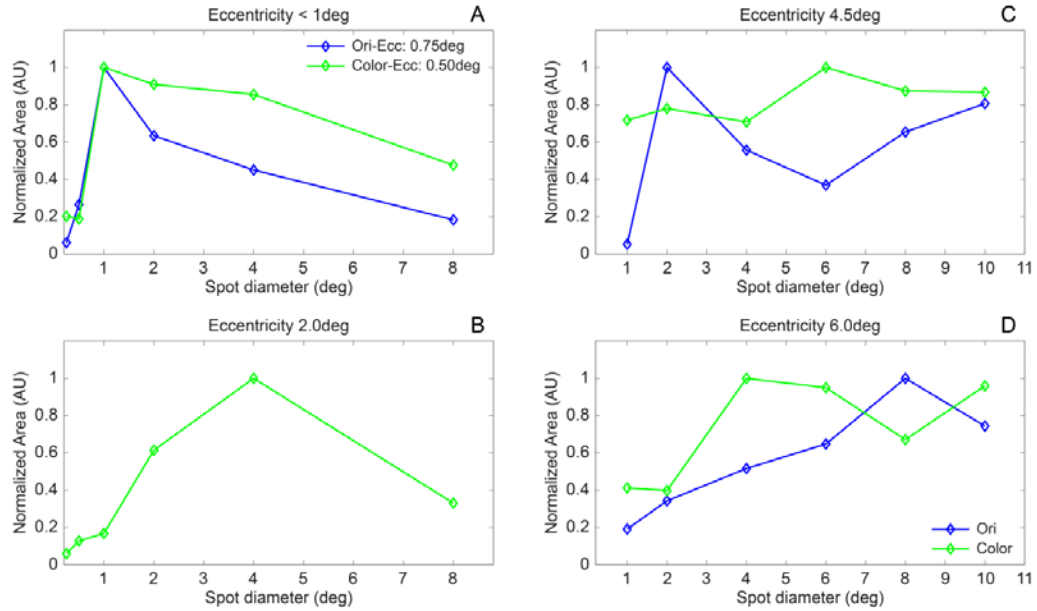


Figure 4- 4. *Effect of spot size on area from exemplar cases.*

Each eccentricity is represented by select cases with the best range of spot diameters. Each data point, in panels A-D, represents the total area based on t-maps. Plots are normalized. Area is calculated as a straight pixel count and which can be converted to millimeters squared but due to normalization the units have been lost. Data points taken from orientation preference domains are in blue and data points taken from color preference domains are shown in green. Panel A: Case L070525O and Case J080324C. Panel B: Case J080318C. Panel C: Case J090703O and Case J090703C. Panel D: Case L071206O and Case L071206C. The peak diameter based on different total area appears to increase consistently for orientation domains but not for color domains. However in the color domains the larger diameters appear to have a more constant relationship. AU = arbitrary units.

presented thus far, provide target locations to sample the IOI signal profile (see Materials and Methods) and indicates, along with Figs. 2 and 3, that orientation domains appear to exert stronger surround suppression effect compared to color domains.

To quickly review, we can sample IOI signal from multiple domains, revealed in the t-maps (Fig. 1D, Fig. 2G-2J and Fig. 3G-3J) and examine changes due to changing spot stimulus diameters. To accomplish this, we compiled data points at different eccentricities as a function of the changing diameter of a spot stimulus. We then fit the data to a second order polynomial and normalized the data to peak of the resultant curve (Fig. 4A-4D) as outlined in the Material and Methods section.

Based on the RF size estimates in V4 reported in by Motter (2009), a reasonable prediction for foveal size preference (for locations below 2° eccentricity) to be within the range of $1.5\text{-}3^\circ$ and then increase with increasing eccentricity. When we take the peaks of our fitted curves in Fig. 4A-4D and plot them by eccentricity, as in Fig. 4E, we see that for color selective domains (green data points and fits in Fig. 4) and orientation domains (blue data points and fits in Fig. 4) the peak values are almost identical by eccentricity and that the size preference is around 4° in diameter for eccentricities below 1° and then climbs to around 7° in diameter at 4.5° eccentricity and then plateaus between 4.5° and 6.0° eccentricity. However if we chose the peak values from Fig. 5A based on the largest sampled signal amplitude (not the peak of the fit), then the best spot diameter would be for a spot 2° in diameter. Based on the total area plots in Fig. 4, the optimal diameter would be locations less than 1° eccentricity would a size of 1° in diameter. The difference in the area and IOI signal peaks could be due to FOV limitations as we suggested before. The difference between peak values for measured signal size and fitted peak size appears

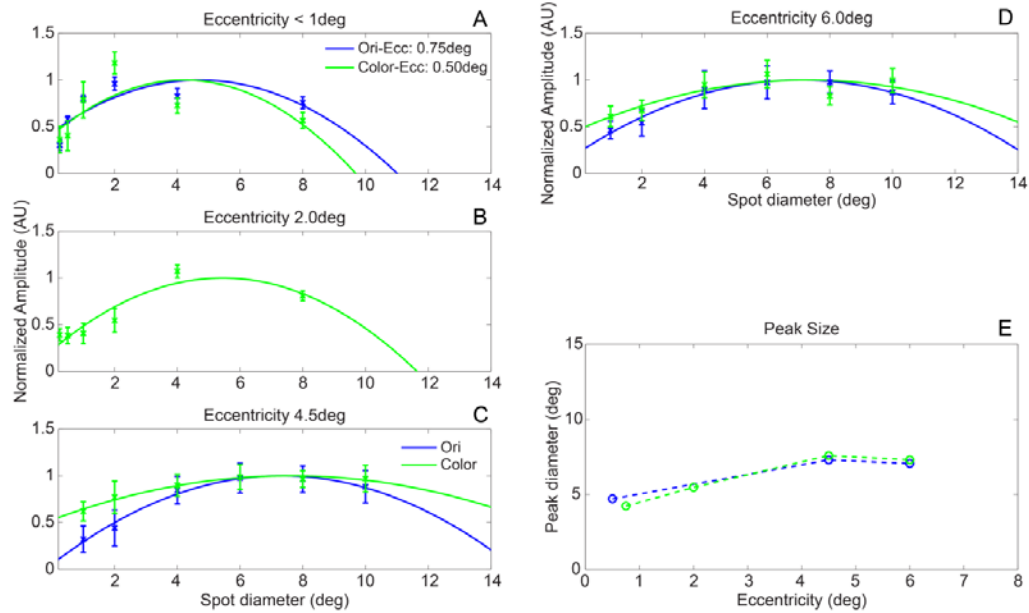


Figure 4- 5. *Effect of spot size on signal strength.*

Each data point, in panels A-D, represents the absolute value of a summed time course (as explained in Fig. 1 and the Materials and Methods). The points are plotted and fitted to a second order polynomial. Plots are normalized from the units percent change in reflectance ($dR/R(\%)$) so that the peak of the fitted data for each curve has a value of 1 AU (arbitrary units). Data points taken from orientation preference domains are in blue and data points taken from color preference domains are shown in green. As we move from foveal to parafoveal representations, the peak signal strength for stimulus size increases to 4.5° and then appears to plateau (E). Peaks are found based on the fitted curves of Normalized signal size vs. Spot diameter (in degrees) (A-D). The peak diameters by eccentricity does not appear to deviate based on feature domain. For the points sample at less than 1° eccentricity (A), there is an apparent difference between the max sampled value (2° in diameter) vs. the peak fitted value ($\sim 4^\circ$ in diameter). However the general trend remains AU = arbitrary units.

to be greatest at the foveal locations and could be due to lack of sampling points. But taking either value does not appear it would affect the general trend of increasing stimulus preference for increasing eccentricity in line. However at 6° eccentricity, the peak measured value is at spot size 8° in diameter for orientation domains and 6° in diameter for color domains. Interestingly, the qualitative assessment of total pixels in t-maps (or total area) in Fig. 4 suggests that after the peak size in color domains is reached, there is less suppression than there is for orientation domains. This is also suggested in the fitted curves at the matching eccentric positions of 4.5° and 6.0° in Fig. 5. This would be consistent with the idea that orientation domains would be more concerned with aspects dealing with edge effects thus would necessarily need to be more sensitive to size changes, while color domains are more concerned with spectral or surface properties where the size of a particular stimulus would be less important.

Optical imaging response of color and orientation preference domains to spatial frequency

Similar to our evaluation of to changes in stimulus size, we evaluate our V4 data with relation to changes the spatial frequency (SF). Previous reports on V4 spatial frequency preferences have provided a wide range of optimal frequencies 0.12-8 cycles/° (Desimone and Schein, 1987; Kumano et al., 2008). We use the same analysis for size preferences for SF and compare orientation and color preference modules to determine if they produce similar or dissimilar trends.

We first present examples of color/luminance domains from Subject J (Fig. 6) and orientation domains from Subject L (Fig. 7) to provide a sense of the effect of changing SF on each feature module. Unlike with spot size, the distribution of the domains in

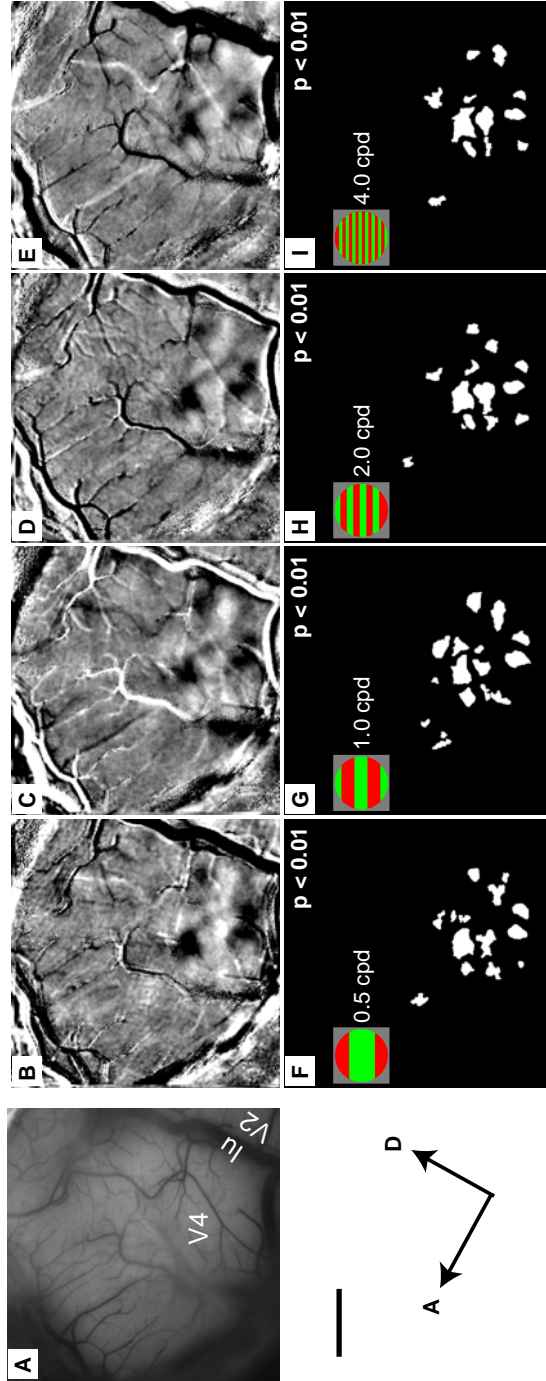


Figure 4- 6. *Example of color domain coverage due to differing spatial frequency.* We present an example color domain maps that results from differing spatial frequencies in V4 of Subject J. Here we illustrate that there is no obvious dependence to changing spatial frequency in the color modules of V4. However, the total area coverage may not reflect the underlying signal dynamics (see Fig. 9 and 10) (A) 8x8mm image of cortex taken under green light (570nm). Gray scale difference maps (B-E) (Red/Green-Luminance) and the corresponding t-maps $p < 0.01$ (F-I), 0.5 cpd (B/F), 1.0 cpd (C/G), 2.0 cpd (D/H), 4.0 cpd (E/I). Qualitatively, the distribution of significant color domains appears very similar regardless across multiple spatial frequency. The illustrated red/green grating spot stimuli examples are relative scales for reference and are not intended to represent true scaling or representation of actual stimuli used. Scale bar = 2mm. lu = lunate. Axis: A = anterior, D = dorsal. cpd = cycles/°.

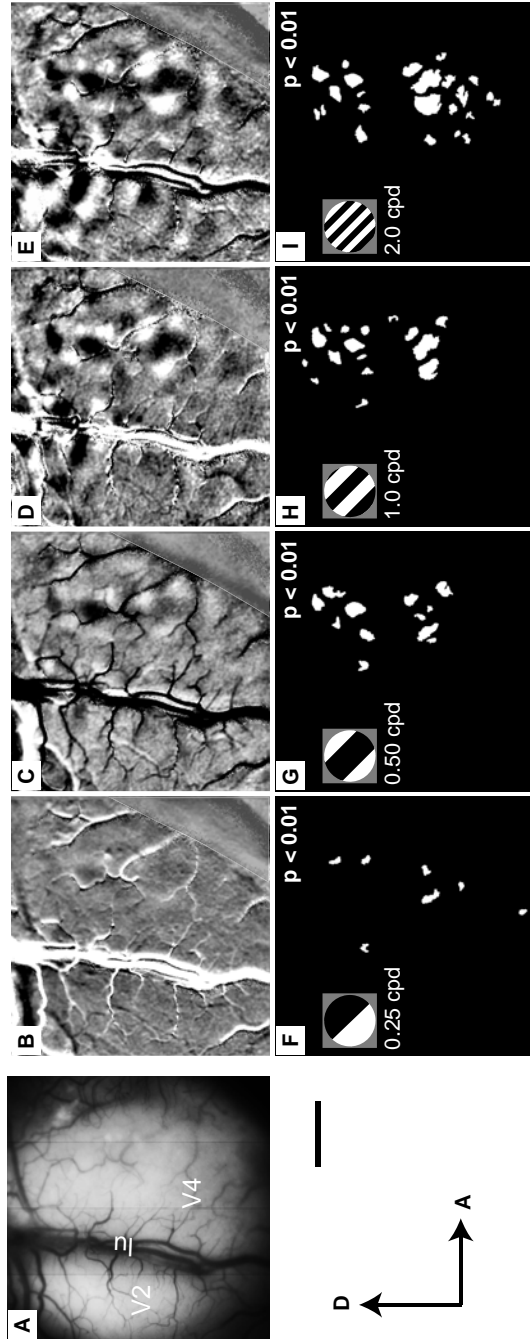


Figure 4- 7. *Example of orientation domain coverage due to differing spatial frequencies.* We present an example orientation domain maps that results from differing spatial frequencies in V4 of Subject L. Here we illustrate that, unlike for color domains, there is clear dependence to changing spatial frequencies in the orientation modules of V4. (A) 8x8mm image of cortex taken under green light (570nm). Gray scale difference maps (B-E) (Acute - Obtuse) and the corresponding t-maps $p < 0.01$ (F-I), 0.25 cpd (B/G), 0.5 cpd (C/H), 1.0 cpd (D/I), 2.0 cpd (E/J). Unlike the distribution of color domains, changing SF appear to influence the distribution of orientation domains. The illustrated blank/white grating spot stimuli examples are relative scales for reference and are not intended to represent true scaling or representation of actual stimuli used. Scale bar = 2mm. lu = lunate. Axis: A = anterior, D = dorsal. cpd = cycles/°.

color/luminance selective modules do not produce an obvious changes in the image maps (Fig 6B-E) or t-maps (Fig 6F-H) as they appear to be very similar across the range of spatial frequencies. In contrast, the orientation domains do show clear differences in image maps (Fig 7B-E) and t-maps (Fig 7F-H) for changing SF (Fig. 7B,F: 0.25 cpd, Fig. 7C,G: 0.5 cpd, Fig. 7D,H: 1.0 cpd, Fig. 7E,I: 2.0 cpd).

Like we did with changing spot size diameter, we select some sample test cases to evaluate the domain area. Here, the total area values show some contrast between the color preference domains and orientation preference domains. First, the total area for color preference domains appears to have a flatter characteristic across the eccentric positions. While there are peak values for the total area of color domains, the range of values are smaller when compared with orientation preference domains. The orientation preference domains show differences in the total area across the different eccentricities that have clear preferences with SF. At 0.5° eccentricity the largest value for orientation domain area is found at 16 cpd (blue line: Fig. 8A), at 0.75° eccentricity there is a clear peak for total area at 4 cpd (blue line: Fig. 8B) and at 4.5° eccentricity, we find the lowest spatial frequency values favored 1cpd (blue line: Fig. 8C). While this more overt change in total area is not obvious for color domains as it is in orientation domains, focusing on the higher spatial frequency values of area (6 cycles/ $^\circ$ and above) there is a relative dip compared to the lower SF values (4° and below) indicating that SF does have some influence in the color domains. However, as we noted with stimulus diameter, the domain area does not necessarily coincide with the underlying signal dynamics. Therefore, as with size, we took sample points from the various t-maps. We plotted signal changes arising from color domains (blue markers and lines) and orientation domains (green

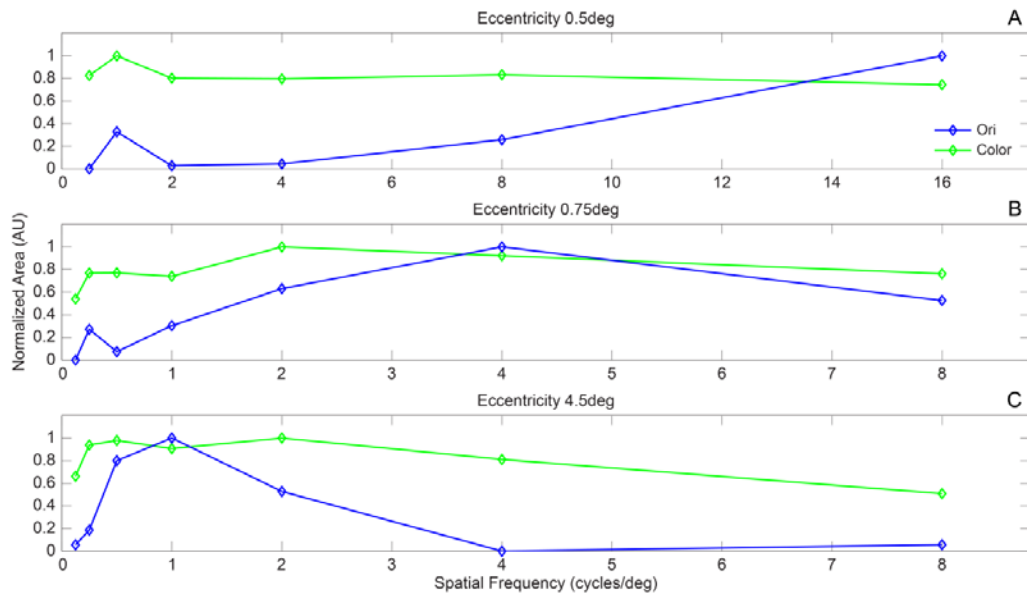


Figure 4- 8. *Effect of Spatial frequency on area from exemplar cases.* Each eccentricity is represented by select cases with the best range of SF values. Each data point, in panels A-C, represents the total area based on t-maps. Plots are normalized. Area is calculated in mm squared however due to normalization, the units have been lost. Data points taken from orientation preference domains are in blue and data points taken from color preference domains are shown in green. Panel A: Case J080411O and Case J080411C . Panel B: Case L070605O and Case L070605C. Panel C: Case J110118O and Case J110118C. For color domains (green), the total area from revealed domains in t-maps is fairly flatter over the prescribed range in A-C when compared to orientation domains. However, the total area measure does not necessarily reflect the underlying signal dynamics (see Figs. 9 and 10). AU = arbitrary units.

markers and lines) in Fig. 9. Interestingly we found that bimodal Gaussians produced better fits for our IOI signal than a standard unimodal Gaussian. The domain area values in Fig. 9 provided no indication that we should expect a bimodal Gaussian. Because this was unexpected (see Discussion) we evaluated the overall improvement from unimodal to bimodal Gaussian fits. Overall there was an improvement in the sum of the absolute error between a unimodal and bimodal Gaussian. The ratio of improvement was fairly wide, between factors of 1.81 to 10292. Because we found that bimodal Gaussians performed universally better, each peak from the bimodal Gaussian fits were found and plotted against eccentricity (Fig. 9D). We also calculated the bandwidths for each Gaussian mode using the theoretical values for half width half max from the final fitted parameters in order to evaluate possible difference in the tuning (Fig. 9E). The calculated bandwidths for each peak (Fig. 9E) are found within ranges that have previously been reported (Desimone and Schein, 1987; Kumano et al., 2008). The bandwidths seem to fall within a tighter range and are, at the more foveal positions, narrower for the orientation preference domains than the color orientation domains. It is interesting that there is a consistent appearance of a low frequency peak around 1 cpd in all of our fits and that there is a similar trend for the high frequency component for both color and orientation domains. But the relative tuning associated with those low frequency components, based on the HWHM values, suggest orientation domains are, in general, more selective than color domains. This is consistent with the total pixel count (or total area) shown in Figs. 6-8. At the most foveal location (0.5° eccentricity) the peak SF value for the high frequency peaks was greater for orientation domains than color domains. However this relationship quickly reversed as we moved to 0.75° eccentricity and remained at the 4.5°

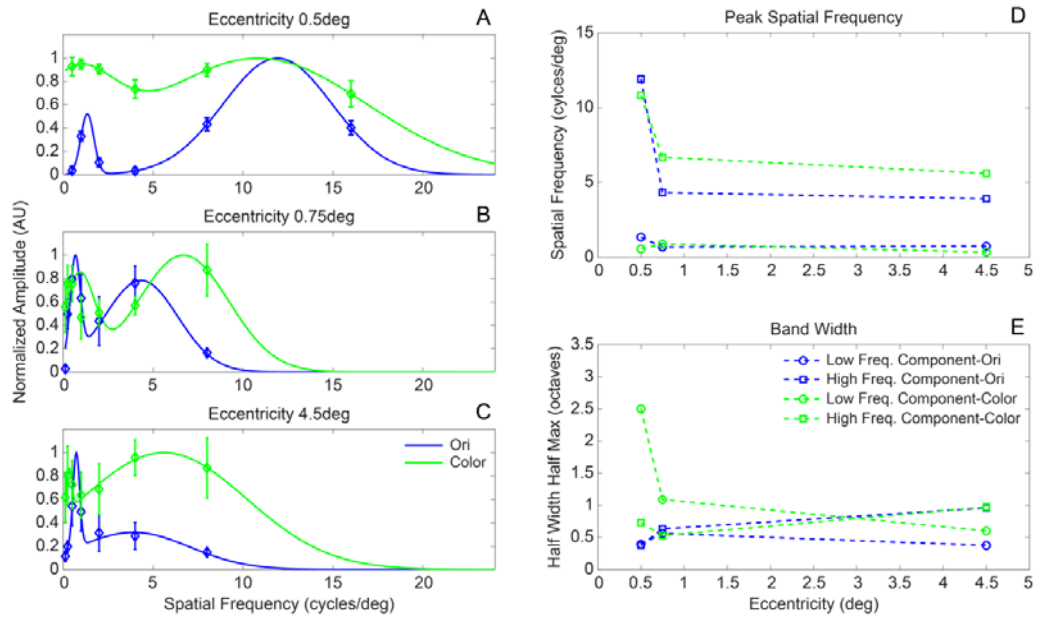


Figure 4- 9. ***Effect of Spatial frequency on signal at various eccentricities.*** Green markers are based on signal strength from orientation preference domains. Blue markers are based on signal strength from color preference domains. Bimodal gaussian fits at 0.5° eccentricity (A), 0.75° eccentricity (B), 4.5° eccentricity (C). Because fits are bimodal, there are two peaks. Peak spatial frequency is plotted against eccentricity (D). Peaks are presented for color and orientation curves divided into higher frequency modal components (square) and lower frequency modal components (circle). The high frequency components shows highest SF peak at the most foveal eccentricity (0.5°). The low frequency modal component is relatively flat for both components by comparison. We also present bandwidth in octaves for each gaussian mode (E). We find no compelling trend other than bandwidths fall within a tighter and lower range when emerging from orientation preference domains when compared to those arising from color preference domains. AU = arbitrary units.

eccentricity location. The orientation domains high frequency component at the 0.5° eccentricity location also showed the most narrow HWHM. At the other locations (0.75° and 4.5° eccentricity) the HWHM values are very similar.

We also grouped the data into eccentricities less than and equal to 2° and eccentricities greater than 2° (Fig. 10). Similar to Fig. 9, the peak SF values for the high frequency component are greater in the foveal collection ($\leq 2^\circ$ eccentricity) vs. the parafoveal collection ($> 2^\circ$ eccentricity) (Fig. 10C). The low frequency peak is also found around the 1 cpd value however the peak is slightly higher for both groupings for orientation domains. For the high frequency peak, we find that SF preference to be slightly higher for orientation for the foveal grouping (similar to the most foveal point in Fig. 9) and then a reversal in the parafoveal grouping (also similar to the relationship more peripherally in Fig. 9). Interestingly, the combination of data influences the relationship of the bandwidths. In this foveal to parafoveal comparison, the range of bandwidth values is nearly identical with the orientation domain bandwidths for the low frequency component being smaller than the color domain bandwidths. The same trend is seen for the high frequency components but to a lesser degree. However the HWHM from the orientation domains, in these groupings, are all smaller with the one exception of the parafoveal high frequency component.

Because the presence of this low frequency peak was unexpected, we wanted to test if its presence could be a collection artifact of during imaging. If this is the case, then it would likely not be specific to V4. To test this hypothesis, we took an imaging case where V2 was well resented (see Fig. 7). We performed the same procedure to acquire the data points for fitting. As can be seen in Fig. 11, in V2 there was no compelling

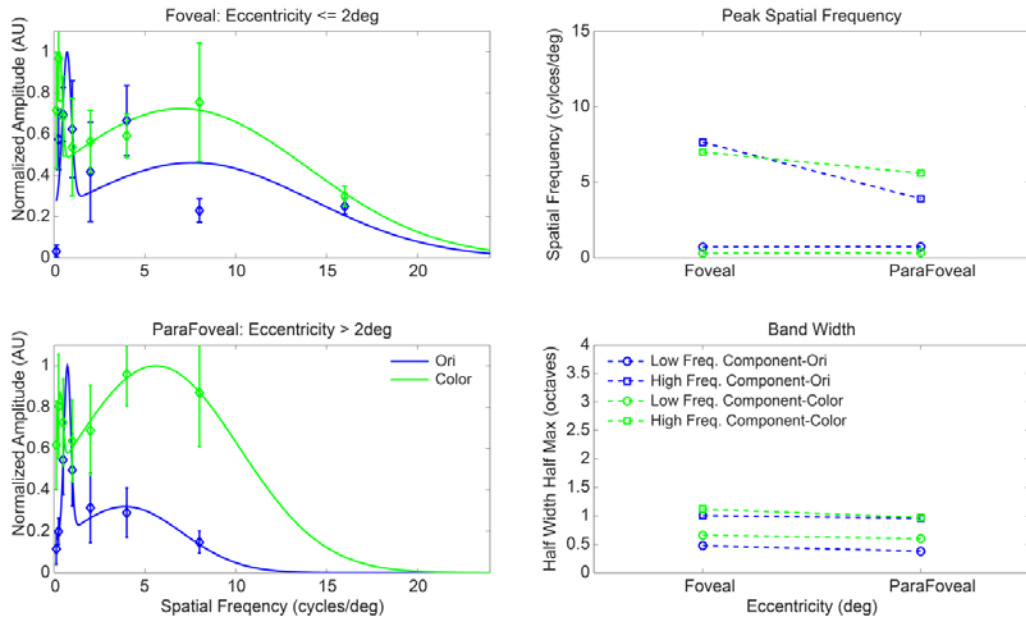


Figure 4- 10. ***Comparing the effect of Spatial frequency from foveal vs. parafoveal eccentricities.***

We combined data from 2° and less eccentricity locations and compared it to data from greater than 2° eccentricity and performed the same analysis as in Fig. 9 by group. Again, the fits are bimodal gaussians and we divide the presentation of the peak spatial frequency and bandwidths into high frequency components and low frequency components. The trends for peak spatial frequency is the same in that the higher frequency mode peaks are larger when presented more foveally and the lower frequency modes are relatively flat by comparison. Similar to the non-grouped data, the range of bandwidths from the data coming from orientation domains is lower than those arising from color domains. However the range is more similar. AU = arbitrary units.

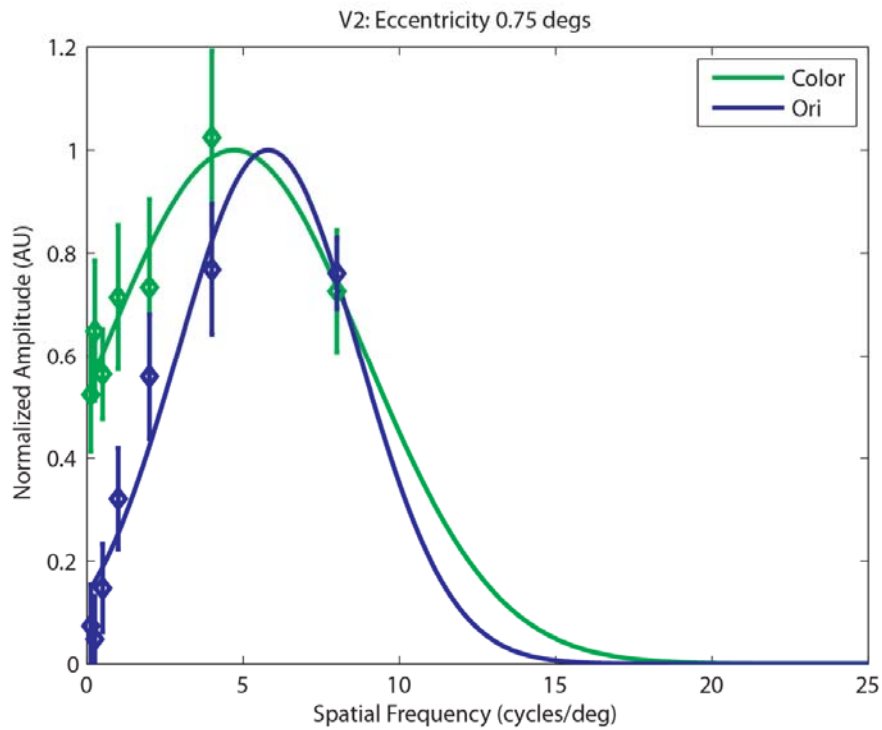


Figure 4- 11. *V2 spatial frequency preference at 0.75° eccentricity.* We evaluated to data at 0.75° eccentricity for V2 to test to see if the low frequency component in Figs. 9 and 10 could be artifact that would appear regardless of visual area. Here we show that a unimodal Gaussian describes the data well and provides no compelling reason that a bimodal Gaussian would be more appropriate. AU = arbitrary units. Color (Green line), Orientation (Blue line).

reason to believe a bimodal Gaussian was appropriate, supporting that the low frequency peak is likely a functional response characteristic to V4, we elaborate on possibilities in the Discussion.

Discussion

Recently, using IOI, Tanigawa et al. (2010) demonstrated the presence of bands of color and orientation modules. Previous investigation into the effect of stimulus size and spatial frequency in V4 (Desimone and Schein, 1987; Kumano et al., 2008; Schein and Desimone, 1990) came before there was a clear way to distinguish territories for specific functional modalities in V4, here we compare the effect of stimulus size to IOI signal in color and orientation preference domains.

IOI signal vs. total domain area

For both color preference domains and orientation preference domains, we provided information regarding the changes in domain area coverage and the IOI signal for different stimulus spot diameters and SF at various eccentricities. As we suggested in the Results section, we can only calculate domain area within the imaging FOV which mean we are missing potential regions outside the FOV. Another potential issue with looking solely at measures that rely on pixel counts is the use of the t-maps which are binary. The underlying signal structure giving rise to the domains is not captured in a binary map and thus total area and signal dynamics may not coincide because we only sample domains that appear in t-maps. For instance, the signal dynamics for SF color indicate slightly worse selectivity to orientation domains but with similar peak preferences. However the area measure in Fig. 8 and visually seen in Figs. 6 and 7 suggest a stronger differentiation

between these two. The reasons for this difference are difficult to reconcile since we are unable to account for aspects outside our FOV that could potentially make these observations slightly more congruent. However, in the Results we do point out that the overall HWHM, our indications of overall tuning, appears to be generally sharper for orientation domains. That is consistent with the idea that our t-maps are binary and do not necessarily capture changes in the signal profile.

Another aspect that is not well captured by evaluating domain area is that the IOI signal is best fit with a bimodal Gaussians (which we discuss below). The relative mixing in the bimodal Gaussians associated with color domains seems to be greater when compared to those associated with orientation domains. This type of variation might contribute (but not completely) to the overall flatter look to the reported color domain area.

Study of parameters of a modular V4 from IOI signal

Stimulus size. Early reports for size optimization in V4 came from bars length and widths (Desimone and Schein, 1987). The size “preference” is due to surround suppression. Reports for surround suppression started very early with Hubel and Wiesel (1965) and have been reported consistently ever since for both cats and monkeys (for review Allman et al., 1985; Cavanaugh et al., 2002; DeAngelis et al., 1994; Levitt et al., 1994). Because increasing size does not result in ever increasing signal from a given RF, defining a “size” preference is a corollary to measuring RF size. Here we show that surround suppression exerts its influence in similar ways between the color and orientation modules in V4 in terms of the size that elicits the strongest IOI signal but the orientation domains appear to exert a stronger influence on the surround suppression that is apparent in the

comparison between Figs. 2 and 3 and is somewhat captured in the Fig 4A. The 2nd order polynomial plots in Fig. 5 also indicate this at the matching eccentric location for color and orientation domains (Fig. 5C-D) where the drop in the curve is steeper for orientation domains after the theoretical peak size value is reached.

Spatial frequency. We sought to understand the relationship of SF with the functional modules within V4. Our IOI analysis uncovered an interesting bimodal Gaussian distribution. By comparison, the SF components for color domains showed more intermixing overall. This is can be observed by the relative size of the “dips” between the two modes for color preference domains and color preference domains (Fig. 9). This flatness (best seen in Fig. 9A green plot) partially explains the more constant value seen across SF in the domain area plots for color domains in Fig. 4 (green plots). Interestingly, in terms of peak SF frequencies, both color and orientation selective domains had similar overall trends, where the higher SF values of the higher frequency component were favored at more central visual field representations and lower SF values of the high frequency component were favored at more peripheral visual field representations. This trend is also apparent when we group the data in to our foveal group ($\leq 2^\circ$ eccentricity) and parafoveal group ($> 2^\circ$ eccentricity). Although the lower frequency mode peak is of similar value in all plots (Fig. 9 and Fig. 10) the higher frequency mode consistently goes from a higher SF value at more foveal visual field locations to lower SF value at more peripheral visual field locations.

Typically SF tuning is fitted with a unimodal Gaussian (e.g. DeAngelis et al., 1993). However we found that fitting with a bimodal Gaussians performed better with our V4 data than a unimodal Gaussians (Fig. 9 and 10). This is somewhat unexpected. The

immediate concern is that IOI signal does not faithfully replicate the underlying neuronal preferences to changing SF. However an IOI study in cat V1 by Issa et al. (2000) showed that SF preferences are highly correlated between IOI and electrophysiological measures. It is then likely that the consistent appearance of a lower frequency Gaussian mode represents a population of cells that respond well to this SF and makes a meaningful contributing to the overall IOI signal. It is known that a wide range of SF preferences can be found in the central 5° of V4, 0.12-8cpd (Desimone and Schein, 1987). The presence of cells in V4 with low pass spatial frequency preferences have been noted in the past but are thought to have no apparent organization (Pollen et al., 2002). This could be a part of the low and high pass SF segregations that results in differential face processing expertise effects to low SF and high SF filtered images (Gauthier et al., 2005).

The stimuli construction itself could be the source of this low frequency component. The high frequency mode does coincide with general relationships observed in V1 and V2 where the SF preference shifts from higher spatial frequency to lower spatial frequency values as we shift from central to more peripheral visual field representations (Foster et al., 1985; Schiller et al., 1976; Xu et al., 2007). It is possible that the report of V4 performing better with square waves (Desimone and Schein, 1987) is because V4 neuronal response can be augmented by the presence of harmonics. While the fundamental is still produces the main power of the wave form, it could be that around the 1 cpd range, the harmonics generated at the lower SF gratings enhances cortical activity on a population level, resulting in these previously unobserved dynamics in V4 that does not appear in imaging artifact control analysis Fig. 11 when assessing V2 SF preference.

Questions regarding differences in SF tuning in regions that primarily process color or orientation are not unique to V4. Spatial frequency responses have been demonstrated to be mapped orderly onto V1 (see Harvey and Dumoulin, 2011; Xu et al., 2007; Yu et al., 2005). But there are studies that demonstrate possible differences exist between the blobs and interblob regions (Born and Tootell, 1991; Edwards et al., 1995). This is consistent with evidence that blobs and interblobs receive differential inputs from the lateral geniculate nucleus (LGN). In V4 it appears that on a population level, there are dynamics in the processing of square waves that result in relationships that might be involved in processing information for low and high pass SF channels.

Conclusions

Here were present preferences for diameter of a spot stimulus and SF for the color and orientation modules of V4 that are similar. However, we find that the effect of surround suppression appears greater for orientation domains based on the t-maps, pixel counts (or total area), and the signal depression after the theoretical peak size values for each modality. Interestingly we find that our SF data fit better with to a bimodal Gaussian distribution. This could be a result of distinct SF frequency processing channels in V4 or a property inherent to V4 processing square waves that is not observed when we make a direct IOI comparison with V2.

References

- Allman J, Miezin F, McGuinness E. 1985. Stimulus specific responses from beyond the classical receptive field: neurophysiological mechanisms for local-global comparisons in visual neurons. *Annu Rev Neurosci* 8:407-430.
- Born RT, Tootell RB. 1991. Spatial frequency tuning of single units in macaque supragranular striate cortex. *Proceedings of the National Academy of Sciences of the United States of America* 88(16):7066-7070.
- Cavanaugh JR, Bair W, Movshon JA. 2002. Nature and interaction of signals from the receptive field center and surround in macaque V1 neurons. *Journal of neurophysiology* 88(5):2530-2546.
- DeAngelis GC, Freeman RD, Ohzawa I. 1994. Length and width tuning of neurons in the cat's primary visual cortex. *Journal of neurophysiology* 71(1):347-374.
- DeAngelis GC, Ohzawa I, Freeman RD. 1993. Spatiotemporal organization of simple-cell receptive fields in the cat's striate cortex. II. Linearity of temporal and spatial summation. *Journal of neurophysiology* 69(4):1118-1135.
- Desimone R, Schein SJ. 1987. Visual properties of neurons in area V4 of the macaque: sensitivity to stimulus form. *J Neurophysiol* 57(3):835-868.
- Edwards DP, Purpura KP, Kaplan E. 1995. Contrast sensitivity and spatial frequency response of primate cortical neurons in and around the cytochrome oxidase blobs. *Vision research* 35(11):1501-1523.
- Fan RH, Baldwin MK, Jermakowicz WJ, Casagrande VA, Kaas JH, Roe AW. 2012. Intrinsic signal optical imaging evidence for dorsal V3 in the prosimian galago (*Otolemur garnettii*). *The Journal of comparative neurology*.
- Foster KH, Gaska JP, Nagler M, Pollen DA. 1985. Spatial and temporal frequency selectivity of neurones in visual cortical areas V1 and V2 of the macaque monkey. *The Journal of physiology* 365:331-363.
- Gallant JL, Braun J, Van Essen DC. 1993. Selectivity for polar, hyperbolic, and Cartesian gratings in macaque visual cortex. *Science* 259(5091):100-103.

- Gallant JL, Connor CE, Rakshit S, Lewis JW, Van Essen DC. 1996. Neural responses to polar, hyperbolic, and Cartesian gratings in area V4 of the macaque monkey. *Journal of neurophysiology* 76(4):2718-2739.
- Gauthier I, Curby KM, Skudlarski P, Epstein RA. 2005. Individual differences in FFA activity suggest independent processing at different spatial scales. *Cogn Affect Behav Neurosci* 5(2):222-234.
- Ghose GM, Ts'o DY. 1997. Form processing modules in primate area V4. *J Neurophysiol* 77(4):2191-2196.
- Harvey BM, Dumoulin SO. 2011. The relationship between cortical magnification factor and population receptive field size in human visual cortex: constancies in cortical architecture. *The Journal of neuroscience : the official journal of the Society for Neuroscience* 31(38):13604-13612.
- Hegde J, Van Essen DC. 2005. Role of primate visual area V4 in the processing of 3-D shape characteristics defined by disparity. *Journal of neurophysiology* 94(4):2856-2866.
- Heywood CA, Gadotti A, Cowey A. 1992. Cortical area V4 and its role in the perception of color. *The Journal of neuroscience : the official journal of the Society for Neuroscience* 12(10):4056-4065.
- Hinkle DA, Connor CE. 2001. Disparity tuning in macaque area V4. *Neuroreport* 12(2):365-369.
- Hubel DH, Wiesel TN. 1965. Receptive Fields and Functional Architecture in Two Nonstriate Visual Areas (18 and 19) of the Cat. *Journal of neurophysiology* 28:229-289.
- Kumano H, Tanabe S, Fujita I. 2008. Spatial frequency integration for binocular correspondence in macaque area V4. *Journal of neurophysiology* 99(1):402-408.
- Levitt JB, Kiper DC, Movshon JA. 1994. Receptive fields and functional architecture of macaque V2. *Journal of neurophysiology* 71(6):2517-2542.
- Livingstone M, Hubel D. 1988. Segregation of form, color, movement, and depth: anatomy, physiology, and perception. *Science* 240(4853):740-749.

- Lu HD, Roe AW. 2008. Functional organization of color domains in V1 and V2 of macaque monkey revealed by optical imaging. *Cereb Cortex* 18(3):516-533.
- Motter BC. 2009. Central V4 receptive fields are scaled by the V1 cortical magnification and correspond to a constant-sized sampling of the V1 surface. *J Neurosci* 29(18):5749-5757.
- Pasupathy A, Connor CE. 1999. Responses to contour features in macaque area V4. *J Neurophysiol* 82(5):2490-2502.
- Pasupathy A, Connor CE. 2001. Shape representation in area V4: position-specific tuning for boundary conformation. *J Neurophysiol* 86(5):2505-2519.
- Pasupathy A, Connor CE. 2002. Population coding of shape in area V4. *Nat Neurosci* 5(12):1332-1338.
- Pollen DA, Przybylski AW, Rubin MA, Foote W. 2002. Spatial receptive field organization of macaque V4 neurons. *Cerebral cortex* 12(6):601-616.
- Rasband WS. 1997-2008. ImageJ. U S National Institutes of Health <http://rsb.info.nih.gov/ij/>.
- Roe AW, Chelazzi L, Connor CE, Conway BR, Fujita I, Gallant JL, Lu H, Vanduffel W. 2012. Toward a unified theory of visual area V4. *Neuron* 74(1):12-29.
- Schein SJ, Desimone R. 1990. Spectral properties of V4 neurons in the macaque. *The Journal of neuroscience : the official journal of the Society for Neuroscience* 10(10):3369-3389.
- Schiller PH, Finlay BL, Volman SF. 1976. Quantitative studies of single-cell properties in monkey striate cortex. III. Spatial frequency. *Journal of neurophysiology* 39(6):1334-1351.
- Sincich LC, Horton JC. 2005. The circuitry of V1 and V2: integration of color, form, and motion. *Annu Rev Neurosci* 28:303-326.
- Tanigawa H, Lu HD, Roe AW. 2010. Functional organization for color and orientation in macaque V4. *Nat Neurosci* 13(12):1542-1548.

- Tsunoda K, Yamane Y, Nishizaki M, Tanifuji M. 2001. Complex objects are represented in macaque inferotemporal cortex by the combination of feature columns. *Nature neuroscience* 4(8):832-838.
- Xu X, Anderson TJ, Casagrande VA. 2007. How do functional maps in primary visual cortex vary with eccentricity? *J Comp Neurol* 501(5):741-755.
- Yu H, Farley BJ, Jin DZ, Sur M. 2005. The coordinated mapping of visual space and response features in visual cortex. *Neuron* 47(2):267-280.
- Zeki SM. 1973. Colour coding in rhesus monkey prestriate cortex. *Brain research* 53(2):422-427.

CHAPTER V

SUMMARY

Elucidating the inner workings of human visual processing requires a detailed understanding of the cortical areas involved and their properties. Because comparative studies provide immeasurable value toward understanding human visual processing, considerable effort is spent toward studying the visual system of other primates. It is presumed that there exists a set of common visual areas to all primates. These homologous visual areas likely provide vital roles in processing visual information, hence their conservation. However the number of homologous primate visual areas is unknown. Currently we only consider V1, V2, and the middle temporal area (MT) as homologous primate visual areas (Kaas and Lyon, 2001).

In this dissertation, we studied two extrastriate areas that lie between V2 and MT, V3 and V4. Traditionally, V3 and V4 are considered to be a part of different visual processing streams, the dorsal stream (also called the “where” pathway) for V3 and the ventral stream (also called the “what” pathway) for V4. However there are some important questions that cloud our understanding of each visual area. In Chapter 2, we used IOI to determine if V3 could be identified in the prosimian primate galago. In Chapter 3, we used IOI to investigate the modular level topography of V4 in awake macaques. In Chapter 4, we further investigated modular properties of V4, also in awake macaques, by studying spatial frequency (SF) and size preferences in color and orientation preference modules.

Chapter 2: Galagos have a V3. In Chapter 2, we used IOI to investigate the rostral border of dorsal V2 in the prosimian primate *galago garnettii*. Based on previous studies among several primates, there were two major proposals for the visuotopic organization along the rostral border of dorsal V2. The first shows the dorsomedial area (DM) as the principle region bordering the rostral border of dorsal V2 (Fig. 1, Chapter 2). DM is described as a complete visual area with both upper and lower visual field representations completely contained in the dorsal aspects of visual cortex. The second proposal shows the dorsal half of V3 as the principle region bordering the rostral border of dorsal V2. The fundamental difference between the two proposals is DM places an upper visual field representation along the rostral border of dorsal V2, while V3 does not. Hence, our main test was to locate the upper visual field representation along the rostral border of dorsal V2 (Figs. 4 and 9, Chapter 2). Consistent with V3, we found no evidence for an upper visual field representation directly rostral to dorsal V2. Also consistent with a V3 organization, was our visuotopic mapping that revealed a mirror reversal across the rostral V2 border. This study supports the notion of V3 as a homologous primate visual area by adding galagos to the list of primates where it has been described.

Implication of a galago V3: There have been descriptions of V3 in a variety of primates. Our IOI study in galagos (Chapter 2) provides strong similarities to IOI evidence in owl monkeys (a New World monkey). Using IOI, it is possible to reveal a mirror reversal in the visuotopic representation of owl monkeys (Lyon et al., 2002) and galagos (Chapter 2) and reveal banding patterns in the orientation selectivity in owl monkey (Xu et al., 2004) and galago (Chapter 2) V3. The visuotopic descriptions are compatible with those found in macaque (Adams and Zeki, 2001; Brewer et al., 2002;

Cragg, 1969; DeYoe et al., 1996; Engel et al., 1997; Press et al., 2001; Zeki, 1969) and human (DeYoe et al., 1996; Engel et al., 1997; Gegenfurtner et al., 1997; Reppas et al., 1997; Sereno et al., 1995; Smith et al., 1998; Tootell et al., 1997) fMRI studies. The orientation selectivity observed in owl monkey V3 (Xu et al., 2004) and galago V3 (Chapter 2) has also been consistently described in macaque V3 throughout its history (Baizer, 1982; Felleman and Van Essen, 1987; Gegenfurtner et al., 1997; Zeki, 1978).

Supporting the visuotopic descriptions of V3 in non-human primates, are studies on cortical connectivity in New World monkeys (owl monkeys, squirrel monkeys, titi monkeys, marmosets) (Lyon and Kaas, 2001; 2002c), Old World monkeys (macaques) (Burkhalter et al., 1986; Felleman et al., 1997a; Lyon and Kaas, 2002b), and a prosimian primate (galagos) (Lyon and Kaas, 2002a). The commonalities (visuotopic, cortical connectivity, and orientation preferences) presented across a variety of primates speaks to the likely conservation of V3 from the earliest primates. This is significant since only 3 areas are well established as homologous visual areas, V1, V2, and MT. What role does V3 play that has maintained its presence through some 65 million years of evolution? Currently we have a very crude understanding of V3 function. As of now, we are only aware of one property that is present in all V3 areas studied, orientation selectivity. This is not overly surprising given that V1, V2, V4, and MT all have been demonstrated to be orientation selective. However V3 is proposed to be a part of the dorsal visual pathway, and accordingly studies have demonstrated a variety of motion processing properties (Baizer, 1982; Cowey et al., 2006; Felleman and Van Essen, 1987; Gegenfurtner et al., 1997; Smith et al., 1998; Zeki, 1978). This belief is strengthened by inactivation studies involving V3 that altered MT response to motion stimuli (Ponce et al., 2008). While this

is a beginning, there is a lack of studies for V3 function where there is good reason to consider homology.

It is notable that there is some dissenting view regarding V3 homology marmoset evidence (Jeffs et al., 2012; Rosa et al., 2005; Rosa et al., 2000; Rosa and Schmid, 1995; Rosa and Tweedale, 2000; 2001). However much of the marmoset evidence supporting DM comes from single electrode recordings and can be re-interpreted to allow for a V3 similar to those described in other primates (Lyon and Connolly, 2012). Additionally, as we line out in Chapter 1, there is evidence from New World monkeys that is consistent with the V3 descriptions in galagos, macaques, and humans. We also pointed out that there is no evidence for functional symmetry between the upper and lower visual fields of DM despite a study that characterized the lower visual field but conspicuously omitted any upper visual field data on the same subject (Lui et al., 2006). For a visual area to respond to the same type of visual stimulus for only lower or upper visual field half would be an unusual and improbable property. Chapter 2 further argues that V3 should be considered a strong candidate for homologous visual area among primates. Since all other homologous visual areas (V1, V2, and MT) are considered crucial to visual function, V3 deserves more attention and study. As a homologous visual area relatively early in the visual processing stream, V3 likely also performs functions integral to visual processing. Compared to V4, there is very little understanding regarding V3 function. But, with the growing sense that V3 is common to all primates, new thoughts about V3 are slowly forming. A recent study demonstrates that V3 is involved in the processing of surface properties of objects (Okazawa et al., 2012). In conjunction with previously reported

color selectivity (Felleman and Van Essen, 1987), V3 could be revealed to operate along both the dorsal and ventral visual processing streams.

Chapter3: Modular influence of V4 visual topography. In Chapter 3, we investigated the influence of modular topography on V4. The ability to use IOI in central V4 of awake macaques was only recently demonstrated (Tanigawa et al., 2010). And while progress has been made toward better understanding of V4 topography, there has been little to assess foveal properties or how modular organization influences V4 organization. To the modular influence of visuotopic organization, we calculated the center of mass from t-maps (see Materials and Methods in Chapter 3) based on comparisons between color vs. achromatic stimuli or two orthogonal orientation grating stimuli. We found that the modules have their own local visuotopic organization that is similar to the repeated representations specific to functional modules in V2 (Roe and Ts'o, 1995). Interestingly, the cortical magnification appears be a scaled version of previous reports of V4 cortical magnification. The scaling is expected if multiple locations of visual space produce multiple cortical representations. For eccentricity, we found a relationship between cortical magnification factor vs eccentricity was a constant factor of 3 off of a well cited report by Gattass et al (1988). However despite this scaling, by making some simple assumptions, we are able to recover similar anisotropy ratios.

When other methods force smooth representation of visuotopy and essentially force a value to a specific location on cortex rather, this dilutes the effect of neighboring areas that may also respond to the given stimulus at that particular visual field position. By ignoring areas where there is cortical activation that may not be considered the center of that cortical regions population receptive field, the distance between cortical

representations can effectively be expanded. In V4 this results in our factor of 3 difference between previous measures and our own.

Implications of local topography: It is common practice to assume that visuotopic representation should be continuous over a given visual area. However, just in V1 and V2, we know this to be false. In V1 there is a repeated representation of the visual field between ocular dominance columns (Blasdel and Fitzpatrick, 1984; Hubel and Wiesel, 1974). In V2 there are representations of the visual field between stripes (Roe and Ts'o, 1995; Shipp and Zeki, 2002). The effect of modular organization is best illustrated in terms of the anisotropy index. The anisotropy index refers to the ratio of linear cortical magnification factors measured as a function of eccentricity or polar angle. In V1 this ratio when measured within ocular dominance columns is roughly 1:1 (Tootell et al., 1988). However if we ignore ocular dominance, then we get a ratio of 2:1 (Polimeni et al., 2006). Similarly, in V2, the ratio within a stripe is approximately 2:1 (Roe and Ts'o, 1995). However, if there are three repetitions in V2, then we theoretically would arrive at a ratio of 6:1 (Polimeni et al., 2006; Roe and Ts'o, 1995). One of the reasons the relationships scale with the number of repetitions is because there is little to no evidence that the repetitions in V1 and V2 repeat across polar angles and eccentricity in V1 and V2. However in V4, the visible repetition is across polar angles (Fig. 8, Chapter 3). Therefore we expect a scaling effect along this axis. Thus as we discussed in Chapter 3, there is potential unequal compression based on our method for measuring cortical magnification factor as a function of eccentricity or polar angle. However when we correct for this, we arrive at a scaling factor of roughly 9:1 at 0.25 degrees eccentricity. It does seem clear that these scaling issues arise due to modular influences. Within our

window, there are no obvious indications of repetitions across eccentricity other than the factor of 3 scaling between cortical magnification factor values between our report and others. But proposed modularity models based on connectivity with V2 suggests that V4 is composed of modular islands (Felleman et al., 1997b; Xiao et al., 1999; Zeki and Shipp, 1989) which is also indicated by IOI evidence from more peripheral locations (Ghose and Ts'o, 1997; also Fig. S5, Chapter 4).

While the difference between continuous vs. non-continuous visual field representation seems purely academic, ignoring modular influence on topography diminishes its role in binding regions of visual field processing features for efficient processing of information (Kaas, 1997). While a more macro approach may be acceptable, ignoring this more micro view and its effect seems unwise. Our report on foveal modularity in V4 provides a unique perspective on topographic organizational principles. While IOI could result in the contraction of the visual field measures because of population averaging, we suggest an alternative explanation. We submit that the contracted view is a more accurate reflection of how modules bind and process local features of a given visual location. This kind of repeated representation of the sensory surface appears to be a strategy that is being used in many visual areas and perhaps is a common theme among them all. It is worth nothing that this strategy of representing the sensory surface does not seem to be unique to visual areas but also appears to be a theme to other sensory cortical areas as well.

Chapter 4: Size and Spatial frequency preferences in V4 modules. In Chapter 4, we studied spatial frequency and size preference for the module function preference type, orientation or color. Looking at size preference, we found little difference between the

preferences between color and orientation preference domains. While this is not unexpected that color domains have a size preference, it is interesting that color domains require any surround suppression, although it appears to be less prominent than in orientation domains. However this could be a necessary attribute for proper figure ground separation, recently proposed as the main function of V4 (Roe et al., 2012). The fact that these domains do employ surround suppression is strong indication that local binding properties of modules are an important aspect of cortical processing. When we examined the V4 spatial frequency preference of these modules, we found qualitative evidence for a bimodal distribution for spatial frequency tuning based on the IOI signal for orientation and color selective domains. When examining bimodal vs. unimodal Gaussian fits for V4 domains we found that the improvement in the least square fits supported the qualitative assessment that these are bimodal distributions. The presence of cells in V4 with low pass spatial frequency preferences have been noted in the past but are thought to have no apparent organization (Pollen et al., 2002). This could be a part of the low and high pass SF segregations that result in differential face processing expertise effects to low SF and high SF filtered images (Gauthier et al., 2005).

The stimuli construction itself could be the source of this low frequency component. It is possible that the report of V4 performing better with square waves (Desimone and Schein, 1987) is because V4 neuronal response can be augmented by the presence of harmonics. While the fundamental is still produces the main power of the wave form, it could be that around the 1 cpd range, the harmonics generated at the lower SF gratings enhances cortical activity on a population level, resulting in these previously unobserved dynamics in V4. Considering that V4 may be involved in object segregation, having

multiple channels or methods to evaluate increasingly complex stimuli would be advantageous.

Perspective on size preferences in V4: Early reports for size optimization in V4 came from bars length and widths (Desimone and Schein, 1987). The size “preference” is due to surround suppression. Reports for surround suppression started very early with Hubel and Wiesel (1965) and have been reported consistently ever since for both cats and monkeys (for review Allman et al., 1985; Cavanaugh et al., 2002; DeAngelis et al., 1994; Levitt et al., 1994). Because increasing size does not result in ever increasing signal from a given RF, defining a “size” preference is a corollary to measuring RF size. However this is simply one type of measure to provide an estimate of RF size. For instance one can choose the more classic minimum response field, which used small bars of light to mark off RF borders (Barlow et al., 1967) or, as we have, expanding patches of drifting gratings (DeAngelis et al., 1994; Sceniak et al., 2001). Thus size “preferences” is an indicator of relative RF sizes but only to a certain extent since induced activity within a given RF is dependent on more than simply coverage, the specific parameters (like contrast) and geometry of the stimulus (spot, annulus, square or bar) can influence the final measure (Petrov and McKee, 2006). When looking at size preferences with IOI, we are measuring the relative relationship of center-surround interaction of a population receptive field for a group of neurons. During passive viewing, we show that in terms of IOI signal dynamics, color domains and orientation domains have similar responses to changing stimulus diameter implying similar RF sizes or RF response relationships to stimulus size at various eccentricities. The presence of a fixation point does present an interesting discussion point. It is well known that attention to specific features can

modulate neural responses (Connor et al., 1996; Connor et al., 1997; Haenny et al., 1988; Haenny and Schiller, 1988; McAdams and Maunsell, 1999a; b; Moran and Desimone, 1985). The dynamic nature of RF size in V4 does present a factor that is important to address in our study. The fixation spot provides is a static point common to all stimuli presented in the visual field. However the fixation spot itself must influence the center-surround interaction to some extent and the amount is likely related to variety of factors such as the size of the fixation spot, the size of the stimulus, and the distance (in visual degrees) between the two. We circumvent this issue in our study by performing subtractions since for a given visual field position its influence is most likely to be roughly constant. However this it would be of interest to know if we altered the parameters of the fixation point alone without changing the rest of our experimental paradigm, what the influence would be.

Implications of bimodal spatial frequency tuning in V4: At this point the full implications are unclear. However it does seem likely that V4 is processing square waves differently than V2. This at least tells us that V4 is performing increasingly complex operations. The long term confirmation of this outcome will clearly increase appreciation of V4 function.

Future directions

V3: Now that we have demonstrated our ability to identify and isolate our proposed galago V3, we need to move into studying other aspects of its function and connectivity. In primates such as galagos and several commonly studied New World species like owl

monkeys and squirrel monkeys, V3 will be exposed on the cortical surface which allows for the use of IOI.

First would be to re-evaluate cortical connectivity of V3. Previous attempts to look at the connectivity directly rostral to dorsal V2 were relatively blind injections with tracers. Injections rostral to V2 were usually based on approximations of ideal models. However using IOI we can better direct injections into V3 with less ambiguity. We would look for cortical connection patterns consistent with our results in Chapter 2. Mostly we expect no upper visual field connections directly rostral to dorsal V2.

A second component to connection studies would be to direct current into specific locations of V3 (or into areas connected to V3) in galagos. By electrically stimulating cortical locations, we could use IOI to observe what cortical locations connected to V3 respond. Based on the basic known visuotopic relationship we know as well as the results we get from initial tracer studies, we can focus our imaging efforts to locations where tracer studies clearly show a relationship with areas like MT or V2. Because of the proposed role of MT and V3, it would be prudent to investigate this relationship. Both MT and V3 in galagos have shown evidence of orientation preference. We can reveal these preferences with IOI. Presumably if MT and V3 are connected, then stimulation of specific orientation preference domain in one area will reveal orientation domains with similar preference and visuotopic relationship within the other. A limitation of the electrical stimulation would arise if an entire column is activated because both orthodromic and antidromic current would be induced so the direction of the connectivity would be unknown. However once we find a region that reveals a relationship between the two areas, we could follow the imaging with retrograde or anterograde tracers to

support any findings of connectivity by electrical stimulation and help assess the cortical connectivity between MT and V3.

V4: At this juncture it would be advantageous to continue studying the modular topography in V4. There have been studies showing motion, disparity, and shape/contour selectivity in V4. How are these mapped in V4? There is preliminary evidence from our laboratory that suggest disparity selectivity has a module. There has also been an early report for domains that are revealed by motion preference (Li et al., 2011). Further study of motion and disparity mapping in V4 will advance our understanding of the potential role V4 plays in the dorsal pathway. But what about a more complex feature like shape/contour? Pasupathy and Connor showed that shape contour can be discriminated at a neuronal level (Pasupathy and Connor, 1999; 2001; 2002). While it would be difficult to study the entire set of 49 basic shapes similar to Pasupathy and Connor (2002), we could study a small subset by looking at a shape that can be unambiguously assigned an orientation and rotate it to see if there is a map to represent the angle of the various chosen shapes.

It would also be fruitful to perform a connectivity study in V4 similar to the one proposed for V3. We could selectively place injections into specific modules of V4 and see if the results are consistent with previous studies that performed the injections without *a priori* knowledge of the modular topography in V4 (Felleman et al., 1997b; Xiao et al., 1999; Zeki and Shipp, 1989). These injections would also provide insight into a previous report suggesting that central V4 preferentially targets temporal lobe areas by tracing injections that were feature specific.

References

- Adams DL, Zeki S. 2001. Functional organization of macaque V3 for stereoscopic depth. *J Neurophysiol* 86(5):2195-2203.
- Baizer JS. 1982. Receptive field properties of V3 neurons in monkey. *Invest Ophthalmol Vis Sci* 23(1):87-95.
- Blasdel GG, Fitzpatrick D. 1984. Physiological organization of layer 4 in macaque striate cortex. *The Journal of neuroscience : the official journal of the Society for Neuroscience* 4(3):880-895.
- Brewer AA, Press WA, Logothetis NK, Wandell BA. 2002. Visual areas in macaque cortex measured using functional magnetic resonance imaging. *J Neurosci* 22(23):10416-10426.
- Burkhalter A, Felleman DJ, Newsome WT, Van Essen DC. 1986. Anatomical and physiological asymmetries related to visual areas V3 and VP in macaque extrastriate cortex. *Vision Res* 26(1):63-80.
- Cowey A, Campana G, Walsh V, Vaina LM. 2006. The role of human extra-striate visual areas V5/MT and V2/V3 in the perception of the direction of global motion: a transcranial magnetic stimulation study. *Exp Brain Res* 171(4):558-562.
- Cragg BG. 1969. The topography of the afferent projections in the circumstriate visual cortex of the monkey studied by the Nauta method. *Vision Res* 9(7):733-747.
- DeYoe EA, Carman GJ, Bandettini P, Glickman S, Wieser J, Cox R, Miller D, Neitz J. 1996. Mapping striate and extrastriate visual areas in human cerebral cortex. *Proc Natl Acad Sci U S A* 93(6):2382-2386.
- Engel SA, Glover GH, Wandell BA. 1997. Retinotopic organization in human visual cortex and the spatial precision of functional MRI. *Cereb Cortex* 7(2):181-192.
- Felleman DJ, Burkhalter A, Van Essen DC. 1997a. Cortical connections of areas V3 and VP of macaque monkey extrastriate visual cortex. *J Comp Neurol* 379(1):21-47.
- Felleman DJ, Van Essen DC. 1987. Receptive field properties of neurons in area V3 of macaque monkey extrastriate cortex. *J Neurophysiol* 57(4):889-920.

- Felleman DJ, Xiao Y, McClendon E. 1997b. Modular organization of occipito-temporal pathways: cortical connections between visual area 4 and visual area 2 and posterior inferotemporal ventral area in macaque monkeys. *The Journal of neuroscience : the official journal of the Society for Neuroscience* 17(9):3185-3200.
- Gattass R, Sousa AP, Gross CG. 1988. Visuotopic organization and extent of V3 and V4 of the macaque. *J Neurosci* 8(6):1831-1845.
- Gegenfurtner KR, Kiper DC, Levitt JB. 1997. Functional properties of neurons in macaque area V3. *J Neurophysiol* 77(4):1906-1923.
- Ghose GM, Ts'o DY. 1997. Form processing modules in primate area V4. *J Neurophysiol* 77(4):2191-2196.
- Hubel DH, Wiesel TN. 1974. Sequence regularity and geometry of orientation columns in the monkey striate cortex. *The Journal of comparative neurology* 158(3):267-293.
- Jeffs J, Federer F, Ichida JM, Angelucci A. 2012. High-Resolution Mapping of Anatomical Connections in Marmoset Extrastriate Cortex Reveals a Complete Representation of the Visual Field Bordering Dorsal V2. *Cereb Cortex* [Epub ahead of print].
- Kaas JH. 1997. Topographic maps are fundamental to sensory processing. *Brain research bulletin* 44(2):107-112.
- Kaas JH, Lyon DC. 2001. Visual cortex organization in primates: theories of V3 and adjoining visual areas. *Prog Brain Res* 134:285-295.
- Li P, Chen M, Han C, Zhu S, Xu H, Roe AW, Lu HD. A motion direction map in macaque V4; 2011 November 12 -16, 2011; Washington, DC, USA.
- Lui LL, Bourne JA, Rosa MG. 2006. Functional response properties of neurons in the dorsomedial visual area of New World monkeys (*Callithrix jacchus*). *Cereb Cortex* 16(2):162-177.
- Lyon DC, Connolly JD. 2012. The case for primate V3. *Proc Biol Sci* 279(1729):625-633.

- Lyon DC, Kaas JH. 2001. Connectional and architectonic evidence for dorsal and ventral V3, and dorsomedial area in marmoset monkeys. *J Neurosci* 21(1):249-261.
- Lyon DC, Kaas JH. 2002a. Connectional evidence for dorsal and ventral V3, and other extrastriate areas in the prosimian primate, *Galago garnettii*. *Brain Behav Evol* 59(3):114-129.
- Lyon DC, Kaas JH. 2002b. Evidence for a modified V3 with dorsal and ventral halves in macaque monkeys. *Neuron* 33(3):453-461.
- Lyon DC, Kaas JH. 2002c. Evidence from V1 connections for both dorsal and ventral subdivisions of V3 in three species of New World monkeys. *J Comp Neurol* 449(3):281-297.
- Lyon DC, Xu X, Casagrande VA, Stefansic JD, Shima D, Kaas JH. 2002. Optical imaging reveals retinotopic organization of dorsal V3 in New World owl monkeys. *Proc Natl Acad Sci U S A* 99(24):15735-15742.
- Okazawa G, Goda N, Komatsu H. 2012. Selective responses to specular surfaces in the macaque visual cortex revealed by fMRI. *Neuroimage*.
- Pasupathy A, Connor CE. 1999. Responses to contour features in macaque area V4. *J Neurophysiol* 82(5):2490-2502.
- Pasupathy A, Connor CE. 2001. Shape representation in area V4: position-specific tuning for boundary conformation. *J Neurophysiol* 86(5):2505-2519.
- Pasupathy A, Connor CE. 2002. Population coding of shape in area V4. *Nat Neurosci* 5(12):1332-1338.
- Polimeni JR, Balasubramanian M, Schwartz EL. 2006. Multi-area visuotopic map complexes in macaque striate and extra-striate cortex. *Vision research* 46(20):3336-3359.
- Ponce CR, Lomber SG, Born RT. 2008. Integrating motion and depth via parallel pathways. *Nat Neurosci* 11(2):216-223.

- Press WA, Brewer AA, Dougherty RF, Wade AR, Wandell BA. 2001. Visual areas and spatial summation in human visual cortex. *Vision Res* 41(10-11):1321-1332.
- Reppas JB, Niyogi S, Dale AM, Sereno MI, Tootell RB. 1997. Representation of motion boundaries in retinotopic human visual cortical areas. *Nature* 388(6638):175-179.
- Roe AW, Ts'o DY. 1995. Visual topography in primate V2: multiple representation across functional stripes. *J Neurosci* 15(5 Pt 2):3689-3715.
- Rosa MG, Palmer SM, Gamberini M, Tweedale R, Pinon MC, Bourne JA. 2005. Resolving the organization of the New World monkey third visual complex: the dorsal extrastriate cortex of the marmoset (*Callithrix jacchus*). *J Comp Neurol* 483(2):164-191.
- Rosa MG, Pinon MC, Gattass R, Sousa AP. 2000. "Third tier" ventral extrastriate cortex in the New World monkey, *Cebus apella*. *Exp Brain Res* 132(3):287-305.
- Rosa MG, Schmid LM. 1995. Visual areas in the dorsal and medial extrastriate cortices of the marmoset. *J Comp Neurol* 359(2):272-299.
- Rosa MG, Tweedale R. 2000. Visual areas in lateral and ventral extrastriate cortices of the marmoset monkey. *J Comp Neurol* 422(4):621-651.
- Rosa MG, Tweedale R. 2001. The dorsomedial visual areas in New World and Old World monkeys: homology and function. *Eur J Neurosci* 13(3):421-427.
- Sereno MI, Dale AM, Reppas JB, Kwong KK, Belliveau JW, Brady TJ, Rosen BR, Tootell RB. 1995. Borders of multiple visual areas in humans revealed by functional magnetic resonance imaging. *Science* 268(5212):889-893.
- Shipp S, Zeki S. 2002. The functional organization of area V2, II: the impact of stripes on visual topography. *Visual neuroscience* 19(2):211-231.
- Smith AT, Greenlee MW, Singh KD, Kraemer FM, Hennig J. 1998. The processing of first- and second-order motion in human visual cortex assessed by functional magnetic resonance imaging (fMRI). *J Neurosci* 18(10):3816-3830.

- Tanigawa H, Lu HD, Roe AW. 2010. Functional organization for color and orientation in macaque V4. *Nat Neurosci* 13(12):1542-1548.
- Tootell RB, Mendola JD, Hadjikhani NK, Ledden PJ, Liu AK, Reppas JB, Sereno MI, Dale AM. 1997. Functional analysis of V3A and related areas in human visual cortex. *J Neurosci* 17(18):7060-7078.
- Tootell RB, Switkes E, Silverman MS, Hamilton SL. 1988. Functional anatomy of macaque striate cortex. II. Retinotopic organization. *The Journal of neuroscience : the official journal of the Society for Neuroscience* 8(5):1531-1568.
- Xiao Y, Zych A, Felleman DJ. 1999. Segregation and convergence of functionally defined V2 thin stripe and interstripe compartment projections to area V4 of macaques. *Cerebral cortex* 9(8):792-804.
- Xu X, Bosking W, Sary G, Stefansic J, Shima D, Casagrande V. 2004. Functional organization of visual cortex in the owl monkey. *J Neurosci* 24(28):6237-6247.
- Zeki S, Shipp S. 1989. Modular Connections between Areas V2 and V4 of Macaque Monkey Visual Cortex. *The European journal of neuroscience* 1(5):494-506.
- Zeki SM. 1969. Representation of central visual fields in prestriate cortex of monkey. *Brain Res* 14(2):271-291.
- Zeki SM. 1978. Uniformity and diversity of structure and function in rhesus monkey prestriate visual cortex. *J Physiol* 277:273-290.